NON-SPECULAR RADAR CROSS SECTION STUDY
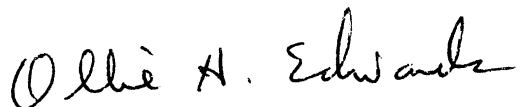
Eugene F. Knott
Thomas B.A. Senior

FOREWORD

This Interim Report describes research performed by The University of Michigan Radiation Laboratory, 2455 Hayward Street, Ann Arbor, Michigan 48105 under USAF Contract F33615-73-C-1174, Project 7633, "Non-Specular Radar Cross Section Study." The research was sponsored by the Electromagnetic Division, Air Force Avionics Laboratory, and the Technical Monitor was Dr. Charles H. Kreuger, AFAL/WRP.

This report covers the time period 15 March through 16 October 1973 and was prepared by E. F. Knott and T. B. A. Senior, Principal Investigators. The authors take pleasure in acknowledging the assistance of Dr. C. H. Kreuger, who supplied some of the experimental data discussed in Chapter V; Professor S. R. Laxpati of the University of Illinois (Chicago Circle), who worked with them during the summer of 1973 and initiated the studies presented in Chapters II and IV as well as directing the computations of the edge diffraction coefficient; and Dr. V. V. Liepa, who has been associated with all major computer programs in the research.

This report has been assigned Radiation Laboratory Report Number 011764-1-T for internal control purposes, and was submitted for sponsor approval on 2 November 1973.

This Technical Report has been reviewed and is approved for publication.

O llie A. Edwards

CLYDE H. EDWARDS
Colonel, USAF
Chief, Electronic Warfare Division

ii

ABSTRACT

The broad objective of this research is to develop techniques to reduce non-specular scattering from objects of interest to the Air Force. The major tools used thus far in the investigations have been two-dimensional computer programs which solve the integral equations for a surface impedance boundary condition and for a thin resistive sheet placed near a conducting obstacle. The existing programs have proven valuable, but the research requirements have now outstripped their capabilities and more inclusive programs are required. The main thrust of this Interim Report is upon the development of the integral equations necessary for the construction of more comprehensive programs, but for the sake of completeness, the equations for the existing programs are also derived as a matter of course. Of considerable importance is the treatment of "magnetic" resistive sheets in addition to conventional electric resistive sheets so that, with but a slight expansion of the concept of resistivity, magneto-dielectric layers of physical materials may be modeled. In addition to the theoretical work, experimental results obtained by both The University of Michigan Radiation Laboratory and the Air Force Avionics Laboratory are compared with computed predictions.

TABLE OF CONTENTS

I

INTRODUCTION

The objective of the research described in this Interim Report is to develop techniques to reduce non-specular scattering from typical aerospace vehicles of interest to the Air Force. Such scattering arises from both smooth and edged structures when viewed in non-specular directions and during this reporting period an ogival cylinder has been used as the basic shape with which to explore promising techniques. The basic tools in the research were a pair of computer programs that solve the appropriate integral equations for the surface fields in two dimensions.

The programs are modified versions of programs furnished by AFAL, the modifications being necessary because the originals lacked the flexibility to conveniently accommodate the shapes of interest in the present study. One of the programs (RAMD) is itself an outgrowth of an earlier modification which has now been abandoned (RAM1B) and is based upon the integral equations in which a surface impedance boundary condition is imposed. RAMD solves the equations for either E- or H-polarization (incident electric or magnetic vector parallel to the cylinder axis, respectively) and a brief description of it, along with a source listing, is given in Appendix B. The other program (REST) solves the integral equations for a metallic cylinder which may have resistive sheets placed on or near the surface, but is applicable only for E-polarization. A source listing of REST may be found in Appendix B of Knott, Liepa and Senior (1973).

The impetus to discard the now defunct RAM1B developed late in the predecessor Contract (F33615-72-C-1439) when it became apparent that the program would never satisfactorily produce the correct solution for edged bodies for E-polarization. At the time the Final Report for that Contract was being prepared, we were still trying to obtain acceptable values by sampling the surface densely in the vicinity of the edges. Although the results tended to converge on what was believed (and has been since demonstrated) to be the correct

behavior, the sampling rate over the remainder of the profile had to be reduced. A summary of these efforts and the consequences of coarse sampling is given in Chapter V; not unexpectedly, accuracy is reduced and ultimately the gain in accuracy by dense packing at the edges will be offset by the loss due to sparse sampling over the rest of the body.

The shortcomings of RAM1B were serious enough to demand a thorough examination of the integral equations for the impedance boundary condition, and in Chapter II the equations are derived using both the scalar and vector approaches. Because the impedance boundary condition rigidly links the electric surface currents to the magnetic ones, a pair of integral equations is produced for each polarization and, from a mathematical viewpoint, one is as good as the other. From a numerical standpoint, however, one of the pair is markedly superior and although RAM1B used the "good" equation for one polarization, it used the "bad" one for the other. This discovery led to the construction of program RAMD, which is sufficiently different from its predecessor to be regarded as a new program, and not merely a modification.

Program REST has been the basic tool in a study still in progress exploring the use of resistive sheets for non-specular scattering reduction, the results of which will be documented elsewhere. The program is designed only for E-polarization, which turns out to be the case when a simple integral equation is sufficient. The H-polarization integral equation, on the other hand, contains a second derivative singularity (and is thus a "bad" equation) that poses annoying, but surmountable, numerical problems, and it was probably for this reason that the original version (RAMC) was restricted to E-polarization. Since both polarizations must be treatable in order to carry out the Contract objectives, we undertook the theoretical study of Chapter IV to secure the necessary equations. Unlike the impedance boundary condition case, there is no choice; only one equation is produced for each polarization be it simple or not, and it must be used to obtain the solution. We should mention in passing that the study in Chapter III, which

2

considers impedance boundary condition sheets, has provided a key result for the analysis and interpretation of the data generated by program REST.

As pointed out in Chapter IV, the principle of duality permits us to immediately write down the equations for a "magnetic" resistance sheet from the electric sheet equations. Since the magnetic and electric currents are independent for each kind of sheet, the sheets may be mathematically superposed to simulate a thin layer of magneto-dielectric material, and we now have the foundation for a computer program capable of modeling physically realizable materials in contrast to the more nebulous specification of surface impedances. The numerical evaluation of second order singularities is an inevitable requirement in a generalized program, of course, but the procedures discussed in Appendix A show that the task can be accomplished with a tolerably small error. And although the thickness of actual or desirable coatings may well prove to be beyond the bounds of a thin layer approximation, a thick coating can be mathematically modeled by a stack of thin layers.

The need for such a generalized program may become apparent from the comparisons between measured and computed results given in Chapter V. The computations were performed by program RAMD and although they agree well with experiment for metallic, and in some cases coated, bodies, the agreement for other coatings is not as good. The disparity in these cases is not necessarily the fault of the program, nor indeed of the experiments, but a consequence of the difficulty of correctly relating the impedance near an edge to the bulk properties of a material coating and the local edge geometry. This specification in itself requires the solution of a boundary value problem, a task we hope to accomplish via a generalized computer program based upon the integral equations developed in this report.

II

INTEGRAL EQUATIONS FOR IMPEDANCE SURFACES

It is desirable to examine the form of integral equations appropriate in a two-dimensional problem involving a scatterer with an impedance boundary condition imposed at its surface. The objectives of this study are not only to show how the equations are affected by the geometry and the boundary conditions, but also to resolve some of the difficulties which have previously been experienced.

2.1 The Impedance Boundary Condition

Consider a closed cylindrical surface whose generators are parallel to the z axis of a cylindrical coordinate system and whose profile in a plane perpendicular to the z axis is the closed curve C. Let $\hat{n}$ be a unit vector normal drawn outwards to C and let $\hat{s}$ be a unit vector in the tangential direction, such that $\hat{s}$, $\hat{n}$, $\hat{z}$ form a right-handed system.

At the surface the impedance boundary condition

$$\underline{E} - (\hat{n} \cdot \underline{E}) \hat{n} = \eta Z_0 \, \hat{n} {}_{\wedge} \underline{H} \tag{2.1}$$

is imposed, where η is the (normalized) surface impedance and may be a function of the distance s along C. For a perfectly conducting surface, $\eta = 0$. By trivial manipulation, eq. (2.1) can be expressed alternatively as

$$\underline{H} - (\hat{n} \cdot \underline{H}) \hat{n} = - \frac{Y_0}{\eta} \, \hat{n} {}_{\wedge} \underline{E} \tag{2.2}$$

(Senior, 1962), which is the "dual" of (2.1) under the transformation $\underline{E} \rightarrow \underline{H}$, $\underline{H} \rightarrow -\underline{E}$, $Z_0 \leftrightarrow Y_0$, $\eta \leftrightarrow 1/\eta$. Of course, this duality is lost if at any point of the surface η is either zero or infinite.

The body is illuminated by a plane wave whose direction of propagation is in a plane perpendicular to the z axis, and it is now sufficient to consider separately the two principal polarizations, that in which $\underline{H}^i = \hat{z} H_z^i$ (H-polarization), and $\underline{E}^i = \hat{z} E_z^i$ (E-polarization). From symmetry it follows that the total fields

4

are similarly oriented and this enables us to treat each problem as a scalar one for the z component of the total magnetic or electric field. Such a simplification is not possible if the plane wave is at skew incidence.

2.2 Scalar Formulation

Let us consider first the case of H-polarization. Then $\underline{H}^i = \hat{z} H_z^i$, implying $\underline{H} = \hat{z} H_z$, and consonant with the usual definition of the surface electric current $\underline{K}$, viz.

$$\underline{K} = \hat{n} \wedge \underline{H} ,$$ (2.3)

we have

$$\underline{K} = \hat{s} K_s \qquad \text{with} \qquad K_s = H_z .$$ (2.4)

On the surface the boundary condition (2.1) requires

$$E_s = \eta Z_0 H_z = \eta Z_0 K_s$$

and since, from Maxwell's equations,

$$\frac{\partial H_z}{\partial n} = -ikY_0 E_s ,$$

we have

$$\frac{\partial H_z}{\partial n} = -ik\eta K_s \qquad\qquad \text{on } C.$$ (2.5)

Application of the scalar Green's theorem to a function $\psi(\rho)$ satisfying the scalar wave equation outside and on the surface gives

$$\psi(\rho) = \psi^i(\rho) + \frac{i}{4} \int_C \left\{ \psi(\rho') \frac{\partial}{\partial n'} H_0^{(1)}(kr) - H_0^{(1)}(kr) \frac{\partial}{\partial n'} \psi(\rho') \right\} ds'$$ (2.6)

where the normal derivatives are with respect to the primed coordinates of the integration point, ρ is the two-dimensional position vector of the observation point

5

and $\underline{r} = \underline{\rho} - \underline{\rho}'$, implying $r = |\underline{\rho} - \underline{\rho}'|$. For simplicity we shall henceforth specify the integration point by its circumferential distance s' along C.

If we identify ψ with H_z, eq. (2.6) becomes

$$H_z(\underline{\rho}) = H_z^i(\underline{\rho}) + \frac{i}{4} \int_C \left\{ (\hat{n}' \cdot \hat{r}) H_1^{(1)}(kr) + i\eta(s') H_0^{(1)}(kr) \right\} K_s(s') d(ks') \qquad (2.7)$$

on making use of (2.5), and if we now allow $\underline{\rho}$ to approach a point s on C, the following integral equation results:

$$H_z^i(s) = K_s(s) + \lim_{\underline{\rho} \to C} \frac{1}{4} \int_C \left\{ \eta(s') H_0^{(1)}(kr) - i(\hat{n}' \cdot \hat{r}) H_1^{(1)}(kr) \right\} K_s(s') d(ks'). \qquad (2.8)$$

The second term in the integrand has a non-integrable singularity when $\underline{\rho}$ is on C, but if this is treated analytically in the usual manner, the limit can be applied to the integrand to yield

$$H_z^i(s) = \frac{1}{2} K_s(s) + \frac{1}{4} \int_C \eta(s') K_s(s') H_0^{(1)}(kr) d(ks')$$

$$- \frac{i}{4} \fint_C K_s(s') (\hat{n}' \cdot \hat{r}) H_1^{(1)}(kr) d(ks') . \qquad (2.9)$$

where the slash across the integral sign indicates a Cauchy principal value. This is identical to the equation obtained by Andreasen (1965) for the special case of incidence in a plane perpendicular to the z axis and was quoted[*] (eq. 3.1) in the first interim report of the previous contract (Knott and Senior, 1973). It is, in fact, the integral equation used for H-polarization in the original computer

---

[*] Since the primes now refer to the point of integration, and in view of the present definition of $\underline{r}$, the last terms on the right hand sides of eqs. (3.1) and (3.2) have the wrong signs.

program RAM1A, and since the kernel has at most a first derivative singularity, the equation is well suited to numerical solution.

However, (2.9) is not the only integral equation that can be obtained. If, for example, the normal derivative of the field $H_z(\rho)$ of eq. (2.7) is taken prior to the observation point reaching C, we find

$$Y_0 E_s^i(s) = \eta(s)K_s(s) + \lim_{\rho \to C} \frac{i}{4k} \frac{\partial}{\partial n} \int_C \left\{ \eta(s')H_0^{(1)}(kr) \right.$$

$$\left. - i(\hat{n}' \cdot \hat{r})H_1^{(1)}(kr) \right\} K_s(s')d(ks') . \qquad (2.10)$$

For the first term in the integrand, the differentiation and integration processes can be interchanged and the non-integrable singularity that results when ρ is on C can be treated analytically as before. This is not true of the second term, however. Hence

$$Y_0 E_s^i(s) = \frac{1}{2} \eta(s)K_s(s) - \frac{i}{4} \int_C \eta(s')K_s(s')(\hat{n} \cdot \hat{r})H_1^{(1)}(kr)d(ks')$$

$$+ \lim_{\rho \to C} \frac{1}{4k} \frac{\partial}{\partial n} \int_C K_s(s')(\hat{n}' \cdot \hat{r})H_1^{(1)}(kr)d(ks') \qquad (2.11)$$

which is not so convenient for numerical solution because of the "second derivative singularity" which it contains.

We now turn to the case of E-polarization. A particular advantage of the impedance boundary condition is that it preserves the duality inherent in Maxwell's equations and, in the present instance, this enables us to deduce the integral equations for E-polarization from those we have already given.

7

As part of the duality transformation, the surface electric current $\underline{K} = \hat{n}_\wedge \underline{H}$ is replaced by the surface magnetic current

$$\underline{K}^* = -\hat{n}_\wedge \underline{E} \ , \tag{2.12}$$

From the boundary condition (2.1), however,

$$\underline{K}^* = -\eta Z_0 \hat{n}_\wedge \underline{K} \tag{2.13}$$

and similarly, from (2.2),

$$\underline{K} = \frac{1}{\eta} Y_0 \hat{n}_\wedge \underline{K}^* \ . \tag{2.14}$$

Hence, as regards the component K_s,

$$K_s \longrightarrow K_s^* = -\eta Z_0 K_z \tag{2.15}$$

where, from (2.3), $K_z = -H_s$ is simply the axial component of the surface electric current. On applying the transformation

$$H_z^i \longrightarrow -E_z^i \ , \quad E_s^i \longrightarrow H_s^i \ , \quad K_s \longrightarrow -\eta Z_0 K_z \ , \quad Y_0 \longrightarrow Z_0, \quad \eta \longrightarrow 1/\eta$$

to eqs. (2.9) and (2.11), we immediately obtain

$$Y_0 E_z^i(s) = \frac{1}{2} \eta(s) K_z(s) + \frac{1}{4} \int_C K_z(s') H_0^{(1)}(kr) d(ks')$$

$$- \frac{i}{4} \oint_C \eta(s') K_z(s') (\hat{n}' \cdot \hat{r}) H_1^{(1)}(kr) d(ks') \ , \tag{2.16}$$

$$H_s^i(s) = -\frac{1}{2} K_z(s) + \frac{i}{4} \oint_C K_z(s') (\hat{n} \cdot \hat{r}) H_1^{(1)}(kr) d(ks')$$

$$- \lim_{\rho \to C} \frac{1}{4k} \frac{\partial}{\partial n} \int_C \eta(s') K_z(s') (\hat{n}' \cdot \hat{r}) H_1^{(1)}(kr) \, d(ks') \ . \tag{2.17}$$

8

Like (2.9) and (2.11), these are alternative equations appropriate, in this case, to E-polarization. The first is identical to that derived by Andreasen (1965) for incidence perpendicular to the z axis, and was quoted by Knott and Senior (1973a; eq. 3.2). Since the highest singularity of the kernel is a first derivative one, the equation is well suited to numerical solution and is the obvious one to choose for E-polarization. In contrast, Eq. (2.17) has (in effect) a second derivative singularity in the kernel and is much less convenient to use, but in spite of this it is apparently the equation employed in RAM1A. This is not entirely unnatural since the computer program was originally developed for skew incidence, but even in this more general case it is still possible to obtain two coupled integral equations having only first derivative singularities at the expense of introducing derivatives of the unknown currents. As Andreasen (1965) shows, these latter derivatives can be eliminated by partial integration, and the resulting equations then degenerate to (2.9) and (2.16) for incidence perpendicular to the z axis.

The fact that the computer program RAM1A is based on eqs. (2.9) and (2.17) explains our differing experiences in running it for H- and E-polarizations. It is now obvious how we can overcome the difficulties which formerly bedevilled us for E-polarization and this matter is taken up in Chapter V.

2.3 Vector Formulation

As we have seen, the problem of a plane wave incident on the cylindrical structure in a plane perpendicular to its axis can be treated as a scalar one, but since Hertz vectors are a convenient tool for any scattering problem, it is of interest to examine the integral equations resulting from this type of vector formulation.

In terms of the electric and magnetic Hertz vectors $\underline{\Pi}$ and $\underline{\Pi}^*$, the scattered field can be written as

$$\underline{E}^S = \nabla_\wedge \nabla_\wedge \underline{\Pi} + ikZ_0 \nabla_\wedge \underline{\Pi}^*,$$

$$\underline{H}^S = \nabla_\wedge \nabla_\wedge \underline{\Pi}^* - ikY_0 \nabla_\wedge \underline{\Pi} \quad . \tag{2.18}$$

The differentiations are with respect to the coordinates of the observation point, and for a two-dimensional problem

$$\underline{\Pi}(\underline{\rho}) = - \frac{Z_0}{4k} \int_C \underline{K}(s')H_0^{(1)}(kr)ds' \quad , \tag{2.19}$$

$$\underline{\Pi}^*(\underline{\rho}) = - \frac{Y_0}{4k} \int_C \underline{K}^*(s')H_0^{(1)}(kr)ds' \quad , \tag{2.20}$$

where $\underline{K}$ and $\underline{K}^*$ are, respectively, the surface electric and magnetic currents defined in eqs. (2.3) and (2.12). Using (2.13) and (2.14) we can express both $\underline{\Pi}$ and $\underline{\Pi}^*$ (and, hence, the scattered field) in terms of either $\underline{K}$ or $\underline{K}^*$ alone.

In view of the duality relations, it is sufficient to restrict attention to the case of H-polarization. As before, we then have $\underline{K} = \hat{s}K_s$ with $K_s = H_z$, implying

$$\underline{\Pi}(\underline{\rho}) = - \frac{Z_0}{4k} \int_C \hat{s}'K_s(s')H_0^{(1)}(kr)ds' \quad . \tag{2.21}$$

Also, $\underline{K}^* = \hat{z}K_z^*$ with $K_z^* = \eta Z_0 K_s$, so that

$$\underline{\Pi}^*(\underline{\rho}) = -\hat{z} \frac{1}{4k} \int_C \eta(s')K_s(s')H_0^{(1)}(kr)ds' \quad , \tag{2.22}$$

and it is now a trivial matter to determine the scattered field. In particular,

$$H_z^s(\underline{\rho}) = - \frac{1}{4} \int_C \eta(s')K_s(s')H_0^{(1)}(kr)d(ks') + \frac{i}{4} \int_C K_s(s')(\hat{n}' \cdot \hat{r})H_1^{(1)}(kr)d(ks') \quad ; \tag{2.23}$$

on allowing $\underline{\rho}$ to approach the surface and using

$$H_z^s(\underline{\rho}) = K_s(s) - H_z^i(s) , \qquad \underline{\rho} \text{ on } C ,$$

the integral equation (2.9) is at once obtained. Similarly for the scattered
electric field: if the component E_s^s is evaluated at a point on the surface, the
fact that

$$E_s^s(\underline{\rho}) = \eta(s)Z_0 K_s(s) - E_s^i(s) , \qquad \underline{\rho} \text{ on } C ,$$

leads immediately to the integral equation (2.11).

Thus, the vector formulation leads to precisely the same integral equations
as the scalar one. For H-polarization, the equation with the first derivative
singularity stems from a consideration of the magnetic field, whilst the electric
field gives rise to the equation having the second derivative singularity. Either
is sufficient to determine the single non-zero component K_s of the surface elec-
tric current. If, instead, we had considered E-polarization, the electric field
would have generated eq. (2.16) and the magnetic field (2.17). This is obvious
from duality and here again either equation is sufficient.

2.4 Thin Sheets

The integral equations derived in the previous sections are valid for a
two-dimensional surface at which an impedance boundary condition is imposed,
and provided its boundary profile C encloses a region of non-zero area, either
of the two equations (2.9) and (2.11) obtained for H-polarization is sufficient to
specify the surface electric current $\underline{K}$. This is also true of the E-polarized
integral equations (2.16) and (2.17), and for each polarization, the equation with the
first derivative singularity is the more attractive one for numerical solution.
However, as the thickness of the body decreases in comparison with its length,
so does the rate of convergence of a numerical solution, and as the two sides of the
body approach one another, these difficulties become severe. In fact, in the limit
of an infinitesimally thin body, neither type of integral equation is capable of

solution as it stands. This limit is the case of a thin sheet (not necessarily planar), and as we shall show, both integral equations are now needed to determine the surface current.

It is again sufficient to restrict our attention to H-polarization. If the cylinder is infinitely thin, the closed contour C can be broken up into two open contours C_+ and C_- lying on the upper (positive) and lower (negative) sides, and the integrals expressed as integrals over C_+ (say) alone. Thus, for a thin sheet whose surface impedances are the same on both sides, eq. (2.7) can be written as

$$H_z(\rho) = H_z^i(\rho) + \frac{i}{4} \int_{C_+} \left\{ J_2(s')(\hat{n}'_+ \cdot \hat{r})H_1^{(1)}(kr) + i\eta(s')J_1(s')H_0^{(1)}(kr) \right\} d(ks') \tag{2.24}$$

where

$$J_1(s) = K_{+s}(s) + K_{-s}(s) \tag{2.25}$$

is the sum of the surface currents on the two sides and

$$J_2(s) = K_{+s}(s) - K_{-s}(s) \tag{2.26}$$

is the difference. $J_1(s)$ and $J_2(s)$ are proportional to the local strengths of the equivalent magnetic and electric current sheets, respectively. We now take the limits of eq. (2.24) as ρ approaches the surface successively from above and below. Addition of the two limits gives

$$H_z^i(s) = \frac{1}{2} J_1(s) + \frac{1}{4} \int_{C_+} \eta(s')J_1(s')H_0^{(1)}(kr)d(ks') \tag{2.27}$$

which is a simple integral equation for $J_1(s)$. Subtraction, on the other hand, yields

$$J_2(s) = \frac{i}{4} \left(\lim_{\rho \to C_+} - \lim_{\rho \to C_-} \right) \int_{C_+} (\hat{n}'_+ \cdot \hat{r})J_2(s')H_1^{(1)}(kr)d(ks') \tag{2.28}$$

12

and by analytical examination of these limits it can be shown that (2.28) is merely the identity $J_2(s) = J_2(s)$. Unless $J_2(s) \equiv 0$ (and this is not in general true even for a uniform planar sheet), the integral equation (2.9) has now served to determine only the sum of the surface currents.

To find $J_2(s)$ and, hence, the currents themselves, it is necessary to use the integral equation (2.11) in addition to (2.9). Paralleling the analysis leading up to (2.11), the normal derivative of (2.24) is taken as the observation point approaches the sheet from above and below. Subtraction of the two limits again yields an identity, this time for $J_1(s)$, but addition produces the following integral equation for $J_2(s)$:

$$Y_0 E^i_{+s}(s) = \frac{1}{2}\eta(s)J_2(s) + \lim_{\underline{\rho} \to C_+} \frac{1}{4k} \frac{\partial}{\partial n_+} \int_{C_+} J_2(s')(\hat{n}'_+ \cdot \hat{r})H_1^{(1)}(kr)d(ks') \ . \quad (2.29)$$

This is analogous to (2.11) in having a second derivative singularity.

For a thin sheet it is therefore necessary to employ both types of integral equation developed in Sections 2.2 and 2.3 and for H-polarization the appropriate equations are most conveniently expressed in the forms (2.27) and (2.29). The equations for E-polarization are similar and can be obtained using duality. Thus, from (2.27) we have

$$-E^i_z(s) = \frac{1}{2}J^*_1(s) + \frac{1}{4} \int_{C_+} \frac{1}{\eta(s')} J^*_1(s')H_0^{(1)}(kr)d(ds') \quad (2.30)$$

where

$$J^*_1(s) = -(E^+_z + E^-_z) = \eta(s)Z_0(H_{+s} - H_{-s}) \ .$$

On writing

$$J^*_1(s) = -\eta(s)Z_0 J_3(s) \ , \quad (2.31)$$

13

eq. (2.30) becomes

$$Y_0 E_z^i(s) = \frac{1}{2}\eta(s)J_3(s) + \frac{1}{4}\int_{C_+} J_3(s')H_0^{(1)}(kr)d(ks') \qquad (2.32)$$

which is an integral equation for the strength of the equivalent electric current sheet. Similarly, from eq. (2.29),

$$Z_0 H_{+s}^i(s) = -\frac{1}{2\eta(s)}J_4(s) - \lim_{\rho \to C_+}\frac{1}{4k}\frac{1}{\partial n_+}\int_{C_+} J_4(s')(\hat{n}_+'\cdot\hat{r})H_1^{(1)}(kr)d(ks') \qquad (2.33)$$

where

$$J_4(s) = (E_z^+ - E_z^-) = -J_2^*(s) \qquad (2.34)$$

is the strength of the equivalent magnetic current sheet. Equations (2.32) and (2.34) are the required integral equations for E-polarization.

A special instance of a thin sheet is a planar strip (or ribbon), and for this geometry it is of interest to pursue our study of E-polarization a little further. If the strip occupies the portion $0 \le x \le L$ of the plane $y = 0$, where x, y, z are Cartesian coordinates, and is illuminated by a plane wave having

$$\underline{E}^i = \hat{z}\, e^{-ik(x\cos\alpha + y\sin\alpha)}, \qquad (2.35)$$

eq. (2.32) becomes

$$Y_0 e^{-ikx\cos\alpha} = \frac{1}{2}\eta(x)J_3(x) + \frac{1}{4}\int_0^L J_3(x')H_0^{(1)}(k|x-x'|)d(kx') \qquad (2.36)$$

while (2.33) reduces to

14

$$-\sin\alpha \, e^{-ikx\cos\alpha} = -\frac{1}{2\eta(x)} J_4(x) - \lim_{y\to 0} \frac{1}{4k^2} \frac{\partial}{\partial y} \int_0^L J_4(x')$$

$$\cdot \frac{\partial}{\partial y} H_0^{(1)}\left(k\sqrt{(x-x')^2+y^2}\right) d(kx') .$$

$$(2.37)$$

For a plane wave at grazing incidence, $\sin\alpha = 0$, and eq. (2.37) gives $J_4(x) = 0$. We are now left with the single equation (2.36) to solve, and since $E_z^- = E_z^+$, its solution specifies the surface fields on the strip. In this case the impedance strip is equivalent to a resistive one (see Chapter IV).

If $L = \infty$ and $\eta = $ constant, the strip is a uniform "metallic" half plane. The integral equations (2.36) and (2.37) are then identical to eqs. (11) and (12) of Senior (1952) and can be solved analytically using the Wiener-Hopf technique. From the resulting expression for the scattered field, the edge diffraction co-efficient can be determined. This is shown in the next Chapter.

III

EDGE DIFFRACTION BY AN IMPEDANCE HALF PLANE

The diffraction of a plane wave by a half plane at which an impedance boundary condition is imposed has been solved for both normal and oblique (skew) incidence (Senior, 1952, 1960), and even for the general problem of an impedance wedge of arbitrary included angle, solutions are available (Senior, 1959; Maliuzhinets, 1960; Lebedev and Skal'skaya, 1963) for normal incidence. Nevertheless, computed data showing the effect of the impedance on the scattering are very scarce. Senior (1952) presented some patterns for a specific complex value of η and Maliuzhinets (1960) has reported that one of the key functions involved in the solutions has been tabulated, but no reference is given.

The analytical solutions can be used to find the diffraction coefficients associated with the edge. Maliuzhinets' expressions are particularly convenient for this purpose, and from the resulting coefficients for an impedance half plane, Bowman (1967) obtained a high frequency approximation to the backscattered field of an absorbing strip at normal incidence. The predicted values are in good agreement with measured data.

If the half plane is illuminated by an E- or H-polarized plane wave of unit amplitude incident at an angle α in a plane perpendicular to the edge, the corresponding diffracted field at large distances from the edge and viewed in a direction θ away from either of the optical boundaries is

$$\sqrt{\frac{2}{\pi k \rho}} \; e^{i(k\rho - \frac{\pi}{4})} \; P(\alpha, \theta)$$

where (Maliuzhinets, 1960)

$$P(\alpha, \theta) = -\frac{i}{4} \frac{\sin \frac{\alpha}{2}}{\psi(\pi - \alpha)} \left\{ \frac{\psi(-\theta)}{\sin \frac{\theta}{2} + \cos \frac{\alpha}{2}} + \frac{\psi(2\pi - \theta)}{\sin \frac{\theta}{2} - \cos \frac{\alpha}{2}} \right\} \tag{3.1}$$

with

$$\psi(\beta) = \psi_{\pi}(\beta + \pi + \chi)\psi_{\pi}(\beta + \pi - \chi)\psi_{\pi}(\beta - \pi + \chi)\psi_{\pi}(\beta - \pi - \chi) ,$$ (3.2)

$$\psi_{\pi}(\beta) = \exp\left\{ -\frac{1}{8\pi} \int_0^{\beta} \frac{\pi \sin v - 2\sqrt{2}\,\pi \sin\frac{v}{2} + 2v}{\cos v}\, dv \right\} .$$ (3.3)

The angle χ is such that

$$\cos\chi = \begin{cases} 1/\eta & \text{for E-polarization} \\ \eta & \text{for H-polarization} \end{cases} .$$ (3.4)

Many properties and alternative definitions of the function $\psi_{\pi}(\beta)$ are listed by Bowman (1967) in the Appendix to his paper.

The edge diffraction coefficient $P(\alpha, \theta)$ is a function of the angle of incidence α, and the case of edge-on incidence $(\alpha = \pi)$ is of particular interest to us. We first consider backscattering, $\theta = \alpha = \pi$, and then examine the more general case of bistatic scattering.

3.1 Backscattering for Edge-on Incidence

From eq. (3.1) with $\theta = \alpha = \pi$, we have

$$P(\pi, \pi) = -\frac{i}{2}\frac{\psi(\pi)}{\psi(0)}$$ (3.5)

since $\psi(\beta)$ is an even function. As shown by Bowman (1967),

$$\psi_{\pi}(2\pi + \chi)\,\psi_{\pi}(\chi) = \frac{1}{2}\frac{\{\psi_{\pi}(\pi/2)\}^4}{\{\psi_{\pi}(\pi + \chi)\}^2}\left(\cos\frac{\pi}{4} - \sin\frac{\chi}{2}\right)$$

so that

17

$$\psi(\pi) = \frac{1}{8} \cos\chi \; \frac{\left\{ \psi_\pi(\pi/2) \right\}^8}{\left\{ \psi_\pi(\pi+\chi)\psi_\pi(\pi-\chi) \right\}^2} \; ,$$

and since

$$\psi(0) = \left\{ \psi_\pi(\pi+\chi)\psi_\pi(\pi-\chi) \right\}^2 \; ,$$

it follows that

$$P(\pi,\pi) = -\frac{i}{16} \cos\chi \; \frac{\left\{ \psi_\pi(\pi/2) \right\}^8}{\left\{ \psi_\pi(\pi+\chi)\psi_\pi(\pi-\chi) \right\}^4} \; .$$

But

$$\psi_\pi(\pi+\chi)\psi_\pi(\pi-\chi) = \frac{1}{2} \; \frac{\left\{ \psi_\pi(\pi/2) \right\}^4}{\left\{ \psi_\pi(\chi) \right\}^2} \; \left(\cos\frac{\pi}{4} + \cos\frac{\chi}{2} \right)$$

and hence

$$P(\pi,\pi) = -i \; \frac{4\cos\chi}{\left(1 + \sqrt{2}\cos\frac{\chi}{2}\right)^4} \; \left\{ \frac{\psi_\pi(\chi)}{\psi_\pi(\pi/2)} \right\}^8 \; . \tag{3.6}$$

Bowman has derived two alternative forms for $\psi_\pi(\beta)$. From the first of these,

$$\frac{\psi_\pi(\chi)}{\psi_\pi(\pi/2)} = (8\cos\chi)^{-1/8} \left(1 + \sqrt{2}\cos\frac{\chi}{2} \right)^{1/2} \exp\left\{ \frac{1}{4\pi} \int_\chi^{i\infty} \frac{v\,dv}{\cos v} \right\} \; , \tag{3.7}$$

giving

18

$$P(\pi, \pi) = -\frac{i}{2} \exp\left\{ \frac{2}{\pi} \int_\chi^{i\infty} \frac{v\,dv}{\cos v} \right\} \quad , \tag{3.8}$$

whereas from the second

$$\frac{\psi_\pi(\chi)}{\psi_\pi(\pi/2)} = 2^{-1/2} \left(1 + \sqrt{2} \cos \frac{\chi}{2}\right)^{1/2} \exp\left\{ -\frac{1}{8\pi} \int_\chi^{\pi/2} \frac{\pi \sin v - 2v}{\cos v}\,dv \right\} \quad , \tag{3.9}$$

giving

$$P(\pi, \pi) = -\frac{i}{4} \cos\chi \exp\left\{ -\frac{1}{\pi} \int_0^{\pi/2 - \chi} \frac{\pi \cos u - (\pi - 2u)}{\sin u}\,du \right\} \quad . \tag{3.10}$$

Equations (3.8) and (3.10) can be used to obtain analytical approximations to $P(\pi, \pi)$ for small and large $|\eta|$. For this purpose, consider E-polarization for which $\cos\chi = 1/\eta$. If $|\eta| \ll 1$,

$$\frac{1}{\eta} \simeq \frac{1}{2} e^{-i\chi}$$

implying

$$\chi \simeq -i \log \frac{\eta}{2} \quad . \tag{3.11}$$

Likewise

$$\frac{v}{\cos v} \simeq 2v e^{iv}$$

and therefore

$$\int_\chi^{i\infty} \frac{v\,dv}{\cos v} \simeq -2(1 - i\chi)e^{i\chi} \simeq -\eta(1 - \log \frac{\eta}{2})$$

from which we obtain

19

$$P(\pi, \pi) \simeq -\frac{i}{2} \exp\left\{-\frac{2\eta}{\pi}\left(1 - \log\frac{\eta}{2}\right)\right\} \qquad . \tag{3.12}$$

When $\eta = 0$, eq. (3.12) gives

$$P(\pi, \pi) = -\frac{i}{2} \tag{3.13}$$

in agreement with the known result for a perfectly conducting half plane. If, on the other hand, $|\eta| \gg 1$, we have

$$\chi \simeq \frac{\pi}{2} - \frac{1}{\eta} \tag{3.14}$$

and

$$\int_0^{\pi/2 - \chi} \frac{\pi \cos u - (\pi - 2u)}{\sin u} \, du \simeq \frac{2}{\eta} \qquad ,$$

so that

$$P(\pi, \pi) \simeq -\frac{i}{4\eta} \exp\left(-\frac{2}{\pi\eta}\right) \qquad . \tag{3.15}$$

To see how successful the approximations (3.12) and (3.15) are in covering the entire range $0 \le |\eta| \le \infty$, $P(\pi, \pi)$ has been computed for real η by direct numerical evaluation of one of its integral expressions. Since

$$\int_0^{i\infty} \frac{v\, dv}{\cos v} = -2\kappa$$

where $\kappa = 0.9159656\ldots$ is Catalan's constant (Bowman, 1967), eq. (3.8) can be written as

$$P(\pi, \pi) = -\frac{i}{2} \exp\left\{-\frac{2}{\pi}\left(\int_0^{\chi} \frac{v\, dv}{\cos v} - 2\kappa\right)\right\} \qquad . \tag{3.16}$$

20

This integral was evaluated using a 32 point Gauss quadrature formula and Fig. 3-1 shows a plot of the normalized diffraction coefficient

$$\tilde{P}(\pi, \pi) = \frac{P(\pi, \pi)}{P(\pi, \pi)\Big|_{\eta=0}} \tag{3.17}$$

for real η, where $P(\pi, \pi)\Big|_{\eta=0}$ is given in eq. (3.13). Results computed using the approximate formulae are included for comparison and it will be observed that (3.12) and (3.15) cover the entire range of $|\eta|$ with surprising accuracy: even for $|\eta| = 1$ the large and small impedance approximations differ by only 20 percent and are individually in error by no more than about 10 percent. Equations (3.12) and (3.15) are therefore adequate for all practical purposes and these are, of course, not restricted to real values of η.

The corresponding results for H-polarization follow on replacing η by $1/\eta$.

3.2 Bistatic Scattering for Edge-on Incidence

The analysis in this more general case is not dissimilar to the one we have already carried out, although the expressions obtained are more complicated.

From eq. (3.1) with $\alpha = \pi$, the bistatic diffraction coefficient is

$$P(\pi, \theta) = -\frac{i}{4} \frac{\cosec \frac{\theta}{2}}{\psi(0)} \left\{ \psi(-\theta) + \psi(2\pi - \theta) \right\} \tag{3.18}$$

which can be written as

$$P(\pi, \theta) = -\frac{i}{2} \cosec \frac{\theta}{2} \frac{\cos\chi}{\cos\chi + \sin\theta} \frac{\psi(\theta)}{\psi(0)} \tag{3.19}$$

on using the relations (A.14) and (A.15) of Bowman (1967). Using relation (A.13) of the same reference, it can be shown that

$$\frac{\psi(\theta)}{\psi(0)} = \frac{\cos\frac{\chi}{2} + \cos\left(\frac{\pi}{4} + \frac{\theta}{2}\right)}{\cos\frac{\chi}{2} + \cos\left(\frac{\pi}{4} - \frac{\theta}{2}\right)} \left\{ \frac{\psi_\pi(\theta - \pi + \chi)\psi_\pi(\theta - \pi - \chi)}{\psi_\pi(\pi + \chi)\psi_\pi(\pi - \chi)} \right\}^2$$

$$= \frac{4i}{\cos\chi} \frac{\cos\frac{\chi}{2} + \cos\left(\frac{\pi}{4} + \frac{\theta}{2}\right)}{\cos\frac{\chi}{2} + \cos\left(\frac{\pi}{4} - \frac{\theta}{2}\right)} \left(\cos\frac{\chi}{2} + \cos\frac{\pi}{4}\right)^2 \left\{ \frac{\psi_\pi(\theta - \pi + \chi)\psi_\pi(\theta - \pi - \chi)}{\psi_\pi(\chi)\psi_\pi(-\chi)} \right\}^2 P(\pi, \pi)$$
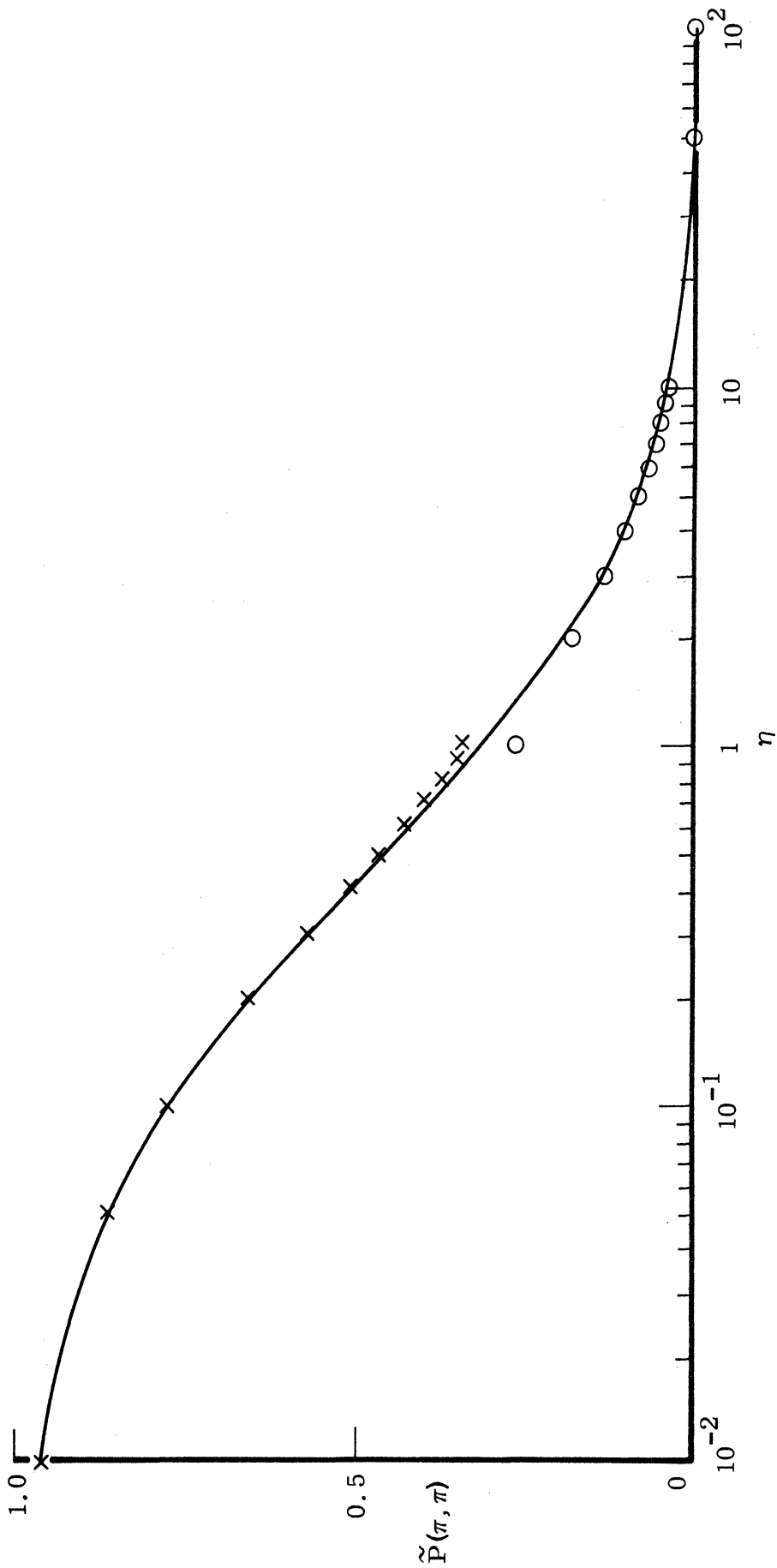
FIG. 3-1: NORMALIZED EDGE DIFFRACTION COEFFICIENT FOR REAL η, E-POLARIZATION: EXACT (———), EQ. (3.16); APPROXIMATE ($\times\times\times$), EQ. (3.12) AND ($\circ\circ\circ$), EQ. (3.15).

and hence

$$\frac{P(\pi, \pi - \delta)}{P(\pi, \pi)} = \sec\frac{\delta}{2} \; \frac{\cos\frac{\chi}{2} + \cos\frac{\pi}{4}}{\cos\frac{\chi}{2} + \cos\left(\frac{\pi}{4} - \frac{\delta}{2}\right)} \; \frac{\cos\frac{\chi}{2} + \cos\frac{\pi}{4}}{\cos\frac{\chi}{2} + \cos\left(\frac{\pi}{4} + \frac{\delta}{2}\right)} \left\{\frac{\psi_\pi(\chi - \delta)\psi_\pi(-\chi - \delta)}{\psi_\pi(\chi)\psi_\pi(-\chi)}\right\}^2$$

(3.20)

where, for brevity, we have written $\delta = \pi - \theta$. As evident from this expression, the bistatic diffraction coefficient is an even function of δ.

From the integral form (3.9),

$$\frac{\psi_\pi(\chi - \delta)}{\psi_\pi(\chi)} = \left(\frac{\cos\frac{\chi - \delta}{2} + \cos\frac{\pi}{4}}{\cos\frac{\chi}{2} + \cos\frac{\pi}{4}}\right)^{1/2} \exp\left\{\frac{1}{8\pi} \int_\chi^{\chi - \delta} \frac{\pi \sin v - 2v}{\cos v}\, dv\right\}$$

and since

$$\left(\int_\chi^{\chi - \delta} + \int_\chi^{\chi + \delta}\right) \frac{\pi \sin v - 2v}{\cos v}\, dv = 2\int_0^\delta \frac{\pi \sin 2u - 4(\chi \sin\chi \sin u + u \cos\chi \cos u)}{\cos 2\chi + \cos 2u}\, du \; ,$$

substitution into eq. (3.20) gives

$$\frac{P(\pi, \pi - \delta)}{P(\pi, \pi)} = \sec\frac{\delta}{2} \exp\left\{\frac{1}{2\pi} \int_0^\delta \frac{\pi \sin 2u - 4(\chi \sin\chi \sin u + u \cos\chi \cos u)}{\cos 2\chi + \cos 2u}\, du\right\} \; .$$

(3.21)

The exponent is a finite range, real-variable integral which converges for all χ and δ, and can be evaluated numerically. The right hand side of eq. (3.21) is unity for $\delta = 0$, as required, but tends to infinity as $\delta \rightarrow \pi$ regardless of χ. This is the forward scatter case in which the direction of observation coincides with the reflected wave and shadow boundaries, and the infinity is attributable to this fact.

Equation (3.21) can be used to obtain analytical approximations to $P(\pi, \pi - \delta)$ for small and large $|\eta|$. If $|\eta| \ll 1$, χ is given approximately by (3.11) and

$$\frac{P(\pi, \pi - \delta)}{P(\pi, \pi)} \simeq \sec \frac{\delta}{2} \exp \left\{ \frac{1}{2\pi} \int_0^{\delta} (-i\chi e^{i\chi} \cos u) du \right\}$$

$$= \sec \frac{\delta}{2} \exp \left\{ -\frac{\eta}{\pi} (1 - \cos \delta) \log \frac{\eta}{2} \right\} \quad .$$

Hence, from (3.12),

$$P(\pi, \pi - \delta) \simeq -\frac{i}{2} \sec \frac{\delta}{2} \exp \left\{ -\frac{\eta}{\pi} \left[2 - (1 + \cos \delta) \log \frac{\eta}{2} \right] \right\} \quad . \tag{3.22}$$

Not surprisingly, this is consistent with eq. (3.12) when $\delta = 0$, and it also reduces to the known bistatic diffraction coefficient for a perfectly conducting half plane when $\eta = 0$. For real η, $P(\pi, \pi - \delta)$ increases monotonically as δ increases from 0 to π.

If $|\eta| \gg 1$, χ can be approximated by the value given in eq. (3.14), but in order to arrive at an expression for the diffraction coefficient it is necessary that

$$|\eta| \cos \frac{\delta}{2} \gg 1 \quad . \tag{3.23}$$

With this restriction,

$$\frac{P(\pi, \pi - \delta)}{P(\pi, \pi)} \simeq \sec \frac{\delta}{2} \exp \left\{ \frac{1}{2} \int_0^{\delta} \left[\tan \frac{u}{2} + \frac{2}{\pi \eta} \left(\frac{u \cos u - \sin u}{\sin^2 u} \right) \right] du \right\}$$

$$= \sec \frac{\delta}{2} \exp \left\{ \frac{1}{\pi \eta} \left(1 - \frac{\delta}{\sin \delta} \right) \right\}$$

and on inserting the expression for $P(\pi, \pi)$ given in eq. (3.15), we have

$$P(\pi, \pi-\delta) \simeq - \frac{1}{4\eta} \sec \frac{\delta}{2} \exp \left\{ - \frac{1}{\pi\eta} \left(1 + \frac{\delta}{\sin \delta} \right) \right\} . \qquad (3.24)$$

This is in agreement with eq. (3.15) when $\delta = 0$ and, consistent with (3.23), remains small as δ increases.

The small and large impedance approximations (3.22) and (3.24) both indicate that $P(\pi, \pi - \delta)$ changes rather slowly as δ increases from zero, and this has been confirmed by a numerical determination of $P(\pi, \pi - \delta)$ using an exact integral expression analogous to that in eq. (3.21).

IV

INTEGRAL EQUATIONS FOR THIN SHEETS

One of the main advantages of the impedance boundary condition is its ability to simulate a variety of surface materials and/or imperfections and to do so in terms of a single parameter only. Unfortunately this generality is also a weakness, and having used the integral equations or some other theoretical approach to arrive at a desirable specification of the surface impedance, it is by no means evident how (or even if) this impedance can be realized in practice.

To avoid the difficulty, it is natural to seek a formulation in which the properties of any surface or coating are included explicitly, both geometrically and electrically. Such a formulation has been considered by Oshiro et al. (1971), who developed the integral equations for the problem of an E-polarized plane wave incident on a metallic cylinder fully or partially clad with a dielectric layer. The geometry and permittivity of the layer are arbitrary, but its permeability is assumed to be that of free space. Since the field scattered by the layer is expressed as a surface integral of the polarization currents, the resulting integral equations are difficult to solve in general, but are amenable to solution in the limiting case of an infinitesimally thin layer. The computer program based on this formulation is designated REST and has proved very helpful in our studies.

Although the problem of a plane wave incident on a resistive sheet in isolation, i.e., without the scatterer present, is of little practical interest in itself, it is instructive to compare it with the problem analyzed in Section 2.4. For this purpose, attention is confined to E-polarization, for which program REST is applicable.

4.1 Electrically Resistive Sheets

Consider a thin sheet of highly conducting material whose permeability μ is that of free space. If σ is the conductivity and Δ is the thickness, we can define a surface resistivity R as

$$R = \frac{1}{\sigma\Delta} = \frac{i}{\omega\epsilon_0\chi_e\Delta} \qquad \text{(ohms)} \qquad\qquad (4.1)$$

where χ_e is the electric susceptibility and ϵ_0 is the permittivity of free space, and as $\Delta \longrightarrow 0$ we can imagine σ to be increased in such a manner that R is finite and non-zero in the limit. The result is an idealized (infinitesimally thin) electric resistive sheet whose electromagnetic properties are specified by the single measurable quantity R.

Mathematically at least, the sheet is simply an electric current sheet whose strength is related to the tangential electric field via the resistivity. Since $\mu = \mu_0$, there is no magnetic current present and

$$\hat{n}\wedge(\underline{E}^+ - \underline{E}^-) = 0 \qquad\qquad (4.2)$$

where the affices $\pm$ refer to the upper (positive) and lower (negative) sides of the sheet and $\hat{n} = \hat{n}_+$ is the outward normal to the upper surface. If $\underline{J}$ is the total electric current flowing in the sheet, i.e., its strength,

$$\hat{n}\wedge(\underline{H}^+ - \underline{H}^-) = \underline{J} \qquad\qquad (4.3)$$

and from the definition of the surface resistivity,

$$\hat{n}\wedge(\hat{n}\wedge\underline{E}^+) = -R\underline{J} \ . \qquad\qquad (4.4)$$

With R specified (it may be a function of position on the sheet), eqs. (4.2) through (4.4) constitute the boundary conditions at the surface.

The field occurring in each of the above equations is the total (incident plus scattered) field, and since $\underline{H}^\pm = \underline{H}^i$ when $\underline{J} = 0$, eq. (4.3) implies for a planar sheet at least,

$$\hat{n}\wedge\underline{H}^\pm = \pm\frac{1}{2}\underline{J} + \hat{n}\wedge\underline{H}^i \ \ .$$

Hence, from (4.4), the surface current density on the upper surface is

$$\underline{K}^+ = \hat{n}\wedge\left\{\underline{H}^i - \hat{n}\wedge\left(\frac{1}{2R}\underline{E}\right)\right\} \qquad\qquad (4.5)$$

and if a surface impedance η is attributable to the sheet, eq. (4.5) suggests that

$$\eta = 2Y_0 R \ .$$
(4.6)

Nevertheless, the problems of a resistive sheet and a sheet at which an impedance boundary condition is enforced are different from one another and, in general, not equivalent. Although there is some similarity between the conditions imposed, an impedance boundary condition specifies a connection between the tangential components of $\underline{E}$ and $\underline{H}$ on each side of the sheet and forces a magnetic current to occur in addition to an electric one. The sheet is therefore a combined electric and magnetic current sheet with the two strengths related via the impedance. In contrast, a resistive sheet supports no magnetic current by virtue of eq. (4.2). Because of this the two problems are basically distinct, and unless the geometry is such that no magnetic current is excited on the impedance boundary condition sheet, it is not possible to relate R and η.

To obtain the integral equations appropriate to a resistive sheet, we consider first the case of E-polarization. If $\underline{E}^i = \hat{z} E_z^i$, then $\underline{J} = \hat{z} J_z$ and the boundary condition (4.4) becomes

$$E_z^{\,+\,-} = R \, J_z$$
(4.7)

where R is the surface resistivity, assumed known. It is a trivial matter to derive an integral equation for the strength J_z of the equivalent electric current sheet, and the vector formulation is (perhaps) even more straightforward than the scalar one. From the definitions (2.19) and (2.20) of the electric and magnetic Hertz vectors describing the scattered field, we have

$$\underline{\Pi}^*(\underline{\rho}) = 0$$
(4.8)

on using (4.2) . Also

$$\underline{\Pi}(\underline{\rho}) = - \frac{Z_0}{4k} \hat{z} \int_C J_z(s')H_0^{(1)}(kr)ds'$$
(4.9)

where the integration is <u>along</u> the sheet (or on <u>one</u> side only), and hence, from (2.18),

$$E_z(\underline{\rho}) = E_z^i(\underline{\rho}) - \frac{Z_0}{4} \int_C J_z(s')H_0^{(1)}(kr)d(ks'). \tag{4.10}$$

If $\underline{\rho}$ is now chosen to lie on the sheet, application of the boundary condition (4.7) gives

$$Y_0 E_z^i(s) = Y_0 R(s)J_z(s) + \frac{1}{4} \int_C J_z(s')H_0^{(1)}(kr)d(ks') , \tag{4.11}$$

which is a rather simple integration equation for the total current $J_z(s)$. Note that consideration of the magnetic field would have produced only an identity for $J_z(s)$. Alternatively, the scalar formulation can be used starting with eq. (2.6) and taking ψ to be the z component of the scattered electric field. The resulting integral equation is identical to (4.11).

From eq. (2.31),

$$J_z(s) = -(H_{+s} - H_{-s}) = J_3(s) \tag{4.12}$$

where $J_3(s)$ is the total current satisfying the integral equation (2.32). Comparison of (4.11) and (2.32) shows them to be identical if R and η are related through eq. (4.6) . With this identification, the electric currents are the same for resistive and impedance boundary condition sheets, but since the latter sheet can also support a magnetic current, the scattered fields will differ in the two cases unless the magnetic current is not excited. A situation where this occurs was noted in Section 2.4 and hence, for a planar sheet at edge-on incidence, a resistive sheet is entirely equivalent to an impedance boundary condition sheet whose surface impedance is given by eq. (4.6) .

This conclusion is important in enabling us to use the analytical information available about the impedance boundary condition sheet in studying the properties of resistive sheets. From the exact analytical solution for a constant impedance half plane, the edge diffraction coefficent can be obtained as shown in the previous chapter. For the particular case of edge-on incidence, this coefficient is also applicable to a resistive sheet for all angles of diffraction provided $\eta = 2Y_0 R$ where R is the surface resistivity in a neighborhood of the edge.

Turning now to H-polarization for which $\underline{H}^i = \hat{z} H_z^i$, the strength of the resulting current sheet is $\underline{J} = \hat{s} J_s$ and the boundary condition (4.4) yields

$$E_s^{\pm} = RJ_s \ . \tag{4.13}$$

For the field scattered by the sheet the magnetic Hertz vector $\underline{\Pi}^*(\rho)$ is again zero, and since

$$\underline{\Pi}(\rho) = - \frac{Z_0}{4k} \int_C \hat{s}' J_s(s') H_0^{(1)}(kr) ds' \ , \tag{4.14}$$

it is a trivial matter to find $E_s^s(\rho)$. When ρ is on the sheet, however, eq. (4.13) implies

$$E_s^s = -E_s^i + R J_s$$

and hence

$$Y_0 E_s^i(s) = Y_0 R(s) J_s(s) + \lim_{\rho \to C} \frac{1}{4k} \frac{\partial}{\partial n} \int_C J_s(s')(\hat{n}' \cdot \hat{r}) H_1^{(1)}(kr) d(ks') \ . \tag{4.15}$$

This is an integral equation from which to determine $J_s(s)$. Unfortunately, it is characterized by the same type of second derivative singularity that we have met before and which is difficult to handle numerically, but in spite of this, eq. (4.15) is the one that must be solved. Indeed, the consideration of the magnetic field scattered by the sheet produces only an identity for $J_s(s)$.

Even for a resistive sheet we are now faced with two integral equations analogous to the ones obtained for an impedance boundary condition sheet, but whereas the latter requires both equations to find the two currents that either an E- or H-polarized wave excites, the resistive sheet needs only a single equation for each polarization. Though one is convenient for numerical solution, the other (for H-polarization) is not. Were we to compare eq. (4.15) with the analogous equation for an impedance boundary condition sheet, we would again find them to be identical if $\eta = 2Y_0 R$.

4.2 Generalized Resistive Sheets

Our attention thus far has been concerned with the concept of an electric resistive sheet whose electromagnetic properties are specified entirely by the surface (electric) resistivity R, but we can also conceive of the electromagnetic dual of such a sheet. This could be simulated using a material having $\epsilon = \epsilon_0$ and high magnetic loss, and we could then define a surface "magnetic resistivity"

$$R^* = \frac{i}{\omega \mu_0 \chi_m \Delta} \qquad \text{(mhos)} \qquad (4.16)$$

analogously to eq. (4.1) , where χ_m is the magnetic susceptibility, μ_0 is the permeability of free space and Δ is the thickness of the layer. If $\chi_m \longrightarrow \infty$ (or, more realistically, $\mathscr{I}m \chi_m$) as $\Delta \longrightarrow 0$ in such a way that the product remains finite, we are then left with an idealized (infinitesimally thin) magnetic resistive sheet whose properties are completely specified by the single measurable quantity R^*.

For a magnetic resistive sheet, the boundary conditions are simply the dual of those in the previous section and are

$$\hat{n}_\Lambda (\underline{H}^+ - \underline{H}^-) = 0 \qquad (4.17)$$

$$\hat{n}_\Lambda (\underline{E}^+ - \underline{E}^-) = -\underline{J}^* \qquad (4.18)$$

$$\hat{n}_\Lambda (n_\Lambda \underline{H}^-) = -R^* \underline{J}^* \qquad (4.19)$$

where the affices $\pm$ again refer to the upper (positive) and lower (negative) sides of the sheet and, say, $\hat{n} = \hat{n}_+$. The sheet supports only a magnetic current $\underline{J}^*$ and, as a result, the tangential components of the magnetic field are continuous across it.

Integral equations from which to compute $\underline{J}^*$ are immediately obtainable from those in Section 4.1 by invoking duality. Thus, for H-polarization, $\underline{H}^i = \hat{z} H_z^i$ and $\underline{J}^* = \hat{z} J_z^*$. Hence, from eq. (4.11),

$$Z_0 H_z^i(s) = Z_0 R^*(s) J_z^*(s) + \frac{1}{4} \int_C J_z^*(s') H_0^{(1)}(kr) d(ks') . \qquad (4.20)$$

Similarly, for E-polarization, $\underline{E}^i = \hat{z} E_z^i$, $\underline{J}^* = \hat{s} J_s^*$ and, from (4.15),

$$Z_0 H_s^i(s) = Z_0 R^*(s) J_s^*(s) + \lim_{\rho \to C} \frac{1}{4k} \frac{\partial}{\partial n} \int_C J_s^*(s')(\hat{n}' \cdot \hat{r}) H_1^{(1)}(kr) d(ks') .$$
$$(4.21)$$

These are analogous to the equations for the magnetic current supported by an impedance boundary condition sheet having surface impedance

$$\eta = Y_0 / (2R^*) , \qquad (4.22)$$

though we remark that the problems of impedance boundary condition and magnetic resistive sheets are completely equivalent only in those cases where an impedance boundary condition sheet supports a single-component current alone. One such situation is a planar sheet at edge-on incidence.

It is now logical to consider a generalized resistive sheet consisting of a superposition of an electric and a magnetic resistive one. With such a sheet, the electric and magnetic currents are produced by the electric and magnetic susceptibilities of the material respectively, and are specified by R and R^* independently of one another. From eqs. (4.2) through (4.4) and (4.17) through (4.19), the electromagnetic boundary conditions at a generalized resistive sheet are

$$\hat{n} \wedge (\underline{H}^+ - \underline{H}^-) = \underline{J} \qquad (4.23)$$

$$\hat{n} \wedge (\underline{E}^+ - \underline{E}^-) = -\underline{J}^* \qquad (4.24)$$

$$\hat{n} \wedge \{\hat{n} \wedge (\underline{E}^+ + \underline{E}^-)\} = -2R\underline{J} \qquad (4.25)$$

$$\hat{n} \wedge \{\hat{n} \wedge (\underline{H}^+ + \underline{H}^-)\} = -2R^*\underline{J}^* \qquad (4.26)$$

where the last two have been deduced from (4.4) and (4.19) by writing these as conditions on the sum fields. This avoids the cross-coupling occurring at each side of the sheet.

The Hertz vectors describing the scattered fields are

$$\underline{\Pi}(\underline{\rho}) = -\frac{\dot{Z}_0}{4k} \int_C \underline{J}(s')H_0^{(1)}(kr)ds' \qquad (4.27)$$

$$\underline{\Pi}^*(\underline{\rho}) = -\frac{\dot{Y}_0}{4k} \int_C \underline{J}^*(s')H_0^{(1)}(kr)ds' \qquad (4.28)$$

from which $\underline{E}^S(\underline{\rho})$ and $\underline{H}^S(\underline{\rho})$ can be computed using the eqs. (2.18). By taking the observation point to lie on the sheet and imposing the boundary conditions (4.15) and (4.16), we then obtain integral equations from which $\underline{J}$ and $\underline{J}^*$ can be computed. Though it is natural to expect that the equations will be coupled, this is not in fact the case.

We shall again confine attention to the principal polarizations and it is actually sufficient to consider E-polarization only. If $\underline{E}^i = \hat{z} E_z^i$, then $\underline{J} = \hat{z} J_z$ and $\underline{J}^* = \hat{s} J_s^*$. From the eqs. (2.18), the fields scattered by the sheet are

$$H_s^S(\underline{\rho}) = -\frac{Y_0}{4k} \frac{\partial}{\partial n} \int_C J_s^*(s')(\hat{n}' \cdot \hat{r})H_1^{(1)}(kr)d(ks')$$

$$-\frac{i}{4} \int_C J_z(s')(\hat{n} \cdot \hat{r})H_1^{(1)}(kr)d(ks') , \qquad (4.29)$$

33

$$E_z^s(\underline{\rho}) = -\frac{Z_0}{4} \int_C J_z(s')H_0^{(1)}(kr)d(ks')$$

$$-\frac{i}{4} \int_C J_s^*(s')(\hat{n}' \cdot \hat{r})H_1^{(1)}(kr)d(ks') . \qquad (4.30)$$

If the observation point $\underline{\rho}$ is now chosen to lie successively on the upper and lower surfaces of the sheet, the resulting fields can be inserted into the boundary conditions

$$H_s^+ + H_s^- = 2R^* J_s^* ,$$

$$(4.31)$$

$$E_z^+ + E_z^- = 2R J_z .$$

Since the contributions of the second integrals in (4.29) and (4.30) cancel, we are left with

$$Z_0 H_s^i(s) = Z_0 R^*(s)J_s^*(s) + \lim_{\underline{\rho} \to C} \frac{1}{4k} \frac{\partial}{\partial n} \int_C J_s^*(s')(\hat{n}' \cdot \hat{r})H_1^{(1)}(kr)d(ks')$$

$$(4.32)$$

$$Y_0 E_z^i(s) = Y_0 R(s)J_z(s) + \frac{1}{4} \int_0^\infty J_z(s')H_0^{(1)}(kr)d(ks') , \qquad (4.33)$$

which are two uncoupled integral equations for J_s^* and J_z. They are identical to the equations (4.21) and (4.11) for individual magnetic and electric resistive sheets, and the scattered fields (4.29) and (4.30) are simply the sums of the fields scattered by the separate sheets. Though a generalized resistive sheet does bear some resemblance to an impedance boundary condition sheet, it should be noted that in the present case $\underline{J}$ and $\underline{J}^*$ are specified independently by R and R^* respectively: the constraint (2.13) or (2.14) which characterizes an impedance boundary condition surface would only exist if $R = 1/(4R^*)$.

An important practical consequence of the above results is that for a generalized resistive sheet it is sufficient to solve only the two integral equations (4.11) and (4.15) for an electric resistive sheet with E- and H-polarizations, respectively. The analogous equations, (4.21) and (4.22), for a magnetic resistive sheet follow by invoking duality; and for a generalized resistive sheet, the integral equations are the same as for a superposition of the two sheets, as are the scattered fields. Of course, we are still faced with the numerical difficulty posed by the second derivative singularity in eq. (4.15), but before turning to this, it is of interest to consider the problem of a generalized resistive sheet in the presence of a body.

4.3 Sheets and Bodies

A resistive sheet is of concern to us because of its potential for reducing the scattering from a body in its vicinity. Until now our studies have been confined to an isolated sheet, and though these have served to pinpoint the types of integral equation which are appropriate, the practically important problem is that of a sheet in the presence of a body. This is the problem that we now address and, as we shall see, the analysis is a rather trivial extension of that which has been done before.

Consider a body whose profile is the (closed) contour C_2 and which has the impedance boundary condition (2.1) or (2.2) imposed at its surface. Somewhere in the vicinity of the body there is a generalized resistive sheet whose profile is the open contour C_1 and which is subject to the boundary conditions (4.23) through (4.26). A plane electromagnetic wave is incident and it is sufficient to assume this to be E-polarized, i.e., $\underline{E}^i = \hat{z} E_z^i$. Hence, $\underline{E} = \hat{z} E_z$ and $\underline{H} = \hat{x} H_x + \hat{y} H_y$, and from the eqs. (4.23) through (4.26),

$$\underline{J} = \hat{z} J_z , \qquad \underline{J}^* = \hat{s} J_s , \qquad (4.34)$$

where $\underline{J}$ and $\underline{J}^*$ are the electric and magnetic currents, respectively, of the equivalent current sheet. The Hertz vectors describing the field scattered by the sheet are therefore

$$\underline{\Pi}^{(1)}(\underline{\rho}) = -\hat{z}\,\frac{Z_0}{4k}\int_{C_1} J_z(s')H_0^{(1)}(kr_{01})ds' \,, \qquad (4.35)$$

$$\underline{\Pi}^{(1)*}(\underline{\rho}) = -\frac{Y_0}{4k}\int_{C_1} \hat{s}'J_s(s')H_0^{(1)}(kr_{01})ds' \,, \qquad (4.36)$$

where $\underline{r}_{0i} = \underline{\rho}-\underline{\rho}_i'$, $i = 1$ or 2.

The body supports surface currents $\underline{K}$ and $\underline{K}^*$ where (see eqs. 2.3 and 2.12)

$$\underline{K} = \hat{z}\,K_z \,, \qquad \underline{K}^* = \hat{s}\,K_s^* \,. \qquad (4.37)$$

Since $K_s^* = -\eta Z_0 K_z$ by virtue of the boundary condition, the Hertz vectors describing the field scattered by the body are

$$\underline{\Pi}^{(2)}(\underline{\rho}) = -\hat{z}\,\frac{Z_0}{4k}\int_{C_2} K_z(s')H_0^{(1)}(kr_{02})ds' \,, \qquad (4.38)$$

$$\underline{\Pi}^{(2)*}(\underline{\rho}) = \frac{1}{4k}\int_{C_2} \hat{s}'\eta(s')K_z(s')H_0^{(1)}(kr_{02})ds' \,. \qquad (4.39)$$

The complete scattered field is given by the eqs. (2.18) with

$$\underline{\Pi} = \underline{\Pi}^{(1)}+\underline{\Pi}^{(2)} \,, \qquad \underline{\Pi}^* = \underline{\Pi}^{(1)*}+\underline{\Pi}^{(2)*} \,,$$

and at an arbitrary point $\underline{\rho}$ in space

36

$$Y_0 E_z(\underline{\rho}) = Y_0 E_z^i(\underline{\rho}) - \frac{1}{4} \int_{C_1} J_z(s')H_0^{(1)}(kr_{01})d(ks')$$

$$- \frac{iY_0}{4} \int_{C_1} J_s^*(s')(\hat{n}' \cdot \hat{r}_{01})H_1^{(1)}(kr_{01})d(ks')$$

$$- \frac{1}{4} \int_{C_2} K_z(s')H_0^{(1)}(kr_{02})d(ks')$$

$$+ \frac{i}{4} \int_{C_2} \eta(s')K_z(s')(\hat{n}' \cdot \hat{r}_{02})H_1^{(1)}(kr_{02})d(ks') \ , \qquad (4.40)$$

$$\underline{H}(\underline{\rho}) = \underline{H}^i(\underline{\rho}) + \left(\hat{x}\frac{\partial}{\partial y} - \hat{y}\frac{\partial}{\partial x}\right)\left[\frac{i}{4k} \int_{C_1} J_z(s')H_0^{(1)}(kr_{01})d(ks')\right.$$

$$- \frac{Y_0}{4k} \int_{C_1} J_s^*(s')(\hat{n}' \cdot \hat{r}_{01})H_1^{(1)}(kr_{01})d(ks')$$

$$+ \frac{i}{4k} \int_{C_2} K_z(s')H_0^{(1)}(kr_{02})d(ks')$$

$$+ \left. \frac{1}{4k} \int_{C_2} \eta(s')K_z(s')(n' \cdot r_{02})H_1^{(1)}(kr_{02})d(ks')\right] \ . \qquad (4.41)$$

We observe that there are three unknown components of the currents, two for the sheet and one on the body, and three integral equations are therefore necessary to determine them.

Let $\underline{\rho}$ approach a point s_1 on the sheet successively from above and below. From the second of the eqs. (4.31) and the fact that

$$\left(\lim_{\rho \to C_{1+}} + \lim_{\rho \to C_{1-}}\right) \int_{C_1} J_s^*(s')(\hat{n}' \cdot \hat{r}_{01})H_1^{(1)}(kr_{01})d(ks') = 0, \qquad (4.42)$$

we have

$$Y_0 E_z^i(s_1) = Y_0 R(s_1)J_z(s_1) + \frac{1}{4}\int_{C_1} J_z(s')H_0^{(1)}(kr_{11})d(ks')$$

$$+ \frac{1}{4}\int_{C_2} K_z(s')H_0^{(1)}(kr_{12})d(ks')$$

$$- \frac{i}{4}\int_{C_2} \eta(s')K_z(s')(\hat{n}' \cdot \hat{r}_{12})H_1^{(1)}(kr_{12})d(ks') \qquad (4.43)$$

where $r_{ij} = \rho_i - \rho_j'$, $i,j = 1$ or 2. Similarly, by considering the magnetic field component $\hat{s}_1 \cdot \underline{H}$ and using the first of the eqs. (4.31),

$$H_s^i(s_1) = R^*(s_1)J_s^*(s_1) + \lim_{\rho \to \rho_1} \frac{Y_0}{4k} \frac{\partial}{\partial n_1} \int_{C_1} J_s^*(s')(\hat{n}' \cdot \hat{r}_{01})H_1^{(1)}(kr_{01})d(ks')$$

$$+ \frac{i}{4}\int_{C_2} K_z(s')(\hat{n}_1 \cdot \hat{r}_{12})H_1^{(1)}(kr_{12})d(ks')$$

$$- \frac{1}{4k}\int_{C_2} \eta(s')K_z(s') \frac{\partial}{\partial n_1}\left\{(\hat{n}' \cdot \hat{r}_{12})H_1^{(1)}(kr_{12})\right\}d(ks').$$

$$(4.44)$$

Equations (4.43) and (4.44) are necessary for the determination of J_z and J_s^*. The first integral on the right hand side of (4.44) has a second derivative singularity of the type referred to earlier. The last integral is similar in form, but the integrand is actually free of singularities if C_1 and C_2 have no point in common, and the differentiation can be carried out explicitly.

38

The third (and last) of the integral equations required is obtained by allowing $\underline{\rho}$ to approach a point s_2 on the body. However, there are two forms that this equation can take. If we consider E_z and use the fact that $E_z = \eta Z_0 K_z$ on C_2, we find

$$Y_0 E_z^i(s_2) = \frac{1}{2} \eta(s_2) K_z(s_2) + \frac{1}{4} \int_{C_2} K_z(s') H_0^{(1)}(kr_{22}) d(ks')$$

$$- \frac{i}{4} \oint_{C_2} \eta(s') K_z(s')(\hat{n}' \cdot \hat{r}_{22}) H_1^{(1)}(kr_{22}) d(ks')$$

$$+ \frac{1}{4} \int_{C_1} J_z(s') H_0^{(1)}(kr_{21}) d(ks')$$

$$+ \frac{iY_0}{4} \int_{C_1} J_s^*(s')(\hat{n}' \cdot \hat{r}_{21}) H_1^{(1)}(kr_{21}) d(ks') \ . \qquad (4.45)$$

Alternatively, from the magnetic field component $\hat{s}_2 \cdot \underline{H}$,

$$H_s^i(s_2) = -\frac{1}{2} K_z(s_2) + \frac{i}{4} \oint_{C_2} K_z(s')(\hat{n}_2 \cdot \hat{r}_{22}) H_1^{(1)}(kr_{22}) d(ks')$$

$$- \lim_{\underline{\rho} \to \underline{\rho}_2} \frac{1}{4k} \frac{\partial}{\partial n_2} \int_{C_2} \eta(s') K_z(s')(\hat{n}' \cdot \hat{r}_{02}) H_1^{(1)}(kr_{02}) d(ks')$$

$$+ \frac{i}{4} \int_{C_1} J_z(s')(\hat{n}_2 \cdot \hat{r}_{21}) H_1^{(1)}(kr_{21}) d(ks')$$

$$+ \frac{Y_0}{4k} \int_{C_1} J_s^*(s') \frac{\partial}{\partial n_2} \left\{ (\hat{n}' \cdot \hat{r}_{21}) H_1^{(1)}(kr_{21}) \right\} d(ks') \ . \qquad (4.46)$$

39

This last equation is similar to (4.44) and the same comments apply. If $J_z(s') = 0 = J_s^*(s')$, i.e., if there is no resistive sheet present, eqs. (4.45) and (4.46) reduce to (2.16) and (2.17), as required.

For the complete problem of a generalized resistive sheet in the presence of a body, the integral equations needed are (4.43), (4.44) and one of (4.45), (4.46). Because of its greater simplicity, (4.45) is the natural one to choose. If the sheet has only an electrical resistivity, so that R^* is infinite, implying $J_s^* = 0$, and if, in addition, the body is perfectly conducting ($\eta = 0$), eqs. (4.43) and (4.45) become

$$Y_0 E_z^i(s_1) = Y_0 R(s_1) J_z(s_1) + \frac{1}{4} \int_{C_1} J_z(s') H_0^{(1)}(kr_{11}) d(ks')$$

$$+ \frac{1}{4} \int_{C_2} K_z(s') H_0^{(1)}(kr_{12}) d(ks') , \qquad (4.47)$$

$$Y_0 E_z^i(s_2) = \frac{1}{4} \int_{C_1} J_z(s') H_0^{(1)}(kr_{21}) d(ks') + \frac{1}{4} \int_{C_2} K_z(s') H_0^{(1)}(kr_{12}) d(ks') ,$$

$$(4.48)$$

and these are the ones used in program REST. However, one of the great advantages of the impedance boundary condition is its preservation of duality, which allows us to deduce the results for H-polarization by applying the following transformation to the E-polarized equations:

$$E_z^i \longrightarrow H_z^i , \qquad H_s^i \longrightarrow -E_s^i , \qquad J_z \longrightarrow J_z^* , \qquad J_s^* \longrightarrow -J_s$$

$$K_z \longrightarrow K_z^* = \eta Z_0 K_s , \qquad R \longleftrightarrow R^* , \qquad \eta \longleftrightarrow 1/\eta , \qquad Y_0 \longleftrightarrow Z_0 .$$

It is therefore sufficient to consider only the three integral equations (4.43), (4.44) and (4.45). Apart from some slight simplifications, these are identical to the equations obtained by Laxpati (1973) using a scalar formulation, and are now

being programmed for numerical solution. Of the three equations, (4.43) and (4.46) are similar in form and rather easy to treat. Indeed, they are not significantly different from those which are employed in programs REST and RAM1D (see Chapter V). Unfortunately, eq. (4.44) is rather difficult to handle because of the "second derivative singularity" which it contains, and an examination of this type of singularity is given in Appendix A.

V

COMPUTED AND EXPERIMENTAL RESULTS

In the process of assembling material for this Interim Report, we found that a great deal of information had been collected since the publication of the previous report (Knott, Liepa and Senior, 1973). The theoretical aspects of a detailed examination of the integral equation formulation have already been presented in Chapters II through IV, but some of the information we had acquired seemed to fit in neither category. We therefore set aside Chapter V as a repository for otherwise unclassifiable topics.

Before presenting the details of these assorted smaller studies, we first review the salient events of the predecessor Contract, and of the present Contract until now, in Section 5.1. The intention is to provide a commentary that bridges the transition between the two and to show why some of the computer programs had to be modified. The review will refresh the memory of the reader who has seen the last report, but will also acquaint the new reader with previous accomplishments. The capability of the impedance boundary condition computer program is assessed in Section 5.2 via comparisons with measured results, and the effect of treating both the leading and trailing edges of an ogival cylinder are discussed in Section 5.3. The effect of sampling rate is taken up in Section 5.4, along with the demonstration that, at least for edge-on incidence, it is the leading edge of the obstacle that dominates the scattering for E-polarized incidence.

5.1 Summary of Previous Efforts

Early in the predecessor Contract we were furnished a computer program (RAM1A) by AFAL, based upon the linearized solutions of integral equations (2.9) and (2.17) derived in Chapter II. RAM1A offered but two options: the solution for a circular cylinder satisfying a (constant) surface impedance boundary condition or the solution for a cylinder of arbitrary shape, but whose profile had to be

specified point-by-point as input data. Since the investigation was to be directed toward non-specular scattering, circular cylinders were of little interest and the feeding of more general profiles into the machine point-by-point was clearly an undesirable task. Moreover, previous experience had shown that the impedance must be variable along the surface in order to permit some measure of control over the far field scattering.

Since our task required more flexibility than was offered by RAM1A, we modified it so as to more fully satisfy the existing needs. The profile-generating subroutine was expanded and it now constructs the body perimeter from a collection of abutting straight line or circular arc segments and assigns variable surface impedances along the profile according to two general mathematical descriptions. A subroutine was also added to the program that prints out "quick-look" plots of the induced surface currents. To distinguish the program from the original it was called RAM1B.

RAM1B was immediately tested for both E- and H-polarizations using a conducting circular cylinder as a test obstacle. The results of these initial test runs duplicated those of the original program, and they also agreed quite well with the exact solution obtained by the method of separation of variables in circular cylindrical coordinates. Satisfied with the capability of RAM1B, we subsequently used it intensively to study methods of reducing traveling wave returns from the trailing edge of an ogival cylinder and the creeping wave contributions from a wedge-cylinder for H-polarization. The results of the study showed that such sources of non-specular scattering can indeed be reduced, but only at the expense of treating a portion of the surface which is a significant fraction of the wavelength (Knott and Senior, 1973; Knott, Liepa and Senior, 1973). Having established favorable surface treatments for this polarization, we turned to E-polarization, for which the leading edges of the bodies become the dominant source.

Preliminary runs of RAM1B were for the bare ogival cylinder so as to

establish reference levels against which to gauge the success of candidate surface treatments. The first test run for the bare body for E-polarization was unacceptable; the surface fields rose to abnormally high levels at the trailing edge and the scattered fields were some 10 dB greater than those observed in experimental work. That the program failed was corroborated by the application of GTD as well, which, at least within 60 degrees of edge-on aspects, agreed with the experimental patterns to within 2 dB. Clearly, something was wrong with RAM1B for E-polarization.

The difficulty had not been resolved by the time the Final Report of the predecessor Contract had been prepared, but a series of tests had been undertaken in an effort to determine if the problem could be circumvented. Reasoning that since the program had worked quite well for the circular cylinder, it must be the sharp edges of the ogival cylinder that gave rise to the problem, so we tried replacing the edges with rounded caps of small radii. Although this ploy tended to destroy the very feature that gives rise to non-specular scattering, it was at once promising: the disagreement between measured and computed results dropped from 10 dB to only 4 dB. Then, reasoning that since the small radii of the caps actually resulted in dense surface sampling near the ends of the cylinder, we reverted back to sharp edges but we clustered the sampling points quite heavily there. Subsequent tests showed that progressively better results were obtainable with progressively heavier sampling but this can be carried only so far; the dense sampling at the edges greatly reduces the number of points available for distribution over the remainder of the body. Although we were able to reduce the disagreement between measured and computed patterns to 2 dB, we were disappointed by the devious means required to do so.

In the meantime we had received another program (RAMC) from AFAL which solved the integral equations (4.47) and (4.48) for a metallic body in the presence of purely resistive sheets for E-polarization. Like RAM1A, RAMC treated a specific geometry, namely a metallic circular cylinder surrounded

44

by a concentric resistive sheet of constant resistivity, and it was too rigid to be used in this form. The program was modified so as to more fully suit our needs and the modification was named REST. Unlike RAMC, REST permits the user to place resistive sheets anywhere (even within the metallic core!) and our first test of REST was for a metallic ogival cylinder with no resistive sheets at all. When compared with experimental patterns, the computed data agreed quite well, but it raised a question: why did REST perform so well while RAM1B did not? The answer is, of course, that REST is based on equations (4.47) and (4.48) for E-polarization while RAM1B is based on equation (2.17), which has the second order singularity in one term.

For the special case of incidence normal to the cylinder axis, equations (2.16) or (2.17) may be used for E-polarization, of course, but for numerical convenience (2.16) obviously has an advantage. In addition, the computer program RAM1B could be greatly simplified since the generation of the matrix elements for both E- and H-polarizations involve identical terms. Thus we put aside program RAM1B and constructed a far more efficient and accurate version. It is called RAMD and a listing of it is given in Appendix B. As will be shown in a moment, RAMD produces satisfactory results for both polarizations, at least within the constraints of the impedance boundary condition.

In summary, we started the predecessor Contract with an impedance boundary condition computer program which was then modified for specific use in non-specular camouflage studies for H-polarization. The present Contract was started with this program on hand, plus another which solved the E-polarized resistive sheet geometry. This second program was also modified for specific use in E-polarization studies. Finally, a streamlined and compressed version of the first program was constructed. We now have available programs REST, for the resistive sheet problem, and RAMD for the impedance boundary condition. As will be pointed out presently, we are in the process of constructing yet a third program that combines the desirable features of both programs, valid for either

polarization. This program will become, we believe, a vital tool in the remainder of our investigation of non-specular camouflage treatments.

5.2 Comparisons of Computed and Measured Results

Programs REST and RAMD solve a two-dimensional problem, of course, whereas laboratory measurements can only be made of finite, three-dimensional obstacles. Thus, in order to compare measured and predicted patterns, one or the other must be scaled by the factor derived in a previous report (Knott, Liepa and Senior, 1973). The relation between two- and three-dimension cross sections is

$$\frac{\sigma_3}{\lambda^2} = 2\left(\frac{L}{\lambda}\right)^2 \frac{\sigma_2}{\lambda} \quad ,$$

where L is the length of the finite cylinder. Measurements were made both by AFAL and the Radiation Laboratory and, since different frequencies and calibration units were used at the two installations, it is convenient to scale the measured patterns down to the two-dimensional system instead of scaling the computed patterns up to the measurements.

The AFAL measurements were made at 7.5 GHz for 18-inch long cylinders; since AFAL routinely presents its data in dB relative to a square meter, 3.79 dB must be added to the patterns in order to obtain the effective two-dimensional results. The Radiation Laboratory measurements were made at 3.0 GHz for a cylinder 35 inches long; since our data are routinely presented in dB relative to a square wavelength, 22.00 dB must be subtracted in order to carry out the comparison with computed results. The Radiation Laboratory patterns were presented in the previous report, but only one comparison was made there with predicted patterns. The AFAL patterns have not yet been published.

Figures 5-1 and 5-2 are comparisons of measured Radiation Laboratory backscattering patterns of a metallic ogival cylinder 3 wavelengths wide for E- and H-polarizations, respectively. Only 90-degree segments of the patterns
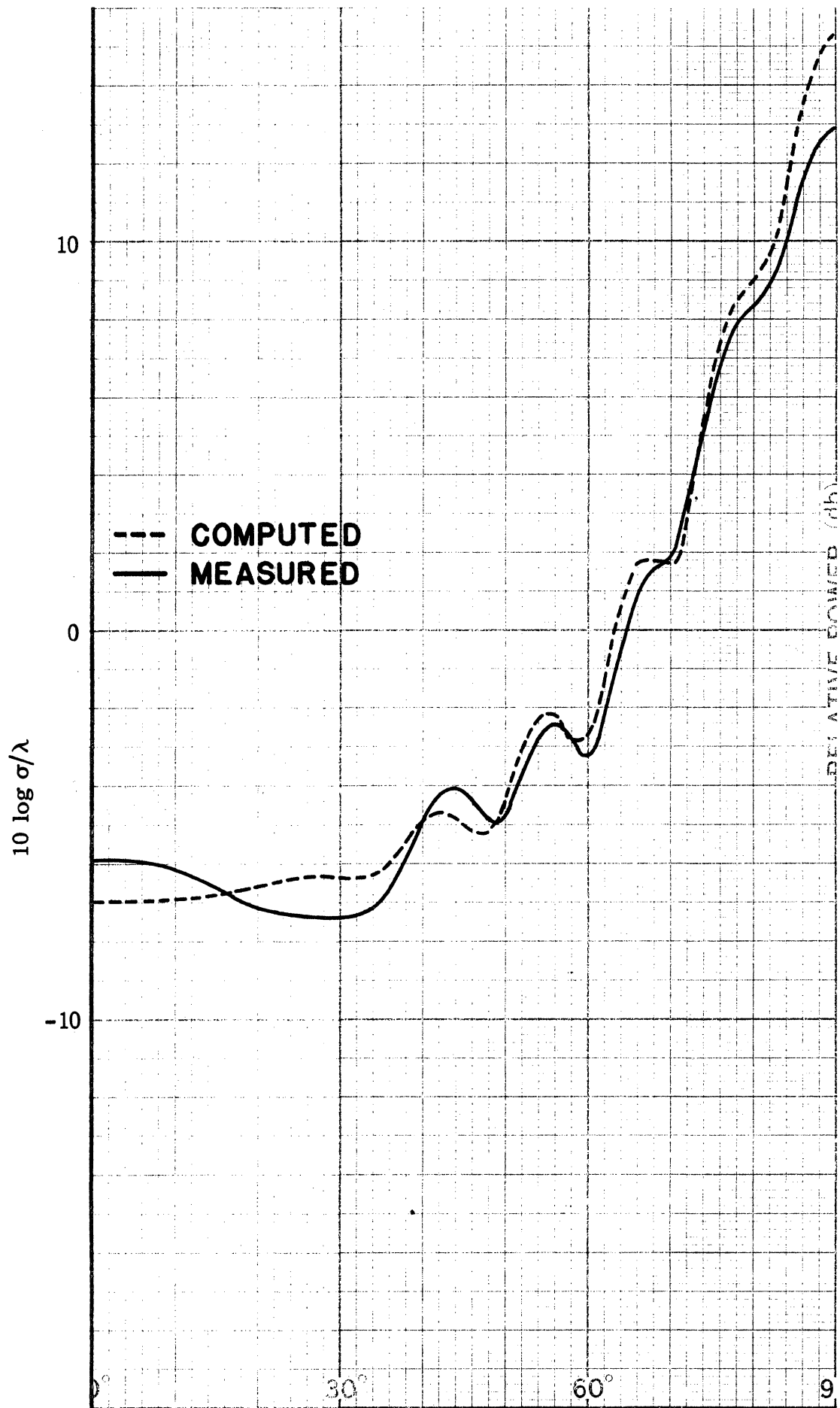
46

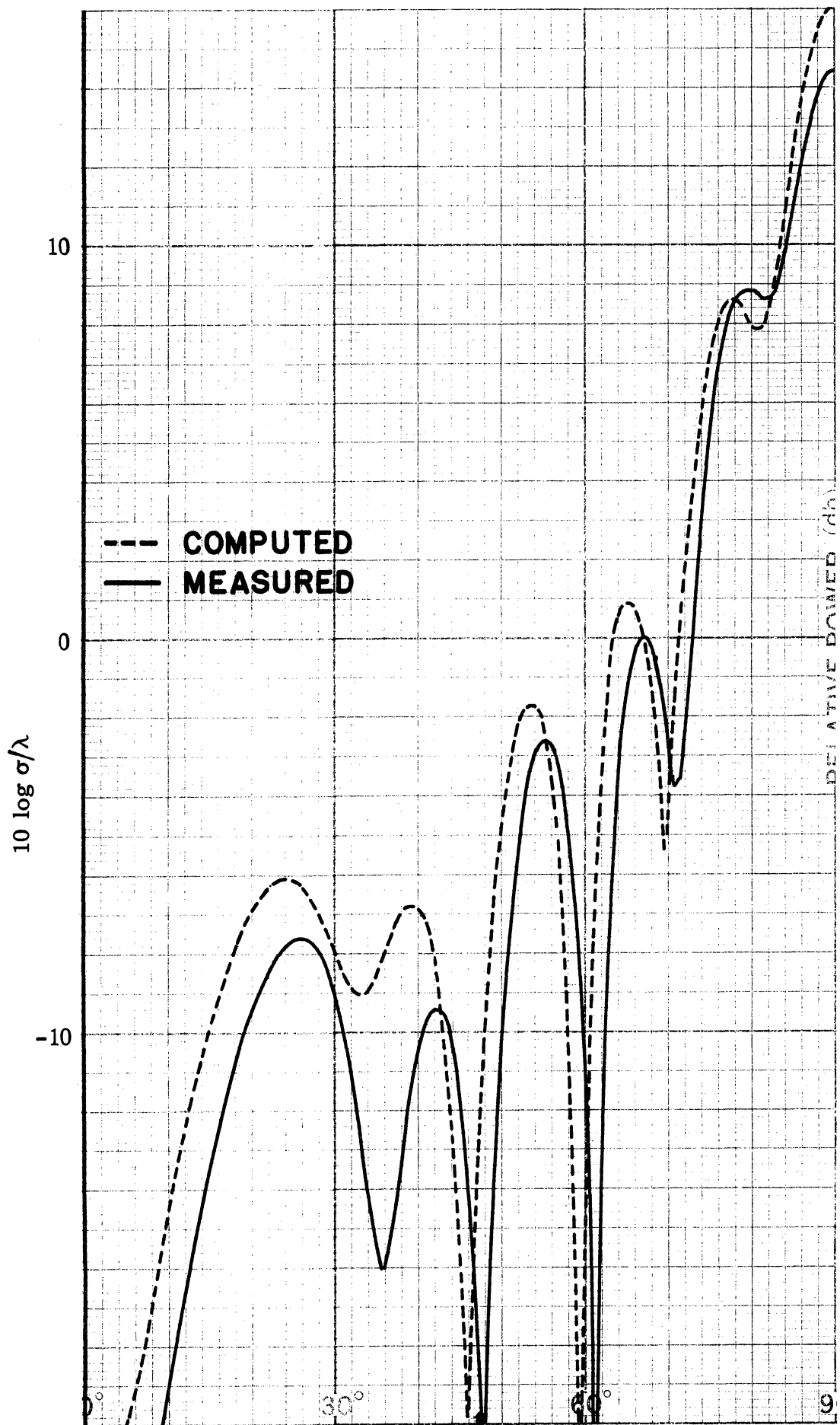FIG. 5-1: BARE OGIVAL CYLINDER, E-POLARIZATION.

FIG. 5-2: BARE OGIVAL CYLINDER, H-POLARIZATION.

48

are presented, and the angular scale runs from edge-on at the left (zero degrees) to broadside incidence at the right (90 degrees). Except for a 1 dB error in the edge-on region and a 2 dB error at broadside, the agreement between measured and predicted patterns for E-polarization (Fig. 5-1) is quite good. And, except for the 4 to 5 dB discrepancy in predicting the null near 35 degrees for H-polarization (Fig. 5-2), the same kind of agreement prevails. It should be noted, however, that the computed H-polarized pattern seems to be shifted 2 degrees toward edge-on incidence. For both polarizations the measured broadside return is less than the computed value, possibly because the target was measured at a range only half of the customary $2L^2/\lambda$.

When the ogival cylinder is covered with a layer of Emerson and Cumming SFT-2.5 absorbing material the agreement is not as good, as may be seen in Figures 5-3 and 5-4. Based upon the measured electromagnetic properties of several samples of this material by AFAL, a constant normalized surface impedance $Z_s = 0.840 + i0.187$ was specified in the computer program input data. This impedance level corresponds to a normal incidence power reflection coefficient of -17.5 dB, and if the computed broadside cross sections in Figures 5-1 and 5-3 are compared, it will be seen that a reduction of 18.7 dB was predicted, reasonably close to that obtained from the measured properties of the material. However, a comparison of the measured and computed patterns of the coated ogival cylinder for E-polarization show no such agreement. In the edge-on region the computed cross sections are of the order of 6 dB greater than the measured values, and at broadside are some 5.5 dB lower. Moreover, such pattern characteristics as lobe structure and null positions are not well produced. The disagreement is not quite so bad for H-polarization (Fig. 5-4), but the measured pattern does not exhibit the deep nulls predicted by the computer program in the broadside aspect angle region. Interestingly enough, the computed broadside cross section reduction is only 16.3 dB (via comparison of Figs. 5-2 and 5-4), and falls short of the normal incidence value by precisely the amount
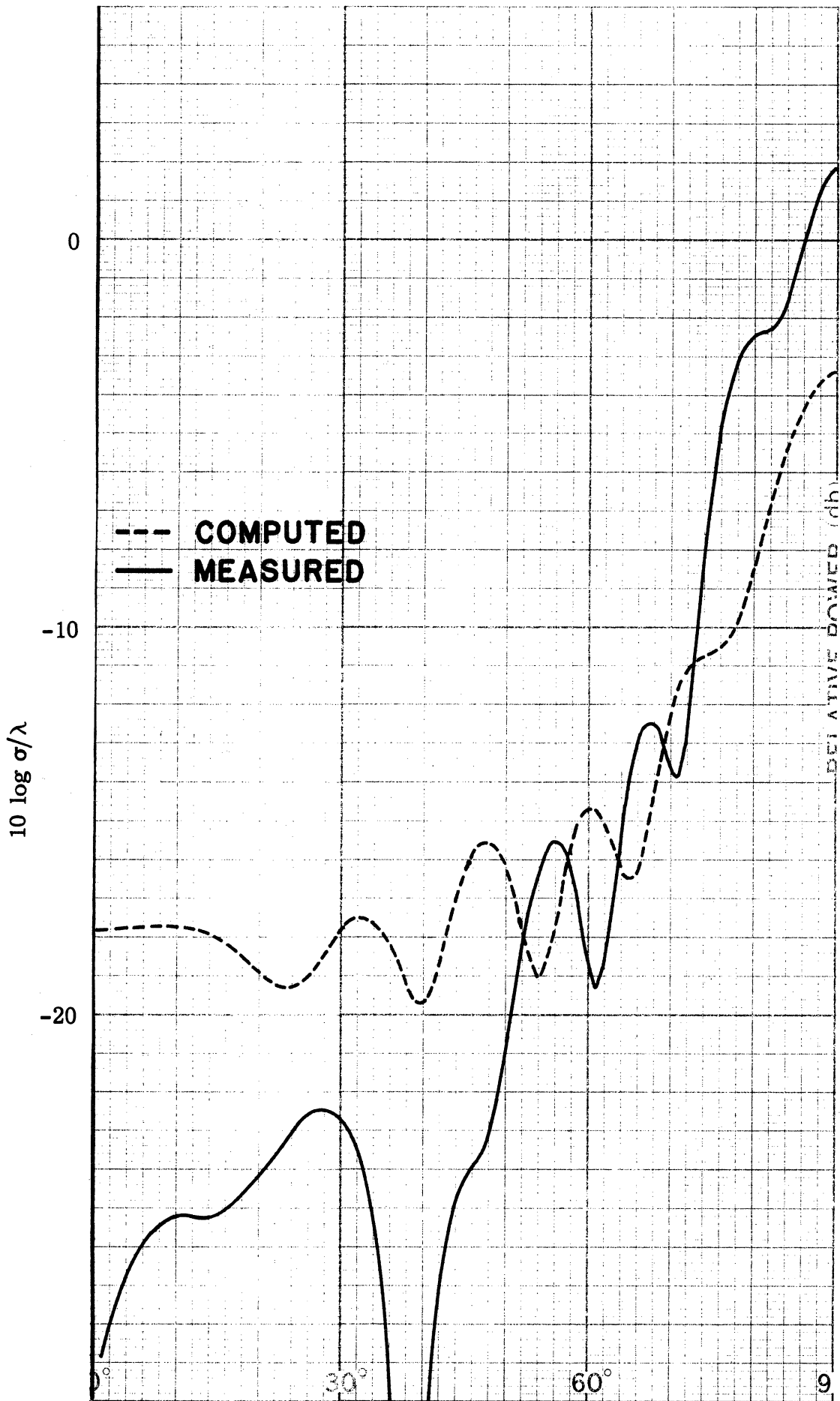
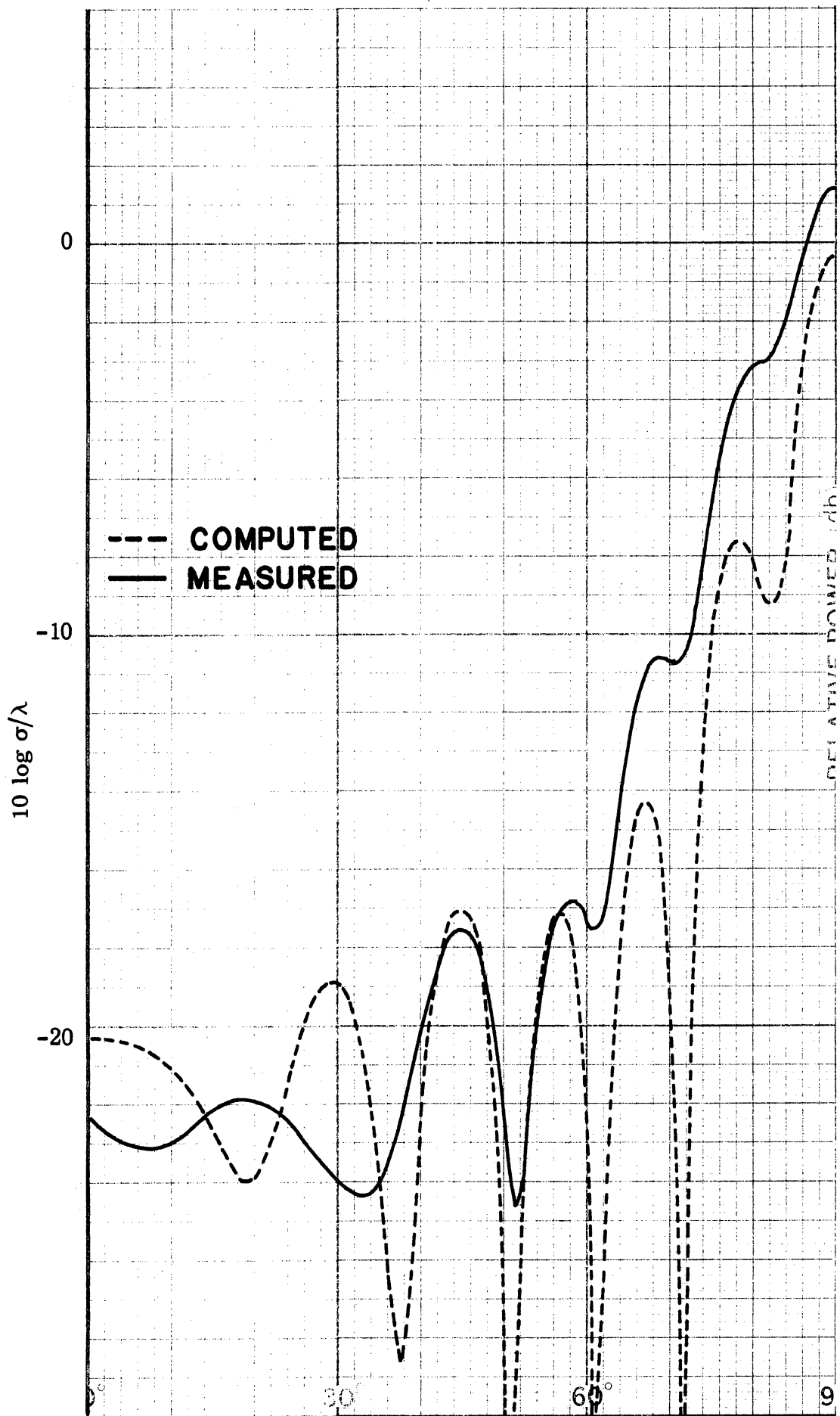FIG. 5-3: COATED OGIVAL CYLINDER, E-POLARIZATION.

FIG. 5-4: COATED OGIVAL CYLINDER, H-POLARIZATION.

51

that the computed E-polarized reduction exceeds it. Nonetheless, we must conclude that even in the presence of possible experimental errors, the back-scattering from the absorber covered ogival cylinder is not well modeled by a constant surface impedance determined by the normal incidence properties of the coating.

Figures 5-5 and 5-6, like Figs. 5-1 and 5-2, are for a metallic ogival cylinder, but in this case the measured patterns were provided by AFAL. The reader will note a change in the amplitude scale on these and the remaining figures, since AFAL uses a 60 dB dynamic range while the Radiation Laboratory uses 40 dB. In both cases the cylinder was 3λ wide and, although the AFAL cylinder was shorter than that measured by the Radiation Laboratory, the difference in length is automatically accounted for by the scaling factor mentioned earlier. The measured pattern for E-polarization (Fig. 5-5) lies below the computed pattern by about 1 dB and were it not for this constant "bias", the fit between the two would be remarkable. The disagreement noted in the Radiation Laboratory data for H-polarization (Fig. 5-2) carries over to the case of the AFAL data in Fig. 5-6, where again it can be seen that the computed pattern seems to be shifted slightly toward the edge-on aspect angle.

Figures 5-7 and 5-8 are for the coated ogival cylinder, but this time the coating was Emerson and Cumming SFT-11.0 material. Based on measurements of the electromagnetic properties of the layer, the normal incidence surface impedance is computed to be $Z_s = 0.471 - i0.400$, and this was the impedance used as input data for program RAMD. Theoretically, at least for normal incidence, the radar cross section should be reduced by 6.97 dB using this impedance, and for E-polarization the computed reduction was in fact 6.9 dB, as judged from a comparison of Figs. 5-5 and 5-7, and for H-polarization 7.4 dB, from Figs. 5-6 and 5-8. The measured E-polarized pattern (Fig. 5-7) is about 1.5 dB greater than the computed one at broadside, and from 1.5 to 2.0 dB lower in the edge-on region, but the agreement is otherwise quite good. For H-polarization
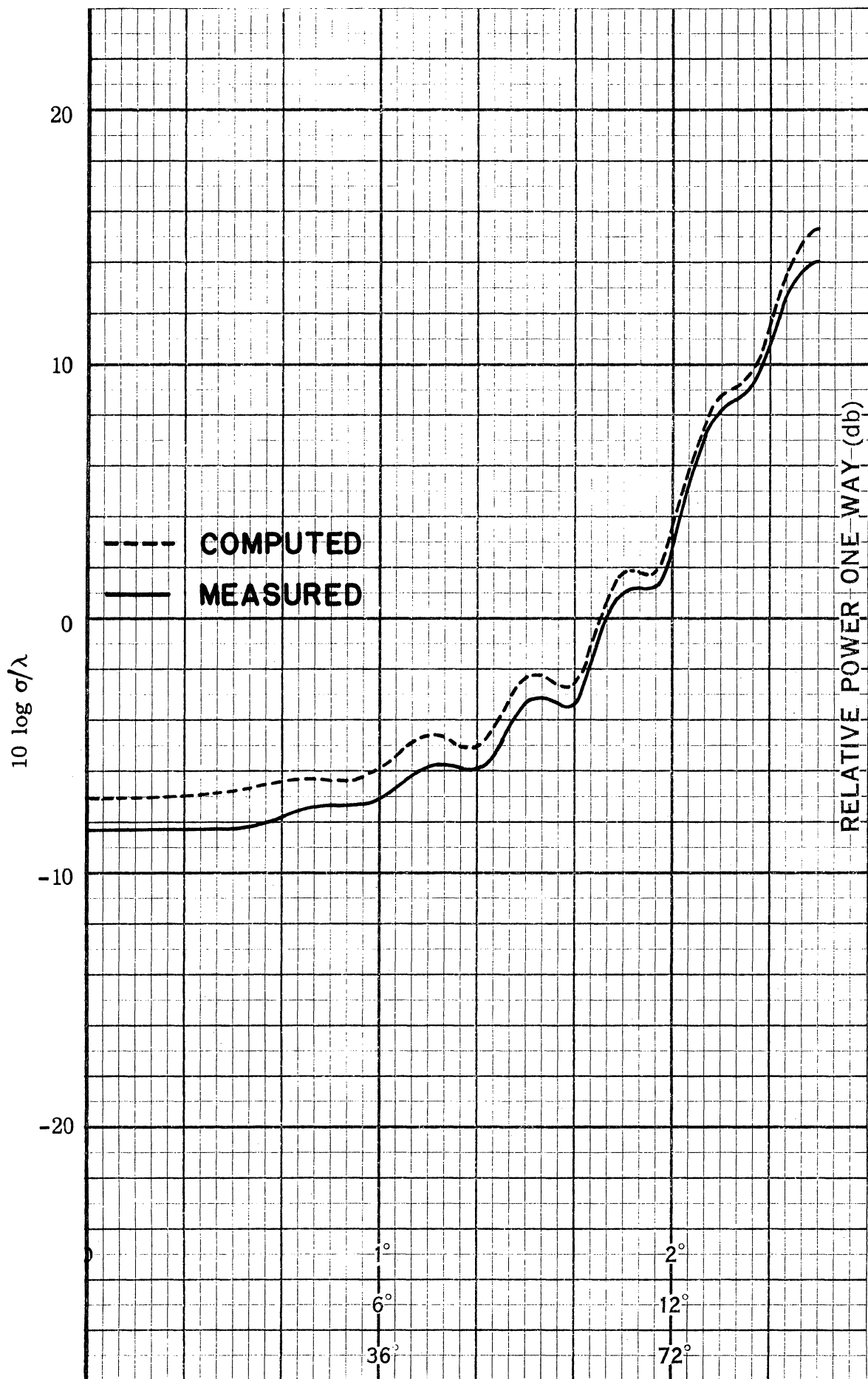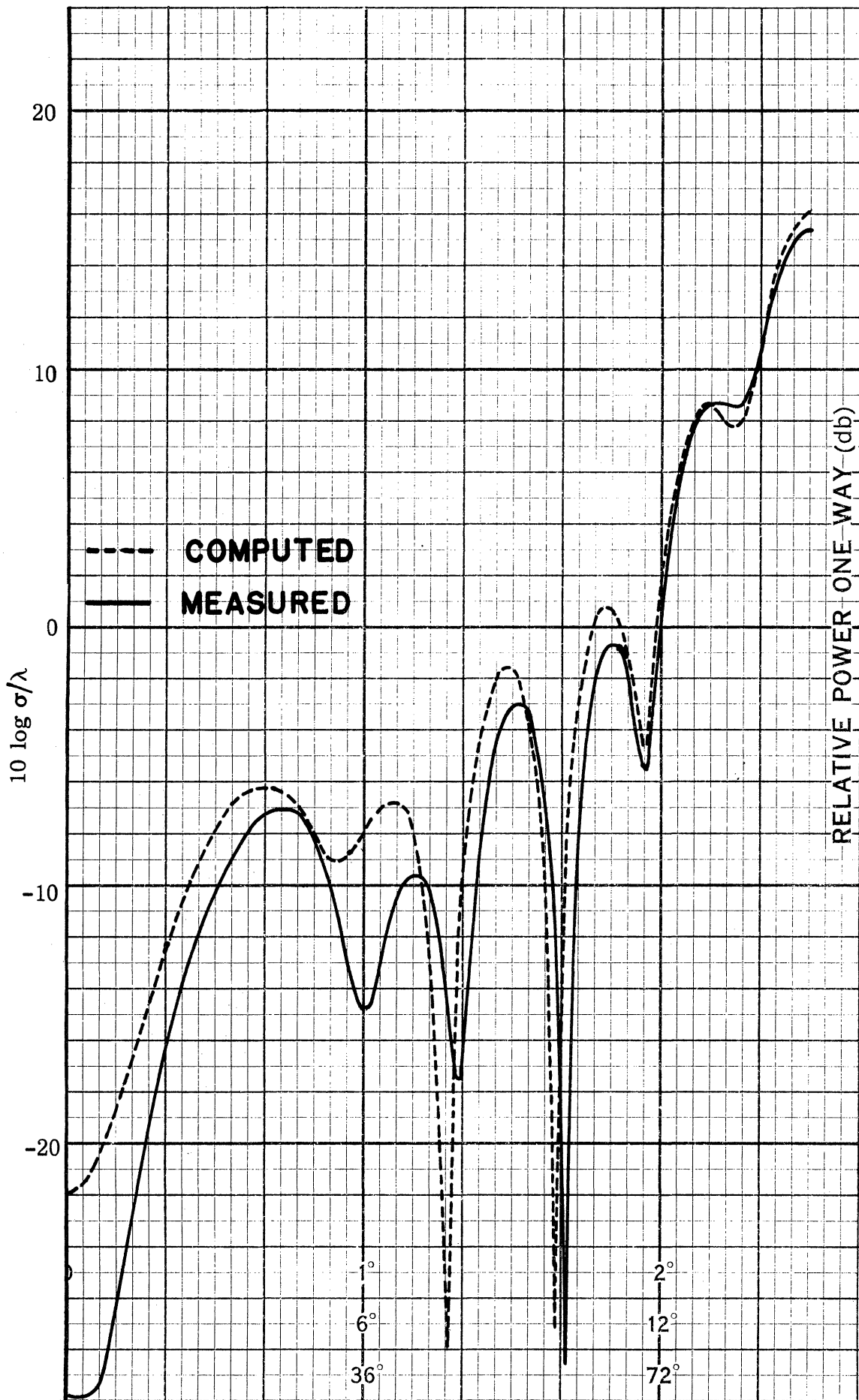
FIG. 5-5: BARE OGIVAL CYLINDER, E-POLARIZATION.
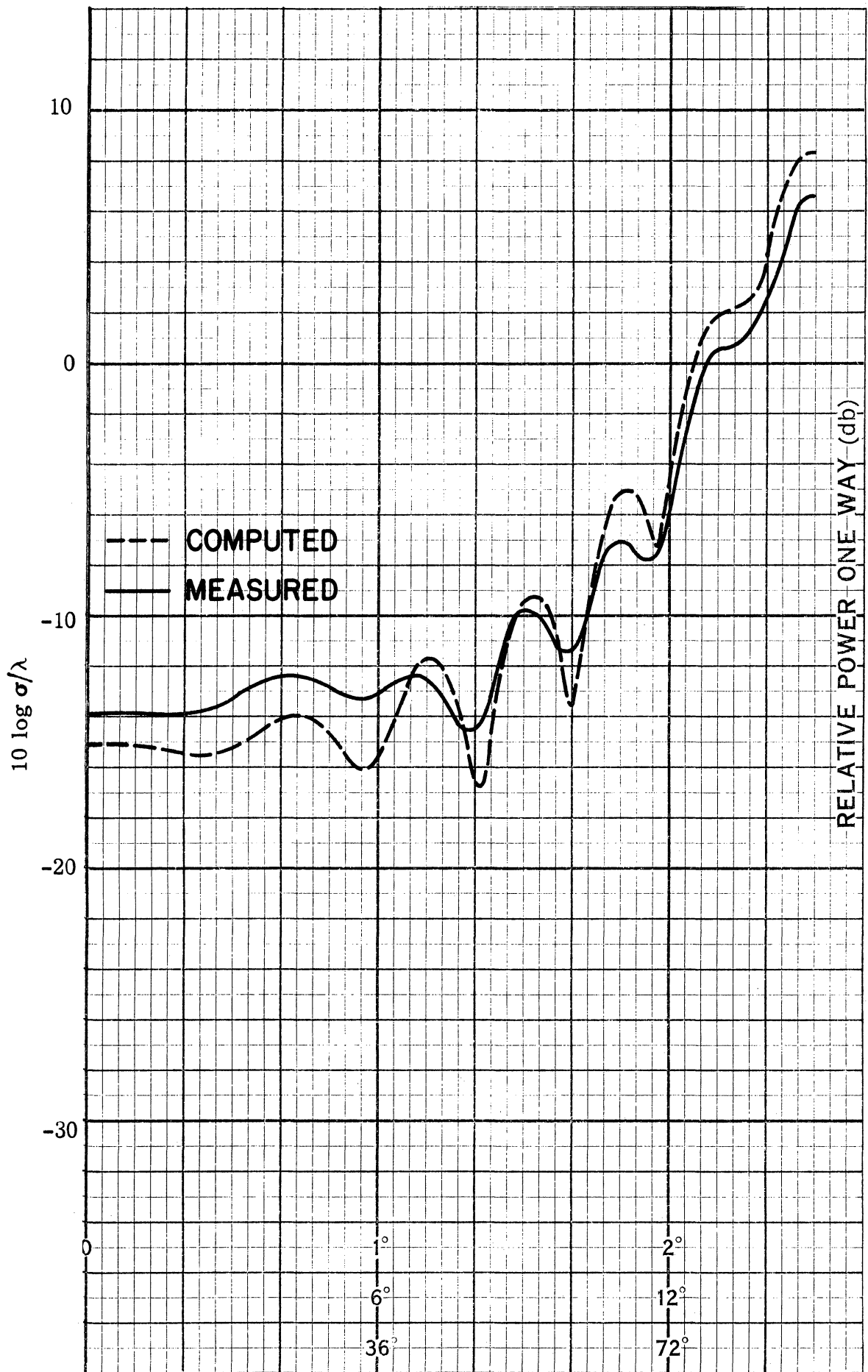
FIG. 5-6: BARE OGIVAL CYLINDER, H-POLARIZATION.

FIG. 5-7: COATED OGIVAL CYLINDER, E-POLARIZATION.

55
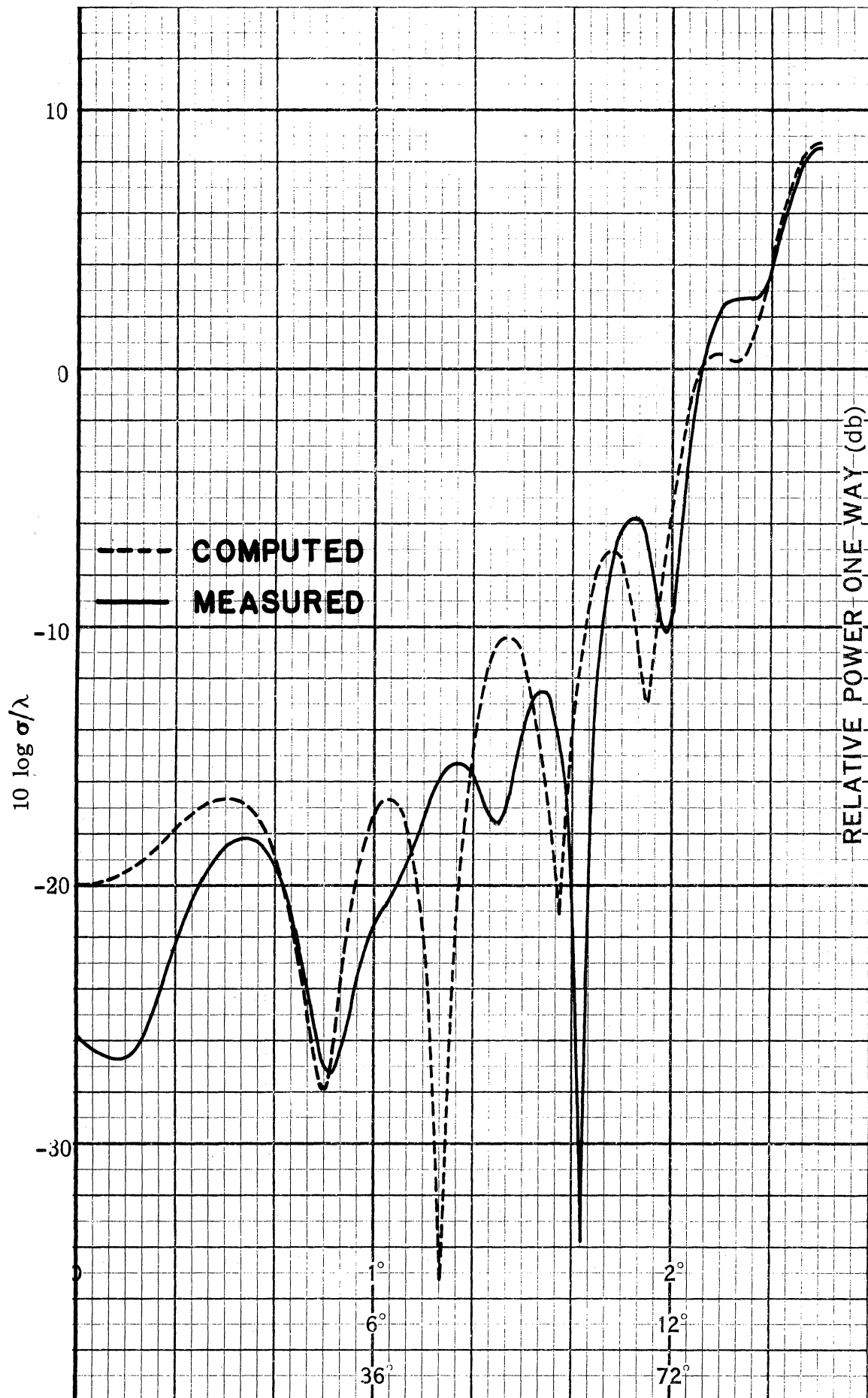
FIG. 5-8: COATED OGIVAL CYLINDER, H-POLARIZATION

56

(Fig. 5-8), the measured and computed patterns nearly coincide at broadside incidence, but there is some disagreement in the details of the lobe structure at edge-on and in the intermediate aspect angle region.

Figures 5-9 and 5-10 are patterns of a metallic wedge cylinder formed by mating a 25-degree (total) angle wedge with a circular cylinder of electrical radius ka = 3.0. The measured pattern for E-polarization (Fig. 5-9), like that of the metallic ogival cylinder, lies about 1.5 dB below the computed one and were it not for this fairly constant difference, the two patterns would be in almost perfect agreement. The agreement for H-polarization (Fig. 5-10) is not quite as good, with some of the computed nulls shifted toward the edge-on incidence side of the pattern and, in particular, with a 6 dB disagreement in amplitude at the edge-on aspect. Note that since the wedge angles of both the wedge-cylinder and the ogival cylinder are the same, the edge-on E-polarized returns of both bodies are the same. Figures 5-1, 5-2, 5-5, 5-6, 5-9 and 5-10 all suggest that the computer program performs quite well for metallic bodies for E-polarization and that, while less accurate, it may still produce acceptable patterns for H-polarization. Some of the differences noted may be due to alignment difficulties and near field effects, and not least, to the neglect of end effects in scaling the three-dimensional patterns down to the two-dimensional computed results.

Figures 5-11 and 5-12 display the wedge-cylinder patterns when the body is coated with the SF-11.0 material mentioned earlier. The agreement for E-polarization (Fig. 5-11) ranges from 1.5 dB at the specular angle to 3 dB or so in the regions of the nulls, and is as good as was noted for the ogival cylinder. The discrepancy for H-polarization (Fig. 5-12) is somewhat greater, about 3 dB, at the specular angle, but rises to as much as 10 dB in the edge-on region. Comparisons of the specular cross sections in these figures show that the computed reduction is 6.1 dB for E-polarization, which is 0.9 dB
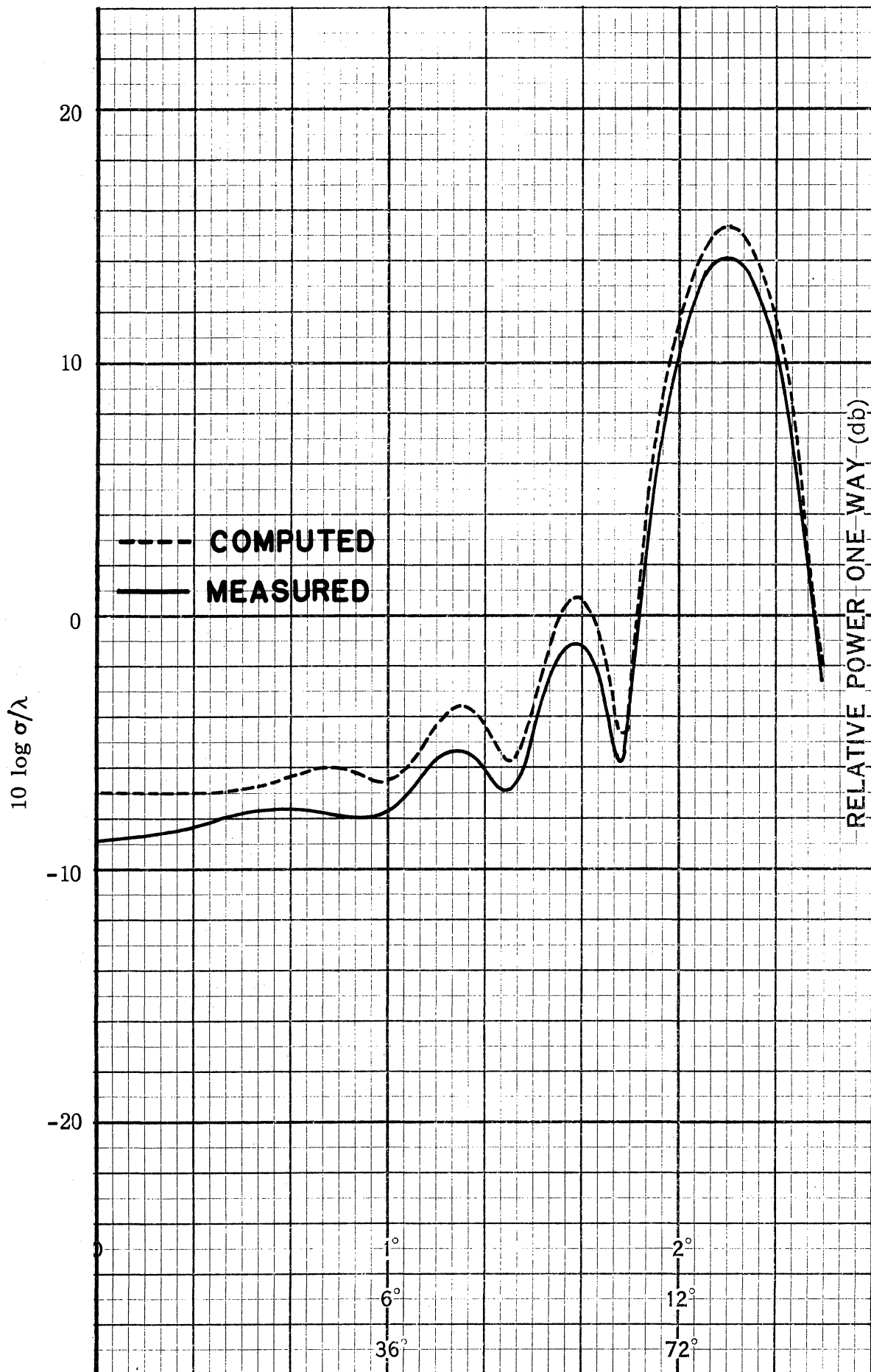
FIG. 5-9: BARE WEDGE CYLINDER, E-POLARIZATION.

58
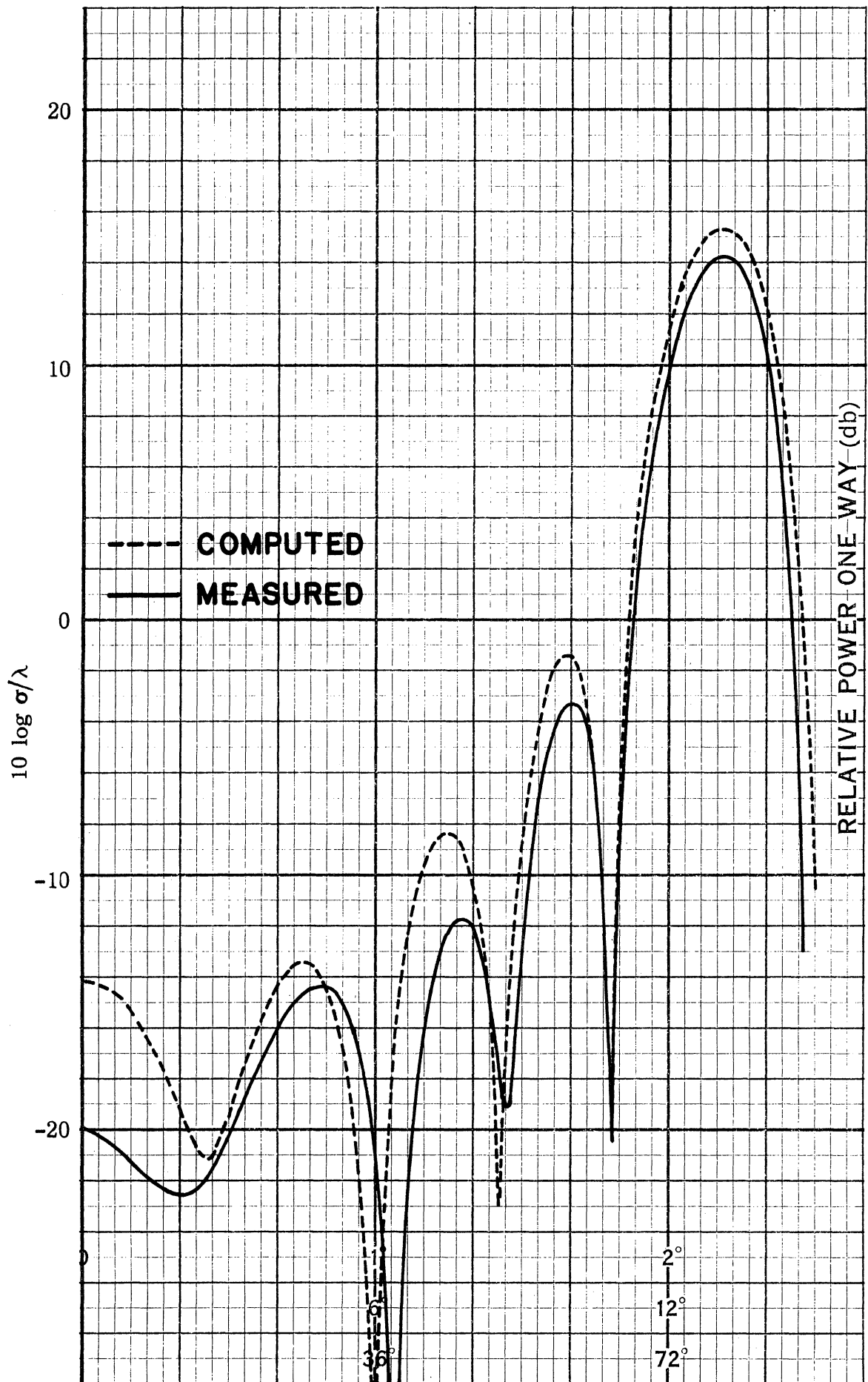
FIG. 5-10: BARE WEDGE CYLINDER; H-POLARIZATION.
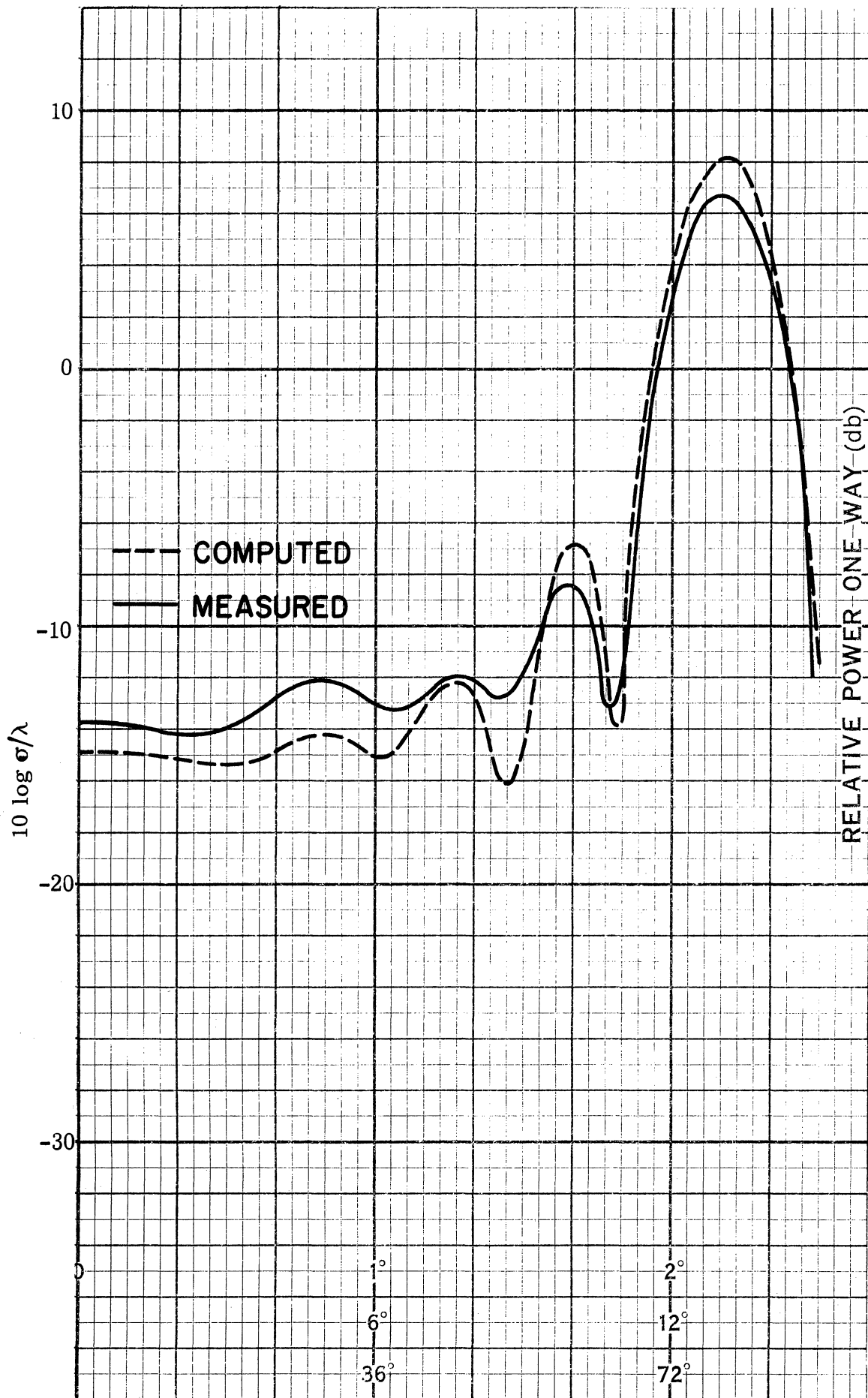
FIG. 5-11: COATED WEDGE CYLINDER, E-POLARIZATION
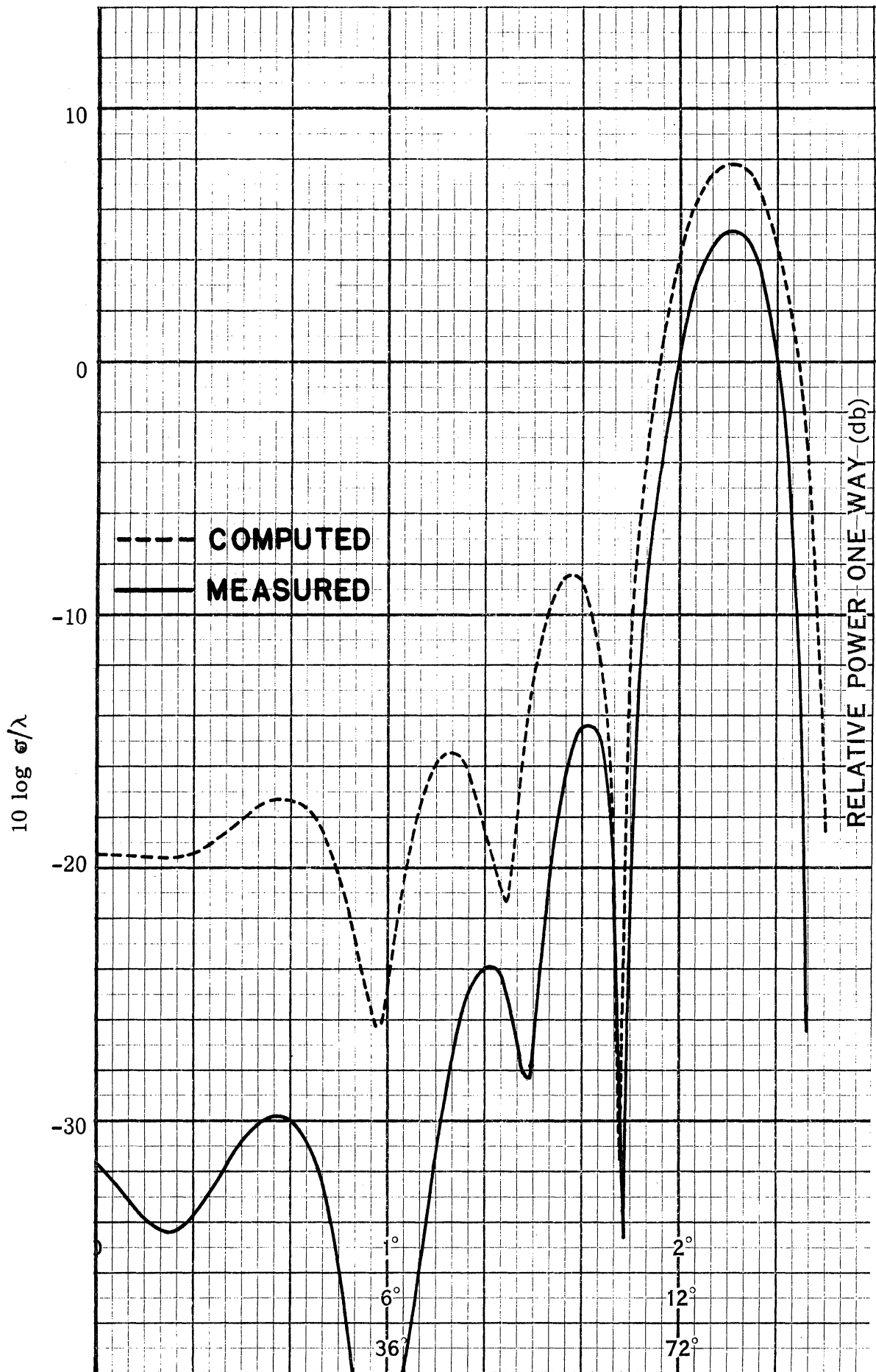
FIG. 5-12: COATED WEDGE CYLINDER, H-POLARIZATION.

61

short of what might be expected for normal incidence as judged from the material properties, and is 7.5 dB for H-polarization, which is 0.5 dB better. The measured cross section reductions considerably exceed the computed ones, however.

The agreement between measured and computed patterns is quite good for metallic bodies, nearly as good for coated bodies for E-polarization, and perhaps disappointing for coated bodies for H-polarization. We believe the errors are traceable, in part, to the shortcomings of the surface impedance boundary condition, which, while conceivably justifiable over smooth surfaces of large radii of curvature for sufficiently lossy materials, is not necessarily valid near edges. From a study of the integral equations presented in Chapter II, one would conclude from that a surface impedance boundary condition tends to interchange the roles of E- and H-polarized scattering sources. Hence the surface impedance would, for example, increase the trailing edge return for E-polarization. If this were truly the case, the design might have to aim for a surface impedance of about unity, since this would be optimum for arbitrary polarizations.

However, the experimental data in Figs. 5-1 through 5-12 show no such inclination. In every case the radar cross section in the edge-on region was reduced; no enhancement took place, as might have been predicted from the duality of the impedance boundary condition integral equations. Therefore the effective surface impedance near the edges was different for the two polarizations, even though the edges were treated with the same physical materials. This is indeed fortunate, for it gives us the kind of control we require: the optimum surface impedance for one polarization is manifestly not optimum for the other. Thus, instead of being disappointed in the lack of agreement between the measured and predicted patterns of these coated objects, we take heart: the disagreement shows that selective control is still available.

5.3 Single and Double Edge Treatment of the Ogival Cylinder

Although it is doubtful that an impedance can be defined near the edges of a coated body on the basis of the normal incidence properties of the coating alone, there is no question that some impedance can be assigned. What is not clear is how we might deduce this impedance from a knowledge of the material properties and the local edge geometry, and indeed, it is via the expansion of program TWOD that we hope to answer the question in the coming months.

The impedance boundary condition integral equations do not in themselves provide the answer. They merely offer the promise of providing a solution to a given scattering problem for whatever particular impedance is selected to represent the relation between the tangential surface fields. Not knowing at present how the H-polarized impedance near an edge is related to the E-polarized impedance there, we shall assume for the time being that they are equal. We now pose the question, how would an optimum treatment for one polarization affect the performance for the other, assuming that the impedance for the two polarizations is the same?

To obtain some idea of the possible degradation in performance, an ogival cylinder was chosen as a test obstacle because the offending source of non-specular scattering shifts from the leading edge to the trailing edge as the polarization is rolled from E to H. We assume that a parabolic (square law) impedance distribution, rising to a terminal value of $Z_s = 2.0 + i\,0$ at the edge, is optimum for H-polarization when 1λ of the trailing edge surface is treated, the constraints of the optimization being due to, say, external considerations such as weight, layer thickness, and the like. Normally, only the trailing edge should be treated, but if the cylinder must also be viewed from the rear, then the leading edge should be included.

Figure 5-13 summarizes the results. As seen on the left side of the diagram, a trailing edge treatment alone (the alternating solid-dashed line) reduces the return by 2 dB at precisely edge-on incidence, but out to about
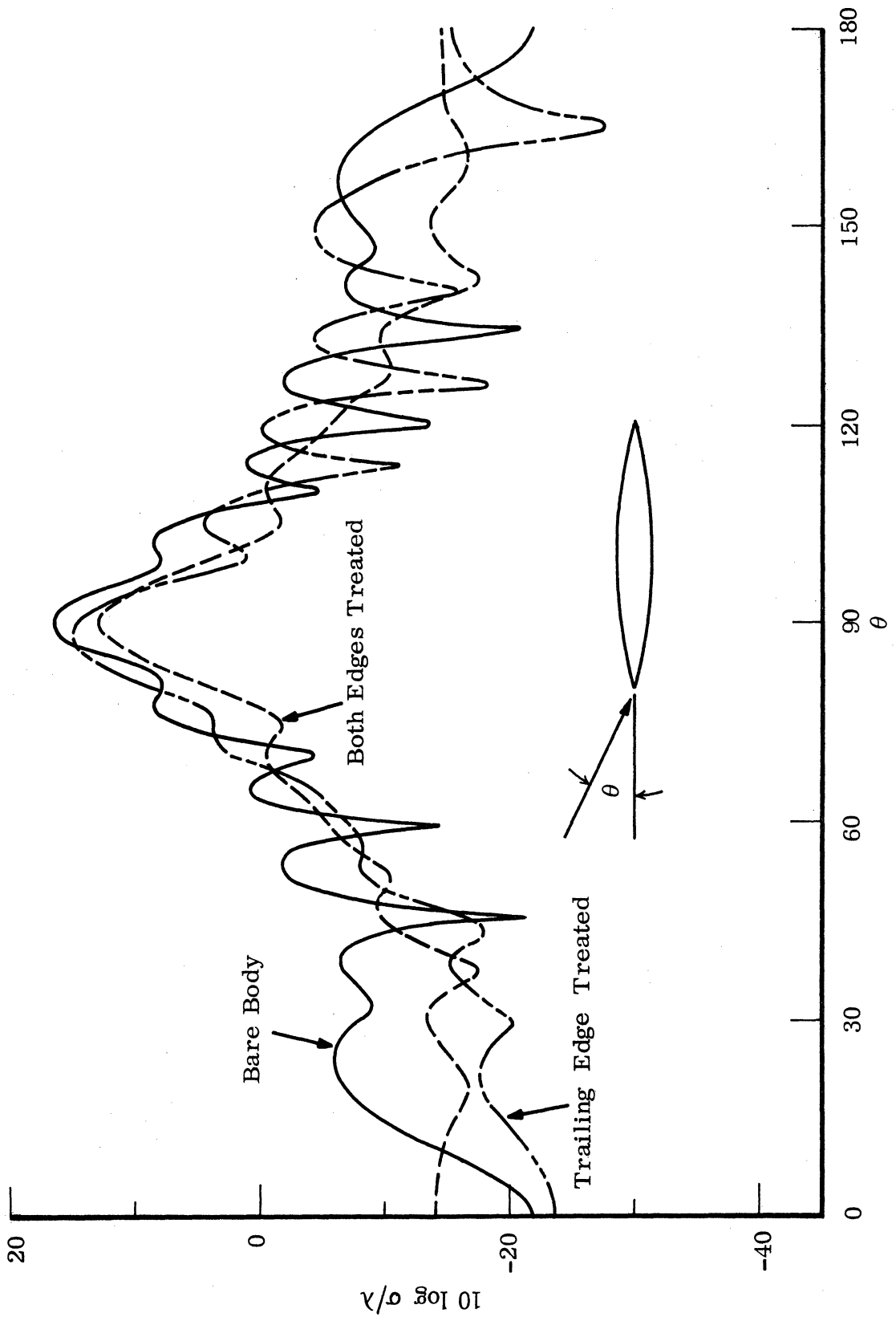
FIG. 5-13: COMPARISON OF SINGLE AND DOUBLE EDGE TREATMENTS FOR H-POLARIZATION USING SURFACE IMPEDANCES.

64

40 degrees an average of 10 dB or so is available. The treated edge becomes a "leading" edge if we shift from the left to the right side of the diagram, and there it can be seen that the cross section is actually enhanced by 5 dB over the bare body level, that a deep null is created at 165 degrees (corresponding to 15 degrees from edge-on), and that the averaged cross section values in the 140 to 180 degree range have not been materially affected. In fact, an envelope sketched through the peaks of the lobes would seem to describe the peak amplitude of the bare body echo as well as that of the body with a single treated edge (when that edge is presented toward the observer). Thus a favorable trailing edge treatment is completely sacrificed if the edge is viewed from the rear.

This being so, it might be expected that treating both edges of the body would be useless, for then a coated edge would be presented to the observer regardless of whether he viewed the cylinder from the front or the rear. Such is not the case, however, as can be seen from the level of the dashed line in Fig. 5-13, representing the effect of a double edged treatment. In the intermediate aspect angle range from 45 to 135 degrees, the double edged treatment smoothes out the peaks and nulls of the bare body pattern, and the averaged cross section levels are scarcely different from those of the metallic objects. But in the edge-on regions, a 7 dB reduction is still available, although there is a substantial enhancement of about 6 dB at precisely edge-on. We conclude that, although a trailing edge treatment offers little benefit if viewed from the wrong direction, a double edged treatment helps to recover the loss in performance. The recovery is not complete, however, and some performance is sacrificed.

This does not seem to carry over to the case of E-polarization, primarily because the trailing edge does not appear to be a source of scattering. As shown in Fig. 5-14, for example, nothing is lost by treating both edges of the cylinder. Aside from a shift in the positions of the peaks and nulls of the pattern, the averaged amplitudes of the scattering from both the single and
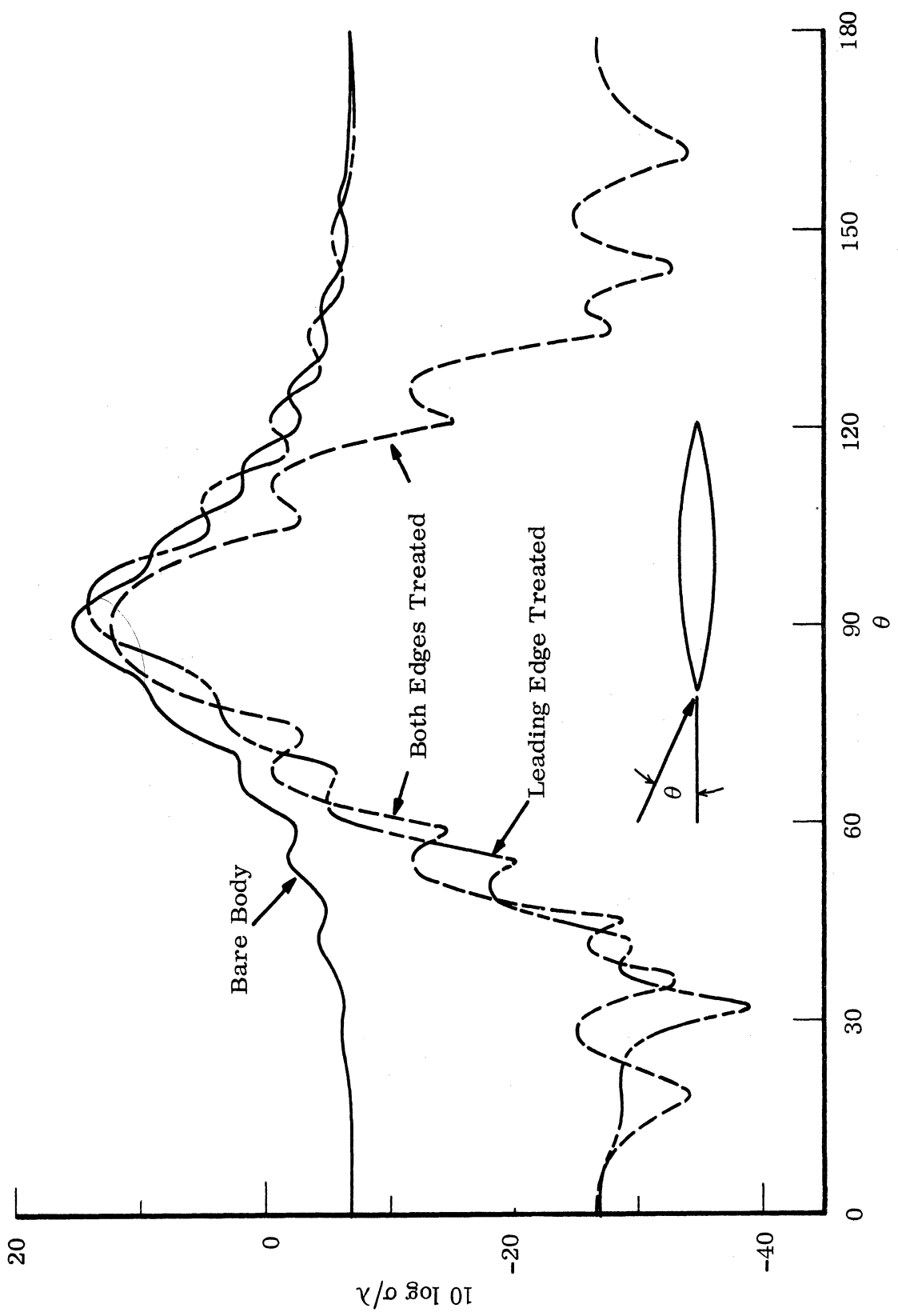
FIG. 5-14: COMPARISON OF SINGLE AND DOUBLE EDGE TREATMENTS FOR E-POLARIZATION USING SURFACE IMPEDANCES.

66

double edged treatments are about the same, but the double edged version does have the virtue of reducing the return in both the forward and backward directions. The cross section reduction available for E-polarization is substantial, amounting to nearly 20 dB within a 40-degree range of edge-on incidence. Thus, at least under the "optimized" conditions specified for this particular case, H-polarization is likely to suffer most from the double edged treatment, with the E-polarized cross section being scarcely of concern.

The above results were obtained using program RAMD and it was of interest to perform the same kind of test using program REST, in which resistive sheets are employed. We chose a sheet 1λ wide having a parabolic resistance variation, with the terminal (outer edge) resistance equal to twice the impedance of free space. Thus the sheet width and the resistance variation were analogous to the surface impedance treatment used in conjunction with RAMD. The results are displayed in Fig. 5-15 and, like those in 5-14, the double edged treatment entails little or no loss in performance compared with that obtained by treating a single edge.

There are two minor differences between the results of the resistive sheet and surface loading methods, however. The first is that the resistive sheet, since it projects outward from the bare body, increases the effective length of the scatterer. Consequently the lobe structure tends to be more detailed and the broadside cross section is slightly greater. For the 1λ sheet width used in the test of Fig. 5-15, this enhancement amounts to about 1.5 dB. The second difference is that the impedance loading method, when extended over a surface distance equal to the sheet width in the above test, offers a slightly better cross section reduction. The improvement amounts to 2 to 4 dB in the end-on region and it persists into the broadside region where the resistive sheet actually produces an enhancement.

As was done under the predecessor Contract for the trailing edge with H-polarization, we also studied the effect of the impedance distribution near the
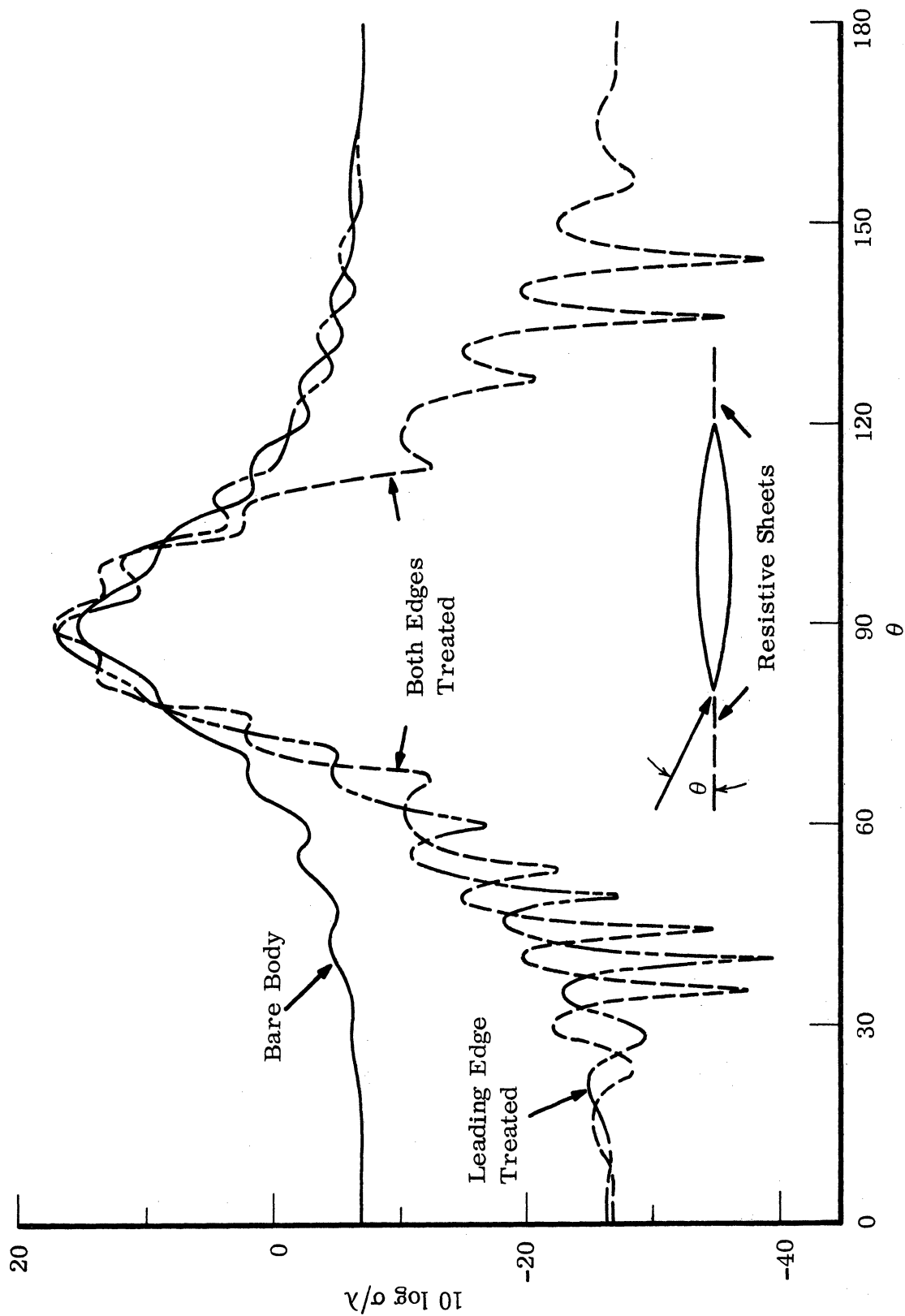
FIG. 5-15: COMPARISON OF SINGLE AND DOUBLE EDGE TREATMENTS FOR E-POLARIZATION USING RESISTIVE SHEETS.

leading edge for E-polarization in the present Contract. The study was not exhaustive, but the results, some of which are shown in Fig. 5-16, suggest that the leading edge treatment is not nearly as difficult to perform for E-polarization as was the trailing edge loading for H-polarization. The angle of incidence was held fixed at 25 degrees from edge-on (as in the H-polarized studies previously mentioned) and two types of distributions were imposed. The length of the treated surface ranged from 0.5λ to 1.5λ, the latter covering half the body.

The four curves plotted in Fig. 5-16 are typical of all the data collected for this case. As the figure shows, slightly less performance is obtained for shorter surface loadings, and it seems to matter little whether a linear or a parabolic distribution is employed. The maximum impedance used in the study was $Z_s = 2.0 + i0$ (at the leading edge) but the curves seem to be continuing downward monotonically. They suggest that the scattering does indeed arise from the edge itself and that the loading might be compressible into a narrow strip of surface near the edge if the impedance can be taken to a high enough level. A cross section reduction of 13 dB is apparently attainable if the leading edge impedance is as low as 1.3 times that of free space. The form of the curves is much like that provided by resistive sheets placed in front of the cylinder.

5.4 Reducing the Number of Sampling Points

The expansion of program TWOD to include magnetic was well as dielectric properties of physical materials, for H-polarization as well as E, will produce a useful tool for our task. The program will be based upon the integral equations for thin layers, but it is not inconceivable that relatively thick coatings may have to be studied, or even coatings whose thicknesses are variable. Hence it may be necessary to synthesize such coatings by stacking up several thin layers. This amounts to sampling in volume instead of area and, unless the total number of sampling points is increased, it will require that the points be
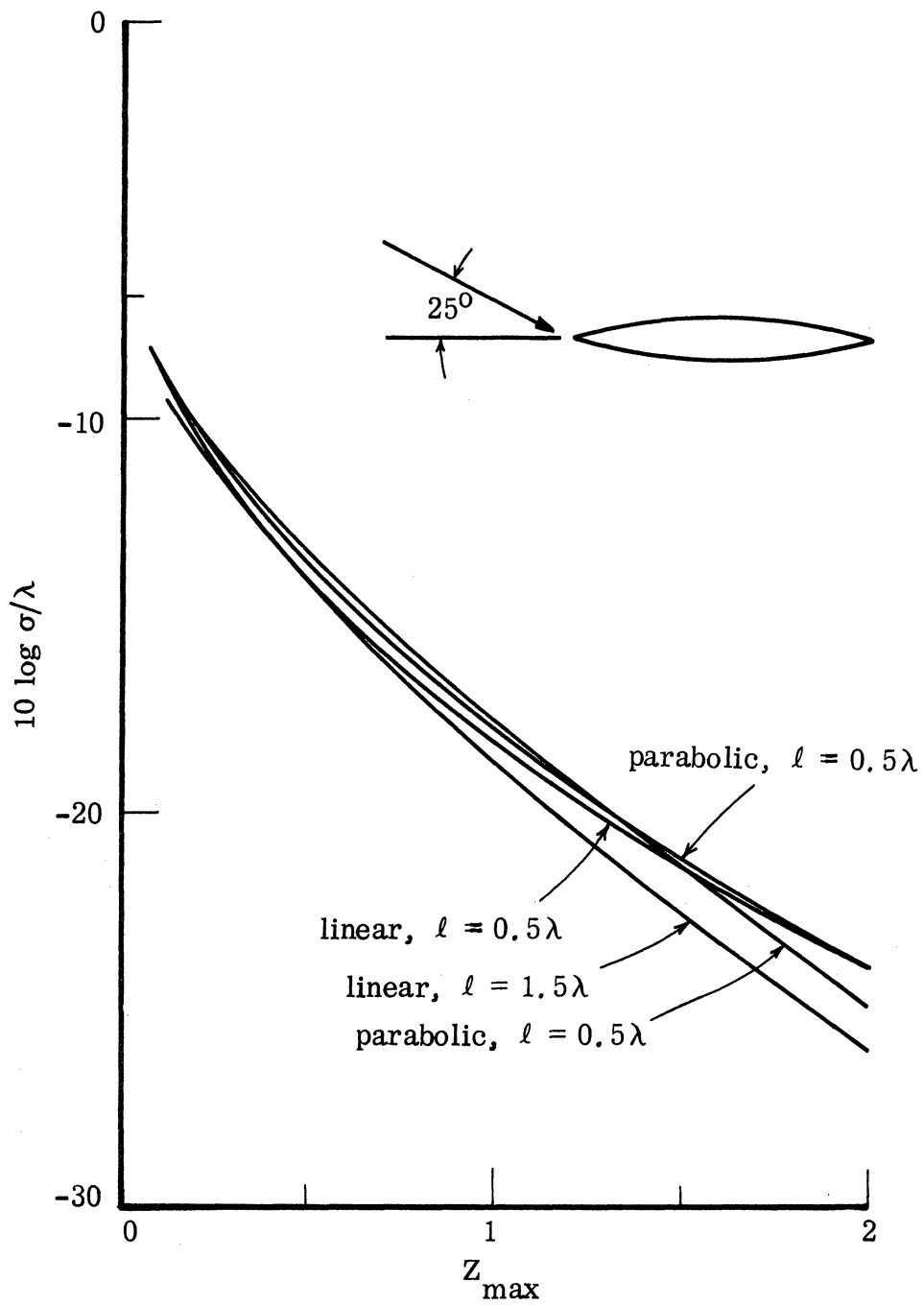
FIG. 5-16: LEADING EDGE TREATMENTS ON THE OGIVAL
CYLINDER USING THE IMPEDANCE BOUNDARY
CONDITION.

70

redistributed. Some parts of the body will therefore be sampled less densely than others, and we ran a sequence of tests to establish how the computed far fields might be affected by sparse sampling.

Again the ogival cylinder was chosen as a test obstacle and program REST was used to compute the backscattering. No resistive sheets were deployed, hence the patterns produced were of the bare body. The total number of sampling points on the profile was increased in steps of six from a minimum of 24 to a maximum of 100, producing nominal surface sampling rates from 4 to $16\frac{2}{3}$ per wavelength. Assuming that the highest sampling rate produces "perfect" results, the errors produced by less frequent sampling can be estimated by comparing the computed backscattering patterns. This comparison is shown in Fig. 5-17 for a selection of 5 sampling rates.

The errors are greatest in the intermediate aspect angle range and are smaller at both the edge-on and broadside aspects. Expectedly, the error increases with decreasing sampling rates. From the data displayed, one finds that 10 samples per wavelength yield 0.5 dB accuracy for the entire aspect angle range, but if only edge-on incidence is of interest, as few as 6 samples per wavelength will suffice. Figure 5-18 is a plot of the errors incurred at three discrete aspect angles, one of the angles ($\theta = 58$ degrees) being that at which the error is greatest. It should be emphasized that these plots are for a bare ogival cylinder and that the behavior depicted may not necessarily apply to other bodies or, indeed, to the same body when coated.

If it is only the leading edge that dominates the far field scattering, as is true for E-polarization, it may be possible to use a small wedge-cylinder, as suggested in Fig. 5-19. In this case, the sampling rate was held fixed at about 16 samples per wavelength, and the electrical size of the body was varied from $ka = 0.625$ to $ka = 3.0$. The number of sampling points ranged from 20 to 96, yet the edge-on return varied by less than 0.3 dB throughout the range. These data suggest that a great number of sampling points may be released for other
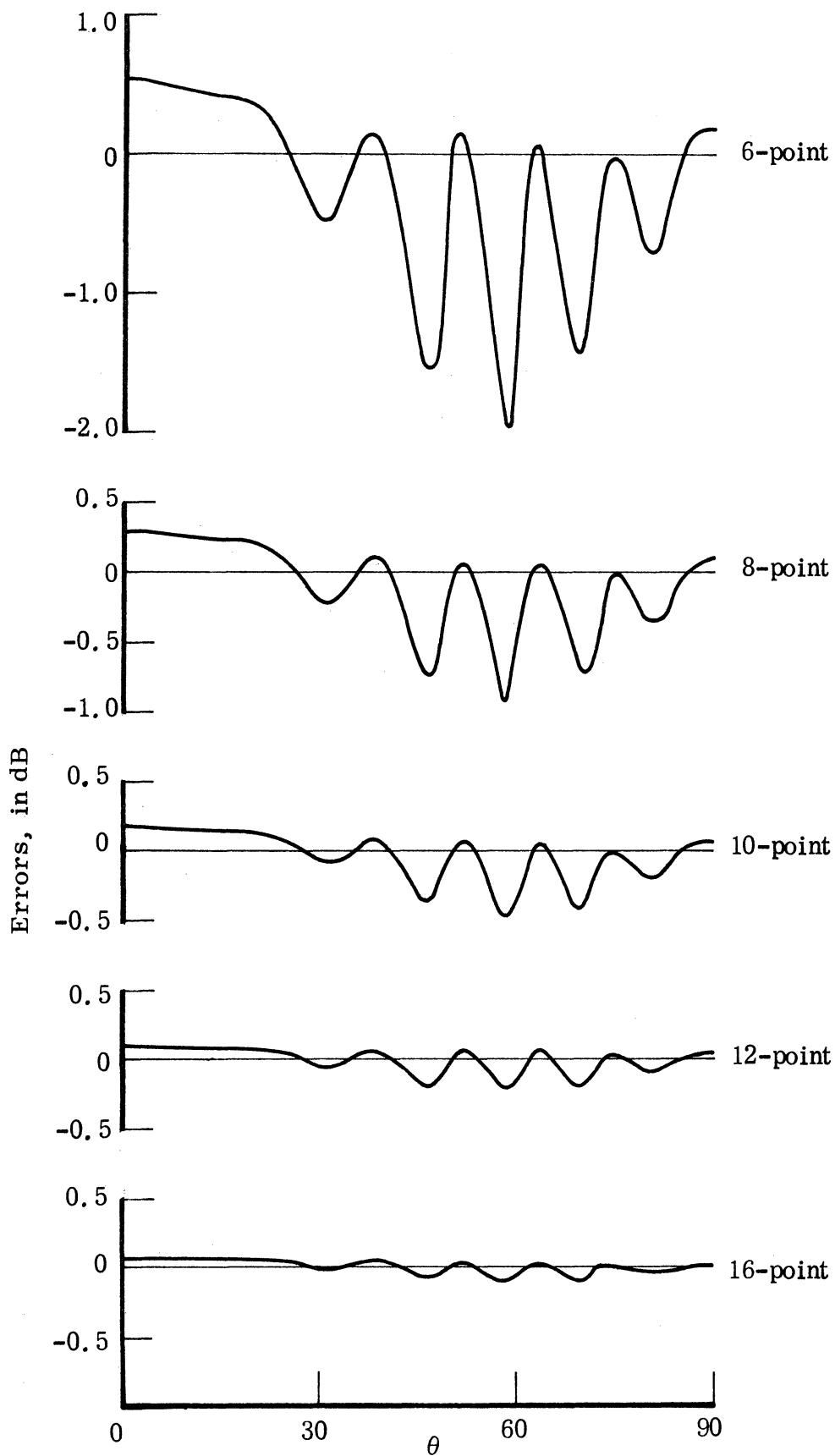
FIG. 5-17: ERRORS IN COMPUTED FAR FIELD PATTERN OF AN
OGIVAL CYLINDER AS A FUNCTION OF ASPECT
ANGLE.

72
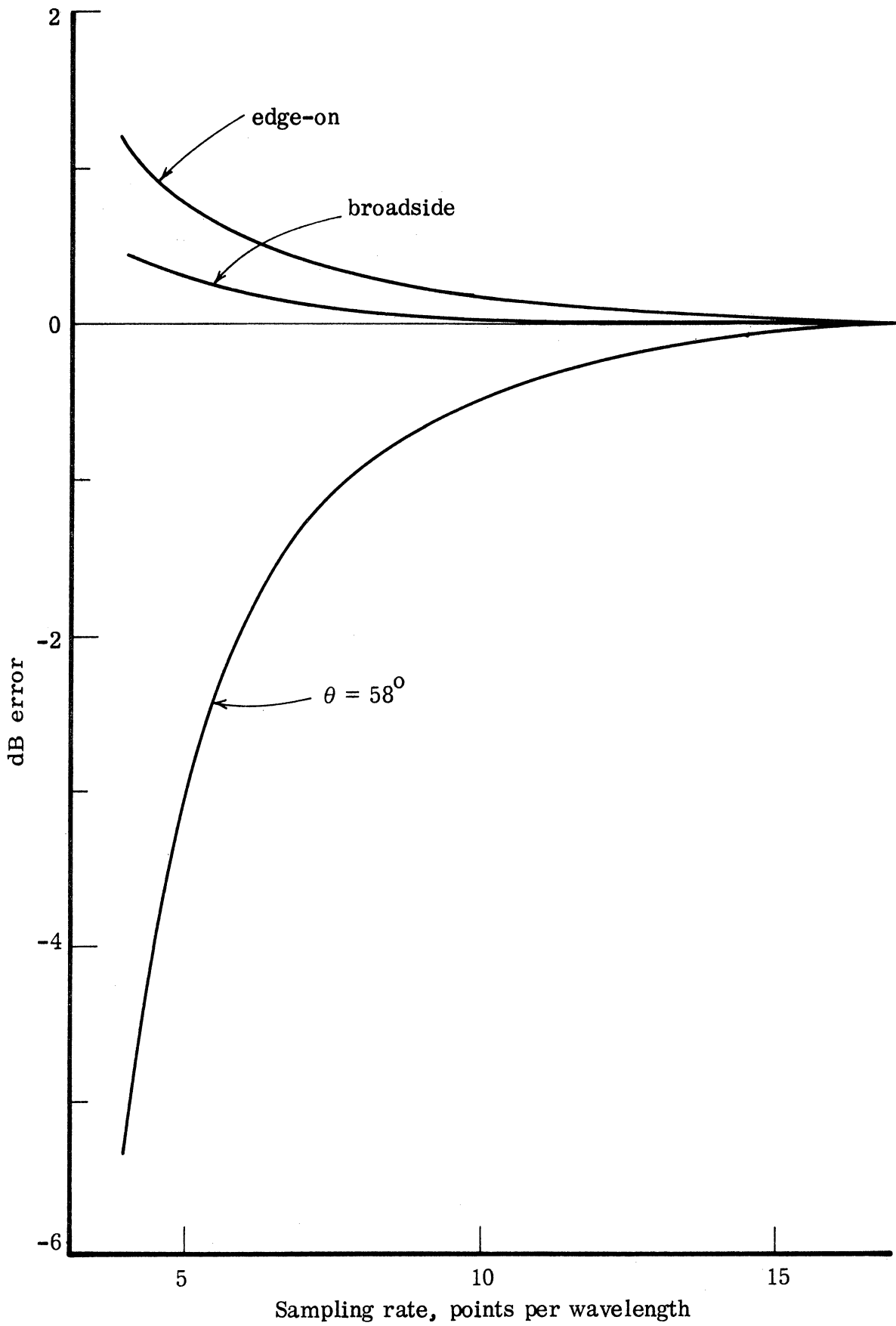
FIG. 5-18: ERRORS IN COMPUTED BACKSCATTERING PATTERN OF AN
OGIVAL CYLINDER AS A FUNCTION OF SAMPLING RATE.

73
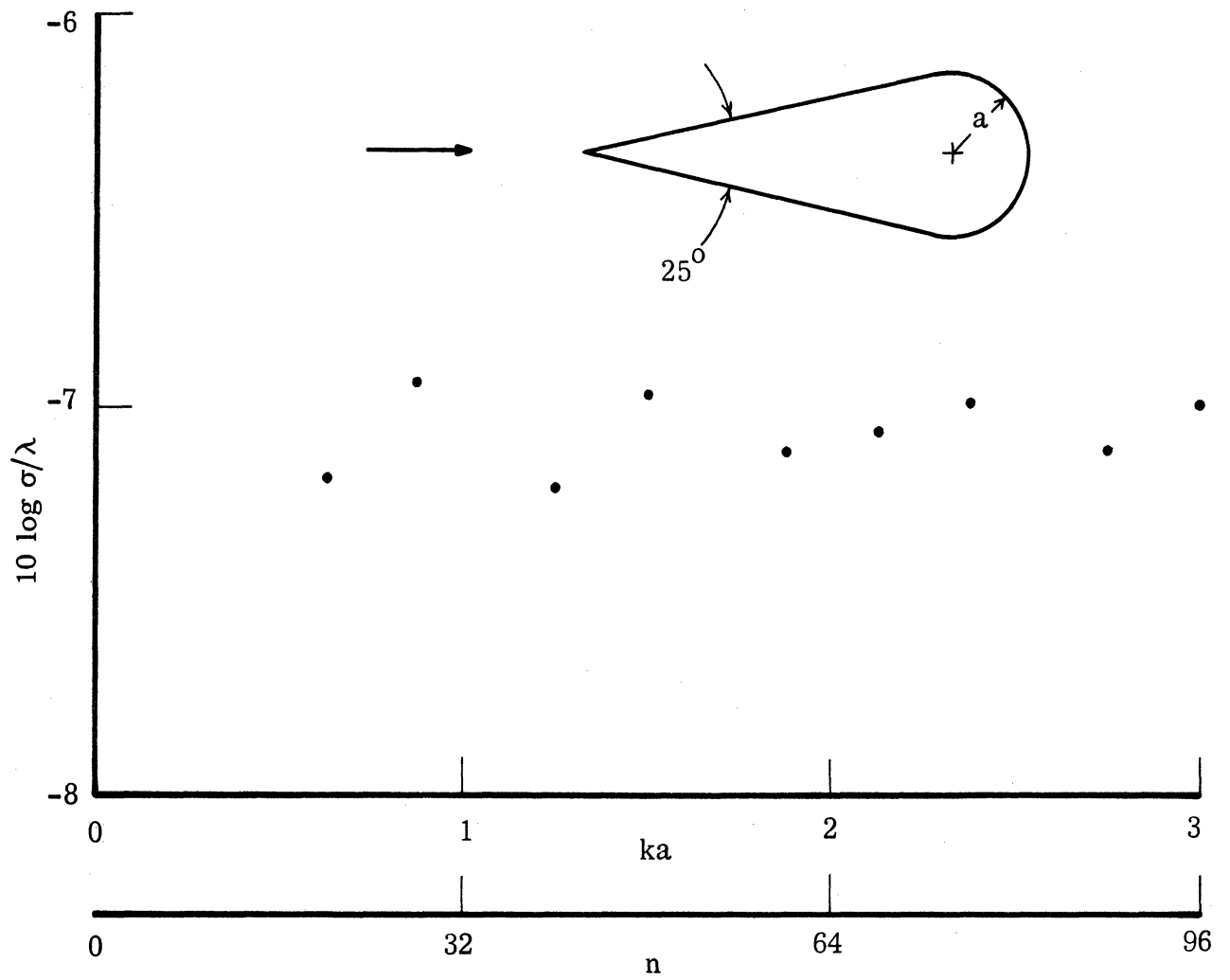
FIG. 5-19: EDGE-ON RETURN OF A METALLIC WEDGE-CYLINDER
FOR E-POLARIZATION.

74

parts of the body (e. g., for the coating), provided the original scattering source is preserved. Since the dominant source then is the leading edge, the size of the cylinder is relatively unimportant, but in other cases, such as H-polarization for the same body, this is no longer true. Thus, in the event that it becomes necessary to re-distribute sampling points, there are certain instances for which it can be accomplished with but a small sacrifice in accuracy. The re-allocation is not possible in all cases, of course, and we may have to search for other techniques should the need arise.

VI

CONCLUSIONS

In this report we have described most of the work carried out since the publication of the Final Report (Knott et al., 1973) under the predecessor Contract. One of the key features of this study is the detailed examination of the integral equations in two-dimensional scattering presented in Chapters II and IV. For an impedance boundary condition imposed at the surface, the analysis has revealed that there is a choice of integral equations appropriate to a solid body, and by using this fact we were able to circumvent the difficulties previously encountered using program RAM1A (B) for E-polarization. The result, now designated RAMD, was a far more efficient and effective program and is listed in Appendix B. RAMD has been used to examine the effect of tapered impedances on the scattering from ogival and wedge-cylinders for E-polarization. Some of the data obtained are presented in Chapter V, and are compared with experimental data.

One of the shortcomings of an impedance boundary condition is the difficulty of relating the surface impedance to the electromagnetic properties of a material necessary to simulate it. To provide a more explicit connection to material properties, we have given considerable attention to the concept of resistive sheets used either individually, or in combination to simulate a layer of finite thickness. For the problem of (electrically) resistive sheets with E-polarization, a computer program is available and is designated REST. We have employed it extensively and successfully to assess the sheet performance, but the results obtained are reserved for a future report. However, it is important to examine the behavior of these same sheets for H-polarization, and since we can also conceive of 'magnetically resistive' sheets, to include these in our study as well.

The derivation of the integral equations for both types of resistive sheets, either in isolation or in the presence of a body having an impedance boundary condition imposed at its surface, is presented in Chapter IV. In essence, this

serves to set the stage for the work we are now doing, and the construction of
a computer program for generalized resistive sheets is now almost complete.
Although at least one of the integral equations is characterized by a 'second
derivative singularity' which is difficult to handle, the analysis and testing
described in Appendix A shows how it can be treated numerically. The
fruits of this work will be the subject of the next report.

APPENDIX A

SOME COMPUTATIONAL CONSIDERATIONS

Many of the integral equations derived in Chapters II and IV resulted from a limiting operation of the form

$$\lim_{\underline{\rho} \to C} \frac{\partial}{\partial n} \int_C f(s')H_0^{(1)}(kr)ds' \ . \tag{A.1}$$

If $\underline{\rho}$ is not on C, the differentiation and integration can be interchanged to give

$$\lim_{\underline{\rho} \to C} \int_C f(s')K(s,s')ds' \tag{A.2}$$

where

$$K(s,s') = k(\hat{n} \cdot \hat{r})H_0^{(1)'}(kr) = -k(\hat{n} \cdot \hat{r})H_1^{(1)}(kr) \ , \tag{A.3}$$

but in the limit as the observation point approaches C, the kernel is characterized by a "first derivative (non-integrable) singularity" and is infinite at $s' = s$. However, (A.2) and, hence, (A.1) can be evaluated by treating analytically a neighborhood of the point $s' = s$, and when this is done we find

$$\lim_{\underline{\rho} \to C} \int_C f(s')(\hat{n} \cdot \hat{r})H_0^{(1)'}(kr)d(ks') = \pm 2if(s) + \rlap{\Big/}\int_C f(s')(\hat{n} \cdot \hat{r})H_0^{(1)'}(kr)d(ks') \tag{A.4}$$

with the upper or lower sign according as $\underline{\rho}$ approaches C in the direction $\pm \hat{n}$, respectively. The slash across the integral sign denotes the Cauchy principal value, and since the first term is simply the self cell contribution, the right hand side of (A.4) is quite convenient for computation.

Unfortunately, several of the key integral equations involve a second derivative kernel in addition or instead, for example

$$\lim_{\rho \to C} \int_C f(s') \frac{\partial}{\partial n} K(s, s') ds' \qquad (A.5)$$

where $K(s, s')$ is given in $(A.3)$, and this is not quite so easy to handle. Even the existence of the limit is mathematically in question, but the form that preceded $(A.5)$, viz.

$$\lim_{\rho \to C} \frac{\partial}{\partial n} \int_C f(s') K(s, s') ds' \qquad (A.6)$$

is capable of justification and physically represents the field of a current sheet evaluated at its surface.

To see how we can treat it, consider

$$I(x,y) = \frac{1}{k} \frac{\partial^2}{\partial y^2} \int_C J(x') H_0^{(1)} \left(k \sqrt{(x-x')^2 + y^2} \right) dx' \qquad (A.7)$$

appropriate to a planar sheet. If x is on C and Δ is a small interval of width 2δ centered on $x' = x$, $I(x,y)$ can be written as

$$I(x,y) = I_1(x,y) + I_2(x,y)$$

where

$$I_1(x,y) = \frac{1}{k} \int_{C-\Delta} J(x') \frac{\partial^2}{\partial y^2} H_0^{(1)} \left(k \sqrt{(x-x')^2 + y^2} \right) dx' , \qquad (A.8)$$

$$I_2(x,y) = \frac{1}{k} \frac{\partial^2}{\partial y^2} \int_\Delta J(x') H_0^{(1)} \left(k \sqrt{(x-x')^2 + y^2} \right) dx' . \qquad (A.9)$$

79

Taking I_1 first and using the differential equation for the Hankel function, we have

$$I_1(x,y) = \int_{C-\Delta} J(x') \left\{ \frac{(x-x')^2 - y^2}{\sqrt{(x-x')^2 + y^2}} H_0^{(1)'}\left(k\sqrt{(x-x')^2 + y^2}\right) \right. $$
$$\left. - ky^2 H_0^{(1)}\left(k\sqrt{(x-x')^2 + y^2}\right) \right\} \frac{dx'}{(x-x')^2 + y^2}$$

and since the integral is convergent for all y including y = 0,

$$\lim_{y \to 0} I_1(x,y) = - \int_{C-\Delta} J(x') \frac{H_1^{(1)}(k|x-x'|)}{|x-x'|} dx' \quad . \tag{A.10}$$

Turning now to I_2, we remark that if $k\sqrt{\delta^2 + y^2} \ll 1$ and $J(x')$ is slowly varying in the vicinity of $x' = x$,

$$\int_{\Delta} J(x') H_0^{(1)}\left(k\sqrt{(x-x')^2 + y^2}\right) dx' \sim \frac{4i}{\pi} J(x) \int_0^{\delta} \log\left(\frac{\Gamma k}{2}\sqrt{(x-x')^2 + y^2}\right) dx'$$

$$= \frac{2}{\pi} J(x) \left[2i\delta \left\{ \log\left(\frac{\Gamma k}{2}\sqrt{\delta^2 + y^2}\right) - 1 \right\} - y \log \frac{y - i\delta}{y + i\delta} \right]$$

where $\Gamma = e^{\gamma}$ with $\gamma = 0.5772\ldots$ (Euler's constant). On carrying out the differentiation with respect to y,

$$I_2(x,y) \simeq - \frac{4i\delta}{\pi k(\delta^2 + y^2)} J(x)$$

from which we obtain

$$\lim_{y \to 0} I_2(x,y) \simeq - \frac{4i}{\pi k \delta} J(x) \quad , \tag{A.11}$$

and hence

80

$$\lim_{y \to 0} I(x,y) \simeq -\frac{4i}{\pi k \delta} J(x) - \int_{C-\Delta} J(x') \frac{H_1^{(1)}(k|x-x'|)}{|x-x'|} dx' \qquad (A.12)$$

It can be verified that this result is unaffected if one or both of the differentiations are carried out prior to integration.

The right hand side of (A. 12) is not inconvenient for numerical evaluation, but in contrast to (A. 4), there is no guarantee of increased accuracy as the cell size 2δ is reduced. The first term is the self cell contribution and is inversely proportional to the cell size. The factor multiplying $J(x')$ in the integrand increases as $(x-x')^{-2}$ as x' approaches x, but since the self cell is excluded, the integrand is finite for all x'. However, over the immediately adjacent cells the integrand can vary by as much as an order of magnitude, and it will almost certainly be necessary to take account of this variation through subdivision of these cells or by integration over them.

This approach can be tested using the simple example of a plane, electrically resistive sheet illuminated by an H-polarized plane wave at non-glancing incidence. If the sheet occupies the portion $0 \le x \le L$ of the plane $y = 0$ and

$$\underline{H}^i = \hat{z} e^{-ik(x \cos \alpha + y \sin \alpha)}, \qquad (A.13)$$

eq. (A. 12) can be written as

$$\sin \alpha e^{-ikx \cos \alpha} = Y_0 R(x) J(x) - \lim_{y \to 0} \frac{1}{4k} \frac{\partial^2}{\partial y^2} \int_0^L J(x') H_0^{(1)} \left(k \sqrt{(x-x')^2 + y^2} \right) dx'$$

and hence, from (A. 12),

$$\sin \alpha e^{-ikx \cos \alpha} = \left\{ Y_0 R(x) + \frac{i}{\pi k \delta} \right\} J(x) + \frac{1}{4} \int_{C-\Delta} J(x') \frac{H_1^{(1)}(k|x-x'|)}{|x-x'|} dx' .$$

$$(A.14)$$

Equation (A. 14) has been programmed for solution and the current $J(x)$ computed in the particular case of a highly conducting (R = 0.01 ohm) strip 3λ long for plane wave incidence at the angle α = 155 degrees, corresponding to the peak of the traveling wave lobe in the backscattering pattern. From an examination of the data, it is believed that 48 sampling points (so that $2\delta = \lambda/16$, implying $k\delta$ = 0.196), with the cells immediately adjacent to the self cell subdivided into 25, and the next 5 cells on either side each subdivided into 10, are sufficient to give data which are effectively "exact". The resulting curve for $|J(x)|$ is shown in Fig. A-1 and has the character expected in a traveling wave situation. The effect of reducing the number of subdivisions is illustrated in Table A-1, from which it appears that if we are to keep the errors less than 1 percent, it is necessary to subdivide two cells on either side of the self cell, with the nearer being more finely subdivided. Many of these same tests have also been performed with 24 and 32 sampling points (or cells). It is found that the errors

TABLE 2-1: ERRORS IN $|J|$

subdivision	aver. (o/o)	max. (o/o)
1 x 25, 5 x 10	assumed 0	
1 x 25, 4 x 10	0.06	0.09
1 x 25, 3 x 10	0.11	0.18
1 x 25, 2 x 10	0.09	0.21
1 x 25, 1 x 10	0.32	0.61
1 x 10, 1 x 10	1.53	2.23
1 x 25	3.39	4.85
1 x 10	4.53	6.38

are significantly increased. As an example, with N = 24 and six cells on each side subdivided as in the first line of Table A-1, the average and maximum errors are 7.31 and 16.03 percent respectively.

In any subdivision process the integrand must be computed a corresponding number of times, and any massive subdivision is therefore an inefficient and time consuming procedure. If the strip is divided into 48 cells, subdivision of the
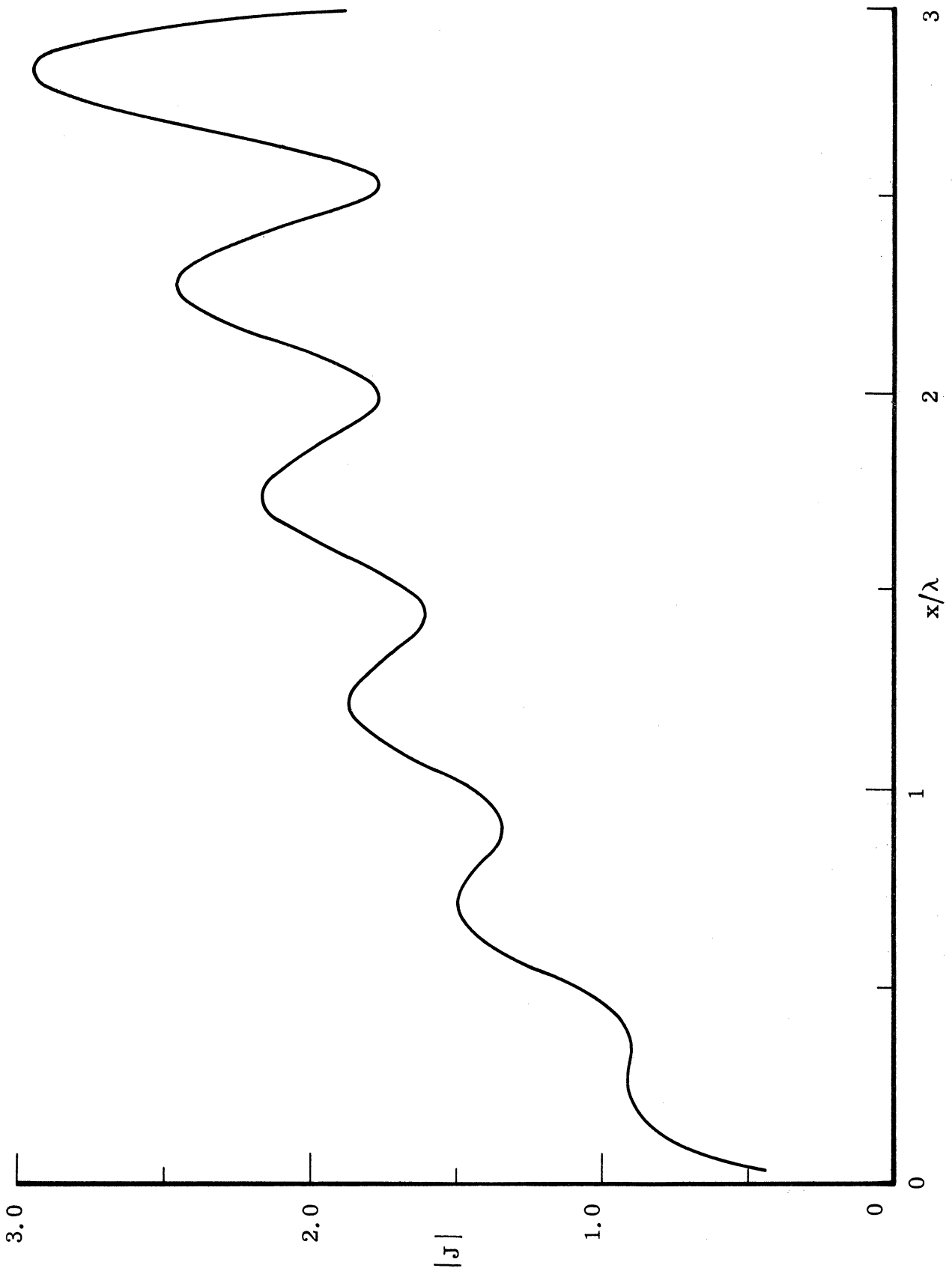
FIG. A-1: TOTAL CURRENT ON A HIGHLY CONDUCTING $(R = 0.01\Omega)$ STRIP 3λ WIDE ILLUMINATED BY AN H-POLARIZED PLANE WAVE WITH $\alpha = 155^\circ$.

cells adjacent and next-to-adjacent to the self cell by 25 and 10 respectively requires almost 1500 additional computations of the Hankel function even when the symmetry of the matrix is taken into account, and this increases considerably the time involved in generating the matrix elements. However, subdivision is just a simple method of numerical integration, and since the unknown current $J(x)$ is still given its value at the midpoint of the cell, the function being integrated is entirely known. This suggests the possibility of an analytical evaluation. The contribution of the kernel from the nth cell on either side of the self cell in eq. (A. 14) is

$$I_n = \int_{(2n-1)\delta}^{(2n+1)\delta} \frac{H_1^{(1)}(kt)}{t} \, dt \tag{A.15}$$

and from the recurrence relations for the Hankel functions (or, alternatively, from the differential equation for $H_0^{(1)}(kt)$), we have

$$I_n = H_1^{(1)}\left(\left[2n-1\right]k\delta\right) - H_1^{(1)}\left(\left[2n+1\right]k\delta\right) + \int_{-k\delta}^{k\delta} H_0^{(1)}(2nk\delta+t)\, dt \ . \tag{A.16}$$

The integrand that now remains is much more slowly varying than the one in (A. 15) , and it is not unreasonable to approximate (A. 16) by

$$I_n \simeq H_1^{(1)}\left(\left[2n-1\right]k\delta\right) - H_1^{(1)}\left(\left[2n+1\right]k\delta\right) + 2k\delta\, H_0^{(1)}(2nk\delta) \ \ .$$

Somewhat surprisingly, when this formula is used for $n = 1, 2$, i.e., for two cells on either side of the self cell, with $k\delta = 0.196$, the current is in error by more than 10 percent. Most of this error is attributable to the evaluation of the integral in (A. 16), and is not substantially reduced when the Hankel function $H_0^{(1)}(x)$ is replaced by its logarithmic approximation for small arguments and the integration carried out analytically. On the other hand, when the cells corresponding to $n = 1, 2$ are subdivided into 5 and 3 parts respectively, the average and maximum errors drop to 0.19 and 0.42 percent respectively, and

even with the coarser subdivision 3 and 2, the errors are still only 0.37 and 0.68 percent. Such a performance is comparable to that achieved on dividing the same cells in (A.15) into 25 and 10 parts (see line 5 of Table A-1), and requires only about 300 additional computations of the Hankel functions in place of 1500. As an alternative to subdivision, integration using the three-point Simpson formula has been tried. When applied to the cells corresponding to $n = 1$ and 2 in eq. (A.16), it turns out to be just slightly more efficient than subdivision of the same cells into 3 and 2 parts respectively, but produces much better accuracy, the average and maximum errors in $|J|$ being 0.12 and 0.40 percent. In contrast, when the same integration formula was applied to the original expression (A.15) for the cell contributions, the errors were larger by two orders of magnitude.

All of the above constitutes the direct approach to an integral of the form shown in eq. (A.7), and though it has turned out to be relatively straightforward, it is not the only way in which the second derivative singularity can be handled. If, for example, we go back to (A.7) and use the fact that

$$\left(\frac{\partial^2}{\partial x^2} + \frac{\partial^2}{\partial y^2} + k^2 \right) H_0^{(1)}\left(k \sqrt{(x-x')^2 + y^2} \right) = 0 \ ,$$

the normal derivatives can be replaced by tangential derivatives and one (or both) of them eliminated by partial integration. This method has been explored in some detail. Integrating only once by parts, we obtain an integral expression for $I(x,y)$ involving the current and its first derivative, plus contributions from the end points of the range of integration. The more singular integral is that containing $\frac{\partial J}{\partial x'}$, but in the limit as $y \to 0$ the self cell contribution can be evaluated analytically and turns out to be zero. Hence, for $0 < x < L$,

$$\lim_{y \to 0} I(x,y) = \int_0^L \frac{\partial}{\partial x'} J(x') \frac{x-x'}{|x-x'|} H_1^{(1)}(k|x-x'|)dx'$$

$$-k \int_0^L J(x') H_0^{(1)}(k|x-x'|)dx'$$

$$+J(L)H_1^{(1)}(k[L-x]) + J(0)H_1^{(1)}(kx) \qquad (A.17)$$

and though we are now left with twice as many unknowns as we had before, the assumption of a locally linear variation of $J(x')$ enables us to express $\frac{\partial J}{\partial x'}$ in terms of the currents over the neighboring cells.

Unfortunately, the end-point contributions pose a problem. Each is infinite when the observation point is at the end in question, and while it can be argued that in the moment method the observation never does lie actually at an end, the contribution will still increase indefinitely with decreasing cell size. In effect, we now have a self cell contribution analogous to (A.11), but appropriate only when the self cell is at an end. If, on the other hand, the self cell contribution is separated out prior to partial integration, the result obtained is no different from integrating by parts the integral in (A.12). Any assumption which then expresses $\frac{\partial J}{\partial x'}$ in terms of J is merely equivalent to an interpolation formula for evaluating this integral.

For these reasons we have found it convenient to use the direct approach and the only task which now remains is to extend it to a non-planar surface or sheet. In place of (A.7) the integral of concern to us is

$$I = \frac{1}{k} \frac{\partial}{\partial n} \int_C J(s')(\hat{n}' \cdot \hat{r}) H_1^{(1)}(kr)d(ks') \qquad (A.18)$$

and a typical integral equation is

86

$$Y_0 E_s^i (s) = Y_0 R(s) J(s) + \frac{1}{4} \lim_{\underset{\sim}{\rho} \to C} I \qquad\qquad (A.19)$$

(see eq. 4.15).

If $\underset{\sim}{\rho}$ is not on C, we can interchange the derivative and integral operations in (A.18) to obtain

$$I = \frac{1}{k} \int_C J(s') \left\{ H_1^{(1)}(kr) \frac{\partial}{\partial n}(\hat{n}' \cdot \hat{r}) + (\hat{n}' \cdot \hat{r}) \frac{\partial}{\partial n} H_1^{(1)}(kr) \right\} d(ks')$$

$$= \int_C J(s') \left\{ (\hat{s}' \cdot \hat{r})(\hat{s} \cdot \hat{r}) \frac{H_1^{(1)}(kr)}{kr} + (\hat{n}' \cdot \hat{r})(\hat{n} \cdot \hat{r}) H_1^{(1)'}(kr) \right\} d(ks')$$

which becomes

$$I = \int_C J(s')(\hat{s}' \cdot \hat{r})(\hat{s} \cdot \hat{r}) H_0^{(1)}(kr) d(ks')$$

$$+ \int_C J(s') \left\{ (\hat{n}' \cdot \hat{r})(\hat{n} \cdot \hat{r}) - (\hat{s}' \cdot \hat{r})(\hat{s} \cdot \hat{r}) \right\} H_1^{(1)'}(kr) d(ks')$$

$$\qquad\qquad (A.20)$$

on using the differential equation for $H_0^{(1)}(kr)$.

To find the limit as the observation point $\underset{\sim}{\rho}$ approaches C, it is necessary to treat analytically the contribution of the self cell Δ to the second integral in eq. (A.20). Since

$$\lim_{\underset{\sim}{\rho} \to C} \int_\Delta J(s') \left\{ (\hat{n}' \cdot \hat{r})(\hat{n} \cdot \hat{r}) - (\hat{s}' \cdot \hat{r})(\hat{s} \cdot \hat{r}) \right\} H_1^{(1)'}(kr) d(ks') = + \frac{4i}{\pi k \delta} J(s)$$

where 2δ is the width of the self cell centered on $s' = s$, we have

$$\lim_{\underline{\rho} \to C} I = + \frac{4i}{\pi k \delta} \, J(s) + \int_C J(s')(\hat{s}' \cdot \hat{r})(\hat{s} \cdot \hat{r}) H_0^{(1)}(kr) d(ks')$$

$$+ \int_{C-\Delta} J(s') \left\{ (\hat{n}' \cdot \hat{r})(\hat{n} \cdot \hat{r}) - (\hat{s}' \cdot \hat{r})(\hat{s} \cdot \hat{r}) \right\} H_1^{(1)'}(kr) d(ks').$$

$$(A.21)$$

But

$$\frac{1}{k} \frac{\partial}{\partial s'} \left\{ (\hat{s} \cdot \hat{r}) H_1^{(1)}(kr) \right\} = - (\hat{s}' \cdot \hat{r})(\hat{s} \cdot \hat{r}) H_1^{(1)'}(kr) - (\hat{n}' \cdot \hat{r})(\hat{n} \cdot \hat{r}) \frac{H_1^{(1)}(kr)}{kr}$$

$$= \left\{ (\hat{n}' \cdot \hat{r})(\hat{n} \cdot \hat{r}) - (\hat{s}' \cdot \hat{r})(\hat{s} \cdot \hat{r}) \right\} H_1^{(1)'}(kr) - (\hat{n}' \cdot \hat{r})(\hat{n} \cdot \hat{r}) H_0^{(1)}(kr)$$

and

$$(\hat{n}' \cdot \hat{r})(\hat{n} \cdot \hat{r}) + (\hat{s}' \cdot \hat{r})(\hat{s} \cdot \hat{r}) = \hat{n}' \cdot \hat{n} \ .$$

Hence

$$\lim_{\underline{\rho} \to C} I = + \frac{4i}{\pi k \delta} \, J(s) + \int_C J(s')(\hat{n}' \cdot \hat{n}) H_0^{(1)}(kr) d(ks')$$

$$+ \int_{C-\Delta} J(s') \frac{\partial}{\partial s'} \left\{ (\hat{s} \cdot \hat{r}) H_1^{(1)}(kr) \right\} ds'$$

and when this is substituted into eq. (A.19), the integral equation for a non-planar sheet becomes

$$Y_0 E_s^i = \left\{ Y_0 R(s) + \frac{i}{\pi k \delta} \right\} J(s) + \frac{1}{4} \int_C J(s')(\hat{n}' \cdot \hat{n}) H_0^{(1)}(kr) d(ks')$$

$$+ \frac{1}{4} \int_{C-\Delta} J(s') \frac{\partial}{\partial s'} \left\{ (\hat{s} \cdot \hat{r}) H_1^{(1)}(kr) \right\} ds'$$

$$(A.22)$$

Equation (A.22) is the analogue of (A.14) and (A.16) combined, and is the desired result. Though the integrand of the second integral is a rapidly varying function of s' for small s'-s, the particular advantage of this form is that if $J(s')$ is constant over a cell (as is assumed in the moment method), the contribution of that cell is given precisely by the difference in the end values of $(\hat{s} \cdot \hat{r})H_1^{(1)}(kr)$. For the first integral in (A.22), the self cell contribution vanishes as the cell size tends to zero. The analogy with the results for a planar sheet is now complete.

APPENDIX B

PROGRAM RAMD

Program RAMD solves the integral equations 2.9 and 2.16 for a cylindrical body satisfying a surface impedance boundary condition. Although its predecessor program, RAM1B, accomplishes this same task, RAMD is a significantly more compact and more efficient program. This compression was achieved by a reduction in the number of arrays created by the program, by the exploitation of the duality between the E- and H-polarization integral equations, and by the elimination of options that were seldom exercised in the former program. As a result, RAMD occupies less than 1/3 the core required by RAM1B, implying that the number of surface sampling points could probably be increased by 50 percent or more. The program is manifestly shorter because it solves the simpler of the two available equations and, not least, it produces the correct solution for E-polarization for edged structures whereas its predecessor did not.

In addition to the MAIN program, RAMD has five subroutines: GEOM, HANK, ADAM, FLIP and ZFUN. The MAIN program reads control information from the input data stream, creates the matrix elements for the geometry at hand, sums the surface currents to obtain the far scattered fields, and indexes through the desired angles of incidence and scattering. MAIN calls subroutine GEOM to create the coordinates of sampling points on the body profile if the profile is describable in terms of straight or circular arc segments but, if necessary, the sampling points may be fed in one at a time by by-passing GEOM. GEOM assigns a specific impedance to each surface sampling point according to two options and, should neither be suitable to the user's needs, a third option invokes a call to subroutine ZFUN. In the program listing below, ZFUN is merely a dummy subroutine necessary for the successful compilation of RAMD and should be replaced by the appropriate version required by the user.

Subroutine HANK generates Hankel functions of order 0 and 1 as required by the integral equations. This particular subroutine differs from previous versions (in REST and RAM1B) in that polynomial approximations of the Hankel

90

functions are employed, a distinct advantage for large arguments; subroutine ADAM assists HANK by summing the terms in the polynomial. Once the matrix elements have been filled in by the MAIN program, subroutine FLIP is called to invert the matrix. FLIP, like its cousin ZVO8 in previous programs, is essentially a copy of subroutine MINV from IBM's Scientific Subroutine Package. FLIP also computes the surface currents on the profile using the inverted matrix. MAIN then sums the currents and, depending on the particular options exercised on input, produces either a bistatic or backscattering pattern of the obstacle, for either E- or H-polarization.

```
C************************************************************************C
C   INPUT FORMAT FOR PROGRAM RAMD---REVISION OF MAY, 1973               C
C************************************************************************C
C   CARD 1  FORMAT (18A4)              TITLE CARD; USE UP TO 72 COLUMNS  C
C************************************************************************C
C   CARD 2  FORMAT (I2,I3,F10.5)    MORE,KODE,ZFAC                       C
C           MORE=0          THIS WILL BE THE LAST RUN FOR THIS DATA SET  C
C           MORE=1          THERE ARE MORE DATA TO BE READ AFTER THIS SET C
C           KODE=0          COMPUTES BISTATIC SCATTERING PATTERN         C
C           KODE=1          COMPUTES BACKSCATTERING PATTERN              C
C           ZFAC            A FACTOR MULTIPLYING ALL ELEMENT IMPEDANCES  C
C************************************************************************C
C   CARD 3  FORMAT (I2,I3,F10.5)    LL,M,WAVE                            C
C           LL              TOTAL NUMBER OF SEGMENTS ON THE PROFILE      C
C           M               TOTAL NUMBER OF POINTS ON THE PROFILE        C
C           WAVE            WAVELENGTH                                   C
C************************************************************************C
C   CARD 4  FORMAT (I2,I3,3F10.5)  IPP,IOPT,FIRST,LAST,INK              C
C           IPP=1           E-POLARIZATION                              C
C           IPP=2           H-POLARIZATION                              C
C           IOPT=0          BODY GEOMETRY READ IN POINT BY POINT        C
C           IOPT=1          BODY GEOMETRY GENERATED INTERNALLY          C
C           FIRST           INITIAL SCATTERING AND INCIDENCE ANGLE      C
C           LAST            FINAL ANGLE                                 C
C           INK             ANGULAR INCREMENT                           C
C************************************************************************C
C   CARD 5  FORMAT (I2,I3,5F10.5)  N,IMP,XA,YA,XB,YB,ANG               C
C           N               NUMBER OF SAMPLING POINTS ON THIS SEGMENT   C
C           IMP=-1          IMPEDANCE GIVEN BY USER-SUPPLIED SUBROUTINE C
C           IMP=0           ZS(I)=ZA+ZB*S(I)**ZEX                       C
C           IMP=1           ZS(I)=ZA+ZB*EXP(-ZEX*S(I))                  C
C           XA,YA,XB,YB     SEGMENT ENDPOINTS                           C
C           ANG             ANGLE SUBTENDED BY THE SEGMENT              C
C************************************************************************C
C   CARD 6  FORMAT (5X,5F10.5)       ZA,ZB,ZEX                          C
C           ZA,ZB           COMPLEX IMPEDANCE CONSTANTS                 C
C           ZEX             REAL IMPEDANCE CONSTANT                     C
C************************************************************************C
C   CARD 7  FORMAT (I2)               INTEGER ZERO IN COLUMN 2: SHUTS    C
C                                     OFF READING OF SEGMENT PARAMETERS  C
C************************************************************************C
C   CARD 8  FORMAT (I2,I3,F10.5)    MORE,KODE,ZFAC                       C
C                                   THIS CARD IS USED ONLY IF, ON CARD 2, MORE=1 C
C************************************************************************C
C   CARD 9  FORMAT (I2,I3,4F10.5)  LUMP(I,1),LUMP(I,2),X(I),Y(I),ZS(I)  C
C           LUMP(I,1)       CELL ID NUMBER                              C
C           LUMP(I,2)       SEGMENT ID NUMBER                           C
C           X(I),Y(I)       CELL COORDINATES                           C
C           ZS(I)           COMPLEX IMPEDANCE OF THE CELL               C
C************************************************************************C
C   NOTE: CARD 9 IS USED ONLY IF IOPT=0 AND THERE MUST BE ONE SUCH CARD C
C   FOR EVERY CELL ON THE BODY.  SIMILARLY, CARDS 5,6 AND 7 ARE USED    C
C   ONLY IF IOPT=1 AND THERE MUST BE ONE EACH OF CARDS 5 AND 6 FOR EACH C
C   SEGMENT SPECIFIED ON INPUT.                                         C
C************************************************************************C
```

```
      COMPLEX A(100,101),PHI(100),PINK(100),SUM,DEL,B1,B2,ZS(100)
      REAL LAST,INK
      DIMENSION X(100),Y(100),XN(100),YN(100),S(100),DSQ(100)
      DIMENSION ID(18),LUMP(100,2),IPOL(2)
      DATA RED,DIG,IPOL/0.01745329,57.29578,'FFFF','HHHH'/
C.....READ INPUT DATA AND GENERATE BODY PROFILE
    5 READ (5,100) ID
      READ (5,200) MORE,KODE,ZFAC
      READ (5,200) LL,M,WAVE
      READ (5,200) IPP,IOPT,FIRST,LAST,INK
      XK=6.283185/WAVE
      WRITE (6,150) ID
      IF (IOPT.EQ.0) GO TO 10
      WRITE (6,300)
      CALL GEOM(LUMP,X,Y,XN,YN,S,DSQ,ZS,M,LL)
      GO TO 20
   10 READ (5,200) LUMP(1,1),LUMP(1,2),X(1),Y(1),ZS(1)
      S(1)=0.0
      DO 15 I=2,M
      READ (5,200) (LUMP(I,J),J=1,2),X(I),Y(I),ZS(I)
      TX=X(I)-X(I-1)
      TY=Y(I)-Y(I-1)
      DSQ(I)=SQRT(TX*TX+TY*TY)
      S(I)=S(I-1)+DSQ(I)
      XN(I)=-TY/DSQ(I)
   15 YN(I)=TX/DSQ(I)
   20 IF (KODE.NE.0) GO TO 25
      NINC=1
      NBIT=1+IFIX((LAST-FIRST)/INK)
      GO TO 30
   25 NBIT=0
      NINC=1+IFIX((LAST-FIRST)/INK)
   30 WRITE (6,400) IPOL(IPP),LL,M,NINC,NBIT,WAVE
      DO 35 I=1,M
   35 DSQ(I)=DSQ(I)/WAVE
C.....CONSTRUCT MATRIX ELEMENTS
   38 DO 55 I=1,M
      DO 55 J=1,M
      IF (I.EQ.J) GO TO 40
      TX=X(I)-X(J)
      TY=Y(I)-Y(J)
      P=SQRT(TX*TX+TY*TY)
      RPQ=P*XK
      CNR=-(TX*XN(J)+TY*YN(J))/P
      CALL HANK(RPQ,1,BJ,BY)
      B1=1.570796*DSQ(J)*CNR*CMPLX(-BY,BJ)
      CALL HANK(RPQ,0,BJ,BY)
      B2=1.570796*DSQ(J)*CMPLX(BJ,BY)
      GO TO 45
```

```
   40  B1=CMPLX(0.5,0.0)
       B2=DSQ(J)*CMPLX(1.570796,0.0287985+ALOG(DSQ(J)))
   45  IF (IPP.EQ.1) GO TO 50
       A(I,J)=B1+B2*ZS(J)*ZFAC
       GO TO 55
   50  A(I,J)=B2+B1*ZS(J)*ZFAC
   55  CONTINUE
C.....COMPUTE INCIDENT FIELD AND INVERT MATRIX
       TETA=RED*FIRST
       CT=COS(TETA)
       ST=SIN(TETA)
       DO 60 I=1,M
       HOLD=-XK*(CT*X(I)+ST*Y(I))
   60  PINK(I)=CMPLX(COS(HOLD),SIN(HOLD))
       CALL FLIP(A,M,PINK,PHI,1)
C.....PRINT OUT CURRENTS AND ELEMENT PROPERTIES FOR FIRST ANGLE
       WRITE (6,150) ID
       WRITE (6,500)
       DO 65 I=1,M
       AMP=CABS(PHI(I))
       PHASE=DIG*ATAN2(AIMAG(PHI(I)),REAL(PHI(I)))
       DEL=ZFAC*ZS(I)
   65  WRITE (6,250) (LUMP(I,J),J=1,2),X(I),Y(I),S(I),DSQ(I),AMP,PHASE,
      &DEL
C.....DOPE OUT THE APPROPRIATE FIELD FACTORS
       THE=FIRST-INK
       IF (KODE.EQ.1) GO TO 70
       WRITE (6,800) FIRST
       GO TO 75
   70  WRITE (6,600)
   75  THE=THE+INK
       IF (THE.GT.LAST) GO TO 105
       IF (THE.EQ.FIRST) GO TO 85
       TETA=RED*THE
       CT=COS(TETA)
       ST=SIN(TETA)
C.....IN THE FOLLOWING LOOP, PINK IS NOT NECESSARILY THE INCIDENT FIELD
       DO 80 J=1,M
       HOLD=-XK*(CT*X(J)+ST*Y(J))
   80  PINK(J)=CMPLX(COS(HOLD),SIN(HOLD))
       IF (KODE.EQ.0) GO TO 85
       CALL FLIP(A,M,PINK,PHI,2)
   85  SUM=CMPLX(0.0,0.0)
C.....ADD UP THE CURRENTS
       DO 95 J=1,M
       DEL=DSQ(J)*PHI(J)*PINK(J)
       IF (IPP.EQ.1) GO TO 90
       SUM=SUM+DEL*(ZFAC*ZS(J)-CT*XN(J)-ST*YN(J))
       GO TO 95
   90  SUM=SUM+DEL*(1.0-ZFAC*ZS(J)*(CT*XN(J)+ST*YN(J)))
   95  CONTINUE
```

```
      SCAT=20.0*ALOG10(CABS(SUM))+1.9612
      WRITE (6,900) THE,SCAT
      GO TO 75
105   IF (MORE.EQ.0) GO TO 5
      READ (5,200) MORE,KODE,ZFAC
      GO TO 38
100   FORMAT (18A4)
150   FORMAT (1H1,18A4)
200   FORMAT (I2,I3,5F10.5)
250   FORMAT (2I5,5F10.5,F10.3,2F10.5)
300   FORMAT (10HOSEG    NUM,11X,24HENDPOINTS OF THE SEGMENT,11X,
     &18HSEGMENT PARAMETERS/11H NUM  CELLS,6X,2HXA,8X,2HYA,8X,2HXB,8X,
     &2HYB,6X,21HANGLE  RADIUS  LENGTH/)
400   FORMAT (//31X,14HKEY PARAMETERS//
     &16X,21HINCIDENT POLARIZATION,22X,1A1//
     &16X,23HNUMBER OF SEGMENTS USED,I21//
     &16X,34HTOTAL NUMBER OF POINTS ON THE BODY,I10//
     &16X,35HNUMBER OF INCIDENT FIELD DIRECTIONS,I9//
     &16X,29HNUMBER OF BISTATIC DIRECTIONS,I15//
     &16X,10HWAVELENGTH,F34.5)
500   FORMAT (11HO    I    SEG,4X,4HX(I),6X,4HY(I),6X,4HS(I),5X,6HDSQ(I),
     &4X,6HMOD(J),4X,6HARG(J),4X,5HRS(I),5X,5HXS(I)/)
600   FORMAT (1H1,22X,28HBACKSCATTERING CROSS SECTION//24X,
     &28HTHETA    10*LOG(SIGMA/LAMBDA)/)
800   FORMAT (1H1,19X,33HBISTATIC SCATTERING CROSS SECTION/18X,
     &29HFOR INCIDENT FIELD DIRECTION=,F7.2//24X,
     &28HTHETA    10*LOG(SIGMA/LAMBDA)/)
900   FORMAT (16X,F13.2,F15.2)
      END
```

```
      SUBROUTINE GEOM(LUMP,X,Y,XN,YN,S,DSQ,ZS,M,LL)
      COMPLEX ZS(100),ZA,ZB
      DIMENSION X(100),Y(100),XN(100),YN(100),DSQ(100),S(100)
      DIMENSION LUMP(100,2)
      DATA RED/0.01745329/
      I=0
      L=0
C.....READ INPUT PARAMETERS AND PREPARE TO GENERATE SAMPLING POINTS
   10 READ (5,200) N,IMP,XA,YA,XB,YB,ANG
      IF (N.EQ.0) GO TO 120
      LIM=2*N-1
      READ (5,250) ZA,ZB,ZEX
      TX=XB-XA
      TY=YB-YA
      D=SQRT(TX*TX+TY*TY)
      IF (ANG.EQ.0.0) GO TO 20
      T=0.5*RED*ANG
      TRX=TX+TY*COTAN(T)
      TRY=TY-TX*COTAN(T)
      RAD=0.5*D/SIN(T)
      ARC=2.0*RAD*T
      ALF=T/N
      DID=2.0*RAD*ALF
      GO TO 30
   20 RAD=999.999
      ARC=D
      DID=D/N
C.....START GENERATING
   30 DO 110 JIM=1,2
      L=L+1
      DO 100 J=1,LIM,2
      I=I+1
      LUMP(I,1)=I
      LUMP(I,2)=L
      IF (I.EQ.100) WRITE (6,400)
      IF (JIM.EQ.2) GO TO 90
      IF (ANG.EQ.0.0) GO TO 40
      SINQ=SIN(J*ALF)
      COSQ=COS(J*ALF)
      X(I)=XA+0.5*(TRX*(1.0-COSQ)-TRY*SINQ)
      Y(I)=YA+0.5*(TRX*SINQ+TRY*(1.0-COSQ))
      XN(I)=-0.5*(TRX*COSO+TRY*SINQ)/RAD
      YN(I)= 0.5*(TRX*SINQ-TRY*COSQ)/RAD
      GO TO 50
   40 X(I)=XA+0.5*J*TX/N
      Y(I)=YA+0.5*J*TY/N
      XN(I)=-TY/D
      YN(I)= TX/D
   50 S(I)=0.5*J*DID
```

```
C.....COMPUTE THE IMPEDANCES
      IF (IMP) 60,70,80
  60  CALL ZFUN(ZA,ZB,ZEX,S(I),ZS(I))
      GO TO 100
  70  ZS(I)=ZA+ZB*S(I)**ZEX
      GO TO 100
  80  ZS(I)=ZA+ZB*EXP(-ZEX*S(I))
      GO TO 100
C.....FROM HERE TO 100 WE CREATE THE SEGMENT IMAGE
  90  K=I-N
      X(I)=X(K)
      Y(I)=-Y(K)
      XN(I)=XN(K)
      YN(I)=-YN(K)
      S(I)=S(K)
      ZS(I)=ZS(K)
 100  DSQ(I)=DID
      IF (JIM.EQ.1) GO TO 110
      YA=-YA
      YB=-YB
 110  WRITE (6,300) L,N,XA,YA,XB,YB,ANG,RAD,ARC
      GO TO 10
 120  M=I
      LL=L
 200  FORMAT (I2,I3,5F10.5)
 250  FORMAT (5X,5F10.5)
 300  FORMAT (I3,I6,3X,4F10.5,F8.2,F8.3,F8.4)
 400  FORMAT (36HOWARNING: WE'VE GENERATED 100 POINTS/)
      RETURN
      END
```

```
        SUBROUTINE HANK(R,N,BJ,BY)
C......SUBROUTINE REQUIRES R>0 AND N EITHER 0 OR 1
        DIMENSION A(7),B(7),C(7),D(7),E(7),F(7),G(7),H(7)
        DATA A,B,C,D,E,F,G,H/1.0,-2.2499997,1.2656208,-0.3163866,
       &0.0444479,-0.0039444,0.00021,0.36746691,0.60559366,-0.74350384,
       &0.25300117,-0.04261214,0.00427916,-0.00024846,0.5,-0.56249985,
       &0.21093573,-0.03954289,0.00443319,-0.00031761,-0.00001109,
       &-0.6366198,0.2212091,2.1682709,-1.3164827,0.3123951,-0.0400976,
       &0.0027873,0.79788456,-0.00000077,-0.0055274,-0.00009512,
       &0.00137237,-0.00072805,0.00014476,-0.78539816,-0.04166397,
       &-0.00003954,0.00262573,-0.00054125,-0.00029333,0.00013558,
       &0.79788456,0.00000156,0.01659667,0.00017105,-0.00249511,
       &0.00113653,-0.00020033,-2.35619449,0.12499612,0.0000565,
       &-0.00637879,0.00074348,0.00079824,-0.00029166/
        IF (R.LE.0.0) GO TO 50
        IF (R.GT.3.0) GO TO 20
        X=R*R/9.0
        IF (N.NE.0) GO TO 10
        CALL ADAM(A,X,BJ)
        CALL ADAM(B,X,Y)
        BY=0.6366198*ALOG(0.5*R)*BJ+Y
        RETURN
10      IF (N.NE.1) GO TO 50
        CALL ADAM(C,X,Y)
        BJ=R*Y
        CALL ADAM(D,X,Y)
        BY=0.6366198*ALOG(0.5*R)*BJ+Y/R
        RETURN
20      X=3.0/R
        IF (N.NE.0) GO TO 30
        CALL ADAM(E,X,Y)
        FOOL=Y/SQRT(R)
        CALL ADAM(F,X,Y)
        GO TO 40
30      IF (N.NE.1) GO TO 50
        CALL ADAM(G,X,Y)
        FOOL=Y/SQRT(R)
        CALL ADAM(H,X,Y)
40      T=R+Y
        BJ=FOOL*COS(T)
        BY=FOOL*SIN(T)
        RETURN
50      N=100
        RETURN
        END
```

```
      SUBROUTINE FLIP(A,N,X,Y,IAT)
      COMPLEX A(100,101),X(100),Y(100),D,BIGA,HOLD
      DIMENSION L(100),M(100)
      IF (IAT.GT.1) GO TO 150
      D=CMPLX(1.0,0.0)
      DO 80 K=1,N
      L(K)=K
      M(K)=K
      BIGA=A(K,K)
      DO 20 J=K,N
      DO 20 I=K,N
   10 IF (CABS(BIGA).GE.CABS(A(I,J))) GO TO 20
      BIGA=A(I,J)
      L(K)=I
      M(K)=J
   20 CONTINUE
      J=L(K)
      IF (J.LE.K) GO TO 35
      DO 30 I=1,N
      HOLD=-A(K,I)
      A(K,I)=A(J,I)
   30 A(J,I)=HOLD
   35 I=M(K)
      IF (I.LE.K) GO TO 45
      DO 40 J=1,N
      HOLD=-A(J,K)
      A(J,K)=A(J,I)
   40 A(J,I)=HOLD
   45 IF (CABS(BIGA).NE.0.0) GO TO 50
      D=CMPLX(0.0,0.0)
      RETURN
   50 DO 55 I=1,N
      IF (I.EQ.K) GO TO 55
      A(I,K)=-A(I,K)/BIGA
   55 CONTINUE
      DO 65 I=1,N
      DO 65 J=1,N
      IF (I.EQ.K.OR.J.EQ.K) GO TO 65
      A(I,J)=A(I,K)*A(K,J)+A(I,J)
   65 CONTINUE
      DO 75 J=1,N
      IF (J.EQ.K) GO TO 75
      A(K,J)=A(K,J)/BIGA
   75 CONTINUE
      D=D*BIGA
   80 A(K,K)=1.0/BIGA
      K=N
  100 K=K-1
      IF (K.LE.0) GO TO 150
      I=L(K)
      IF (I.LE.K) GO TO 120
```

```
          DO 110 J=1,N
          HOLD=A(J,K)
          A(J,K)=-A(J,I)
110       A(J,I)=HOLD
120       J=M(K)
          IF (J.LE.K) GO TO 100
          DO 130 I=1,N
          HOLD=A(K,I)
          A(K,I)=-A(J,I)
130       A(J,I)=HOLD
          GO TO 100
150       DO 200 I=1,N
          Y(I)=CMPLX(0.0,0.0)
          DO 200 J=1,N
200       Y(I)=A(I,J)*X(J)+Y(I)
          RETURN
          END
```

```fortran
      SUBROUTINE ADAM(C,X,Y)
      DIMENSION C(7)
      Y=X*C(7)
      DO 10 I=1,5
10    Y=X*(C(7-I)+Y)
      Y=Y+C(1)
      RETURN
      END




      SUBROUTINE ZFUN(ZA,ZB,ZEX,S,ZS)
      ZS=ZA+ZB+ZEX
      RETURN
      END
```

REFERENCES

Andreasen, M. G. (1965) "Scattering from cylinders with arbitrary surface impedance", Proc. IEEE 53, 812-817.

Bowman, J. J. (1967), "High-frequency backscattering from an absorbing infinite strip with arbitrary face impedances", Can. J. Phys. 45, 2409-2430.

Knott, E. F., V. V. Liepa and T. B. A. Senior (1973), "Non-specular Radar Cross Section Study", The University of Michigan Radiation Laboratory Report No. 011062-1-F (AFAL-TR-73-70), April 1973.

Knott, E. F. and T. B. A. Senior (1973), "Non-specular Radar Cross Section Study", The University of Michigan Radiation Laboratory Report No. 011062-1-T (AFAL-TR-73-2), February 1973.

Laxpati, S. R. (1973), "Derivation of integral equations for a two dimensional scatterer with impedance boundary condition and partially clad by an absorptive sheet", The University of Michigan Radiation Laboratory Memorandum No. 011764-505-M.

Lebedev, N. N. and I. P. Skal'skaya (1963), "A new method for solving problems of diffraction of electromagnetic waves by a wedge with finite conductivity", Sov. Phys. - Tech. Phys. 7, 867-874.

Maliuzhinets, G. D. (1960), "Das Sommerfeldsche Integral und die Lösung von Beugungsaufgaben in Winkelgebieten", Ann. Physik 6, 107-112.

Oshiro, F. K., K. M. Mitzner, S. S. Locus, et al. (1971), "Calculations of Radar Cross-section", Northrop Corporation, Norair Division Technical Report No. AFAL-TR-71-50.

Senior, T. B. A. (1952), "Diffraction by a semi-infinite metallic sheet", Proc. Roy. Soc. 213A, 436-458.

Senior, T. B. A. (1959), "Diffraction by an imperfectly conducting wedge", Commun. Pure Appl. Math. 12, 337-372.

Senior, T. B. A. (1960), "Diffraction by an imperfectly conducting half-plane at oblique incidence", Appl. Sci. Res. 8B, 35-61.

Senior, T. B. A. (1962), "A note on impedance boundary conditions", Can. J. Phys. 40, 663-665.

DOCUMENT CONTROL DATA - R & D

(Security classification of title, body of abstract and indexing annotation must be entered when the overall report is classified)

1. ORIGINATING ACTIVITY (Corporate author)	2a. REPORT SECURITY CLASSIFICATION
The University of Michigan Radiation Laboratory 2216 Space Research Building, North Campus Ann Arbor, Michigan 48105	UNCLASSIFIED
	2b. GROUP NA

3. REPORT TITLE

NON-SPECULAR RADAR CROSS SECTION STUDY

4. DESCRIPTIVE NOTES *(Type of report and inclusive dates)*

Technical. Scientific. Interim (15 March - 16 October 1973)

5. AUTHOR(S) *(First name, middle initial, last name)*

Eugene F. Knott

Thomas B.A. Senior

6. REPORT DATE	7a. TOTAL NO. OF PAGES	7b. NO. OF REFS
October 1973	102	12

8a. CONTRACT OR GRANT NO.	9a. ORIGINATOR'S REPORT NUMBER(S)
F33615-73-C-1174	
b. PROJECT NO. 7633	011764-1-T
c.	9b. OTHER REPORT NO(S) *(Any other numbers that may be assigned this report)*
d.	AFAL-TR-73-422

10. DISTRIBUTION STATEMENT

Distribution limited to U.S. Government Agencies only;

Test and Evaluation Data;

Other requests for this document must be referred to AFAL/WRP.

11. SUPPLEMENTARY NOTES	12. SPONSORING MILITARY ACTIVITY
	Air Force Avionics Laboratory Air Force Systems Command Wright-Patterson Air Force Base, Ohio

13. ABSTRACT

The broad objective of this research is to develop techniques to reduce non-specular scattering from objects of interest to the Air Force. The major tools used thus far in the investigations have been two-dimensional computer programs which solve the integral equations for a surface impedance boundary condition and for a thin resistive sheet placed near a conducting obstacle. The existing programs have proven valuable, but the research requirements have now outstripped their capabilities and more inclusive programs are required. The main thrust of this Interim Report is upon the development of the integral equations necessary for the contribution of more comprehensive programs, but for the sake of completeness, the equations for the existing programs are also derived as a matter of course. Of considerable importance is the treatment of "magnetic" resistive sheets in addition to conventional electric resistive sheets so that, with but a slight expansion of the concept of resistivity, magneto-dielectric layers of physical materials may be modeled. In addition to the theoretical work, experimental results obtained by both the University of Michigan Radiation Laboratory and the Air Force Avionics Laboratory are compared with computed predictions.

14. KEY WORDS	LINK A		LINK B		LINK C	
	ROLE	WT	ROLE	WT	ROLE	WT
Edge diffraction						
Surface currents						
Surface impedance						
Surface sampling						
Resistive sheets						

14.	LINK A		LINK B		LINK C	
	ROLE	WT	ROLE	WT	ROLE	WT